CHALMERS

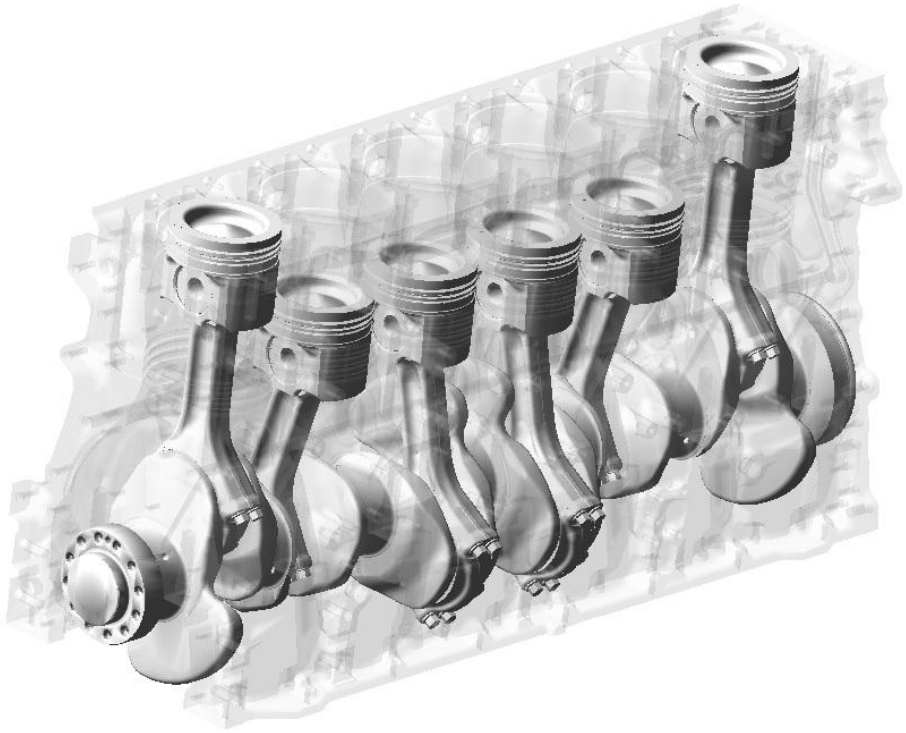

SIMULATION OF AN ENGINE FRICTION STRIP TEST

Master's Thesis in Automotive Engineering

AKHIL KRISHNAN

Department of Applied Mechanics
Division of Combustion
CHALMERS UNIVERSITY OF TECHNOLOGY
Göteborg, Sweden 2014
Master's Thesis 2014:39

MASTER'S THESIS 2014:39

SIMULATION OF AN ENGINE FRICTION STRIP TEST

Master's Thesis in Automotive Engineering

AKHIL KRISHNAN

Department of Applied Mechanics
Division of Combustion
CHALMERS UNIVERSITY OF TECHNOLOGY
Göteborg, Sweden 2014

SIMULATION OF AN ENGINE FRICTION STRIP TEST
Master's Thesis in Automotive Engineering
AKHIL KRISHNAN

Master's Thesis 2014:39
ISSN 1652-8557
Department of Applied Mechanics
Division of Combustion
Chalmers University of Technology
SE-412 96 Göteborg
Sweden
Telephone: + 46 (0)31-772 1000

Cover:
Volvo MD13, Euro 4 – Cranktrain CAD representation.

Chalmers Reproservice
Göteborg, Sweden 2014

SIMULATION OF AN ENGINE FRICTION STRIP TEST

Master's Thesis in Automotive Engineering

AKHIL KRISHNAN
Department of Applied Mechanics
Division of Combustion
Chalmers University of Technology

ABSTRACT

Over the years, internal combustion engine technology development has been targeted towards improving operating efficiency and thereby lowering fuel consumption. Friction Mean Effective Pressure (FMEP) accounts for 7-15% of the total indicative power produced in an engine cycle for large diesel engines, such as in trucks. The base-engine components such as piston rings, bearings, gears, seals and pumps contribute 60% - 70% of this FMEP. Minimizing the friction losses in the engine would translate to a direct reduction in fuel consumption. The development of low friction engine technology requires extensive studies and testing, with major challenges associated with the accurate measurement of individual component contribution to the overall engine friction power loss. Therefore, the requirement for a 'Virtual Engine Friction Strip Test' using modern simulation tools is exigent.

This thesis project, in association with the Tribology and Mechanics research group, at the Advanced Technology and Research department at Volvo Group Trucks Technology aims at developing a full engine strip down test simulation model. Owing to the large number of active components on an engine contributing to the overall friction losses, the scope of this study is restricted to the major friction contributors in the cranktrain – piston rings, skirts, journal bearings on the connecting rods and the main crankshaft journal bearings.

A one-dimensional analytical model was prepared using the Gamma Technologies' GT-Suite simulation tool. The dynamics of the crankshaft and the piston cylinder unit are modeled. The hydrodynamics of the lubrication films for the bearings, rings and skirts are solved quasi-statically, and mixed lubrication and asperity contact lubrication are also modeled. Combined with an oil thermal model, a shear thinning model, and accurate measurement data, a detailed insight of the engine friction can be obtained.

The model was validated against various other simulation approaches and against strip tests of the Volvo MD13 Euro 4 DST Engine. The same test conditions of the strip tests are reproduced on the simulation model, and the results are compared. In order to establish the model fidelity and robust solution methodology, it is also used to perform various studies on friction reduction techniques. This *Virtual Engine Strip Test* simulation model provides an opportunity to analyze new friction reduction methods and unconventional engine designs, towards the development of a low friction engine.

Key words: Simulation, GT-Suite, GT-Power, Friction, 1-dimensional, Validation, Hydrodynamics, Rings, Bearings, Tribology, Cranktrain.

SIMULERING AV ETT MOTORSFRIKTIONSAVSKALNINGSTEST

Examensarbete i Automotive Engineering
AKHIL KRISHNAN
Institutionen för tillämpad mekanik
Förbränningsavdelningen
Chalmers tekniska högskola

SAMMANFATTNING

Genom åren har utvecklingen av förbränningsmotortekniken varit inriktat på att förbättra effektiviteten och därmed sänkning bränsleförbrukningen. Friction Mean Effektiv Pressure (FMEP) står för 7-15% av den totala kraften som produceras under en motorcykel för stora dieselmotorer, som t.ex. i lastbilar. Basmotorkomponenterna såsom kolvringar, lager, kugghjul, tätningar och pumpar bidrar till 60% - 70% av denna FMEP. Att minimera friktionsförlusterna i motorn skulle kunna översättas till en direkt minskning av bränsleförbrukningen. Utvecklingen av lågfriktionsmotorteknik kräver omfattande studier och tester, med stora utmaningar i samband med den noggranna mätningen av de enskilda komponenterna som bidrar till den totala motorfriktionseffektförlusten. Därav kommer kravet på en "Virtual Engine Friktion Strip Test" med moderna simuleringsverktyg.

Detta examensarbete, i samarbete med Tribologi och mekanik-forskargruppen vid Advanced Technology and Research avdelningen på Volvo Group Trucks Technology syftar till att utveckla ett komplett motoravskalnings av en simuleringsmodell. På grund av det stora antalet aktiva komponenter på en motor som bidrar till de totala friktions förlusterna, är omfattningen av denna studie begränsat till de stora friktionsbidragsgivarna i vev- och kolvparti - kolvringar, kolvkjolar, vevstakslager och vevaxellager.

En endimensionell analytisk modell framställdes med användning av simuleringsverktyg GT-Suite från Gamma Technologies. Dynamiken hos vevaxeln och kolvcylinderenheten modelleras. Hydrodynamiken för smörjfilmerna för lagren, ringarna och kolvkjolarna löstes kvasistatiskt. Blandad smörjning och skrovlighetskontaktsmörjning modelleras också. I kombination med en oljetermisk modell, en skjuvförtunning modellen och en exakt datamätning kan ge en detaljerad inblick i motorns friktion.

Modellen validerades mot olika andra simulerings metoder och mot avskalningstester av Volvo MD13 Euro 4 DST Engine. Samma testförhållanden på avskalningstesterna återges i simuleringsmodellen och resultaten jämförs. I syfte att fastställa en modelltrohet och en robust lösningsmetodik och även för att utföra olika studier på friktionsreduceringstekniker. Denna *Virtual Engine Strip Test* simuleringsmodellen ger en möjlighet att analysera nya metoder för att minska friktion och okonventionella motorkonstruktioner, samt för att utveckla lågfriktionsmotorer.

Nyckelord: Simulering, GT-Suite, GT-Power, friktion, 1-dimensionell, validering, hydrodynamik, kolvringar, lager, tribologi, vev- och kolvparti.

Acknowledgements

This Master's Thesis project has been a phenomenal learning experience, thanks to the encouragement, guidance and support of many who helped shape it into a valuable academic project. I would like to extend my heartfelt gratitude to their contributions.

This Thesis project has been completed in association with the Tribology and Mechanics research group at the Advanced Technology and Research department at Volvo Group Trucks Technology. I would like to thank my manager, Arne Andersson for giving me this opportunity to work with this research based project and for all his involvement and support. I would also like to extend my gratitude to Per Salomonsson, Mark Fowell and Lars Mattsson, from the Tribology and Mechanics research group at Volvo GTT/ATR for their unparalleled support with the project.

I extend my gratitude to Professor Ingemar Denbratt, Head of the Division of Combustion at the Department of Applied Mechanics at Chalmers University of Technology, for his guidance and support, also to Professor Sven B. Andersson for his personal guidance and ever cheerful wit!

My colleagues at Volvo Group Trucks Technology have truly made my time with Volvo thoroughly exciting and have amplified my engineering knowledge many fold. I would like to thank my mentor Ola Styrenius, through whom my connection with Volvo began! This thesis project would not have been complete without the support of Bengt Olsson, Martin Svensson, Lina Wramner, Bincheng Jiang, Bengt Otterholm, Per H Nilsson, Jimmy Kling and Ramadan Salif and many others from Volvo.

Thank you, Pete T. Nguyen, from Gamma Technologies for answering dozens of queries about the GT-Suite simulation program and for the excellent support! I also thank Dr. Rifat Keribar and Alex Molnar from Gamma Technologies for their continued support through the course of this Master's Thesis project.

Göteborg, June 2014.

Akhil Krishnan

Contents

1 Introduction

1.1 Motivation

Heavy and medium duty truck engines lose between 7-15% of the fuel energy due to mechanical friction losses. A majority of the friction losses originate from three major sources – The Piston Cylinder Unit, the Crankshaft and the Pumps and some contribution from the gear drive and the Valvetrain. The piston Cylinder Unit contributes to about 30 to 40 % of the mechanical friction losses through the system and these numbers include the power loss from the piston rings, the skirt and the Connecting Rods in roughly equal proportions. The Crankshaft bearings and seals also contribute to 20-25% of the share of friction power. Apart from the Base engine components, the air compressor and the coolant and water pump cover the rest of the loss of engine power. A small contribution of around 1-7% is from the Valvetrain and the gear drive assembly. A pie graph of this result is shown from a study conducted by MIT on a stationary 16l Waukesha engine [1], and a similar strip down study conducted by Volvo in Japan also captures the same trends in friction power loss distribution. [2].

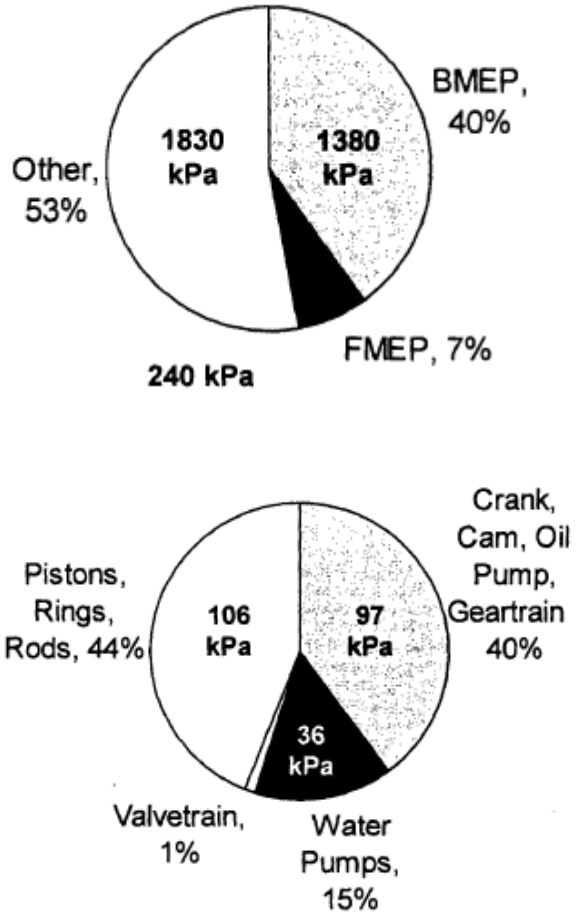

Figure 1.1: Pie graph showing FMEP and Friction distribution between engine components [1]

Lowering of the mechanical friction losses in an engine leads to a direct saving in fuel consumption and improves the operating efficiency of the system. An important aspect to friction reduction involves the evaluation of various methods and designs that can be employed in order to achieve a lower engine friction power los. This requires extensive testing and leads to long development times. The need for physical friction modelling which is capable of running fast simulation cycles for minor design changes and provide significant relative results is dominant.

Most work performed with friction reduction and the modelling and simulation of friction have been either through 3-dimensional CFD simulations or simple empirical models. This thesis project evaluates the possibility of providing a 1-dimensional simulation modelling approach to evaluate engine friction.

1.2 Objective

The objective of this thesis project is to build a 1D simulation model based on first principles which is capable of calculating engine friction contribution due to individual engine components, focused towards the cranktrain bearings and the piston ringpack. The model should be useful to analyse the effects of a variety of design changes on said components and should provide robust results. The model should be useful to evaluate both steady state and transient simulations to evaluate parameter identification for the whole system.

Due to the high degree of complexity involved with full physical modelling of individual components of the engine system, and the solution of a complete engine model including pumps and valvetrain systems involves very high computing resources, the scope of this thesis project is restricted to the evaluation of the friction contribution of the piston ring pack and the cranktrain bearings. As it was explained earlier, the major portion of the friction power is lost through these sources. Therefore, they have been selected as the primary focus of this thesis project.

The second phase of this project is to validate said model against results from fired friction evaluation experiments conducted by FEV and Volvo, and motored strip down tests. Model calibration for varying load cases and operating conditions are performed at this stage. The model developed using specific software tools are to be analysed against results obtained from dedicated solvers and physical models based on first principles.

The final phase of this thesis project is to provide a frame work of Friction analysis models which are capable of providing a better overview towards engine friction losses compared to empirical models such as the Chen Flynn or the Schwarzreimer Reulien models [3]. These models are to be applied on the new engine concepts being developed by Volvo GTT, in order to evaluate early stage friction reduction designs.

1.3 Limitations and Assumptions

Physical modelling based on first principles requires a large number of input data parameters. Some of these parameters require extensive measurements, such as, surface toughness, ovality and cylinder roundness etc. Some of the physical input parameters have been assumed. The list of parameters is presented in Appendix A.

Traces of Crank-angle resolved Cylinder pressure and Peak Cylinder Pressure, are not available for all engine speeds. Extrapolations of the pressure curves have been used for cases where data was unavailable.

Due to computational limitations, the resolution of the Reynold's equation solvers and the number of cells in the piston rings and bearing surfaces has been limited. Variations in output results vs. the resolution of the calculations are presented in the Results section.

Comparisons between empirical solutions and other modelling approaches are presented in this report, and the input data between the simulations are maintained the same for all, but few insignificant parameters.

A number of model assumptions have been made in place of unavailable data. The selection of the assumptions has been reasoned through this report.

1.4 Thesis overview

This report provides a brief overview of the complete project including the modelling approach and presents the results obtained from the simulation studies in comparison with the strip tests. Chapter 2 presents a simple description of the Engine components involved in this study. Chapter 3 presents an overview of the fundamentals of engine friction and lubrication Chapter 4 focuses on the modelling approach and comparisons between modelling approaches are described in this section. Chapter 5 presents an overview of the theory behind the modelling used in GT Suite. Chapter 6 presents insight into engine testing for friction and also provides details on the engine strip tests conducted by FEV for Volvo, Chapter 7 shows the results from the simulation model developed. A complete summary of the study and future applications of the model framework towards friction reduction designs are presented in Chapter 8.

2 Engine Component description

This section contains a description of the Engine components that will be studied as a part of this thesis project. Some engine components such as the piston rings may be installed or designed in varying configurations and designs suited to particular engines. The description provided in this section is with regard to the Volvo MD 13 engine, though similar to other heavy and medium duty truck engines.

2.1 Power Cylinder Unit (PCU)

A diagram of the Power Cylinder Unit is shown in Figure 2.1. The main components that contribute to friction power loss in the PCU are the ringpack and the piston skirt as they move against the cylinder liner. The functions of the ringpack are to ensure sealing against high pressure combustion gases from leaking through the crevice between the piston and the cylinder and also another function of the ringpack is to distribute lubricant as required through the liner. The third function of the ringpack is to regulate heat flow from the piston to the cylinder. The skirt is part of the piston, and enables the guidance of the piston through the strokes of the cycle.

2.1.1 Piston ringpack

The ringpack in heavy duty diesel engines generally consist of three rings. Some ringpack designs may involve even two or four rings. But the three major types of rings are described in this section.

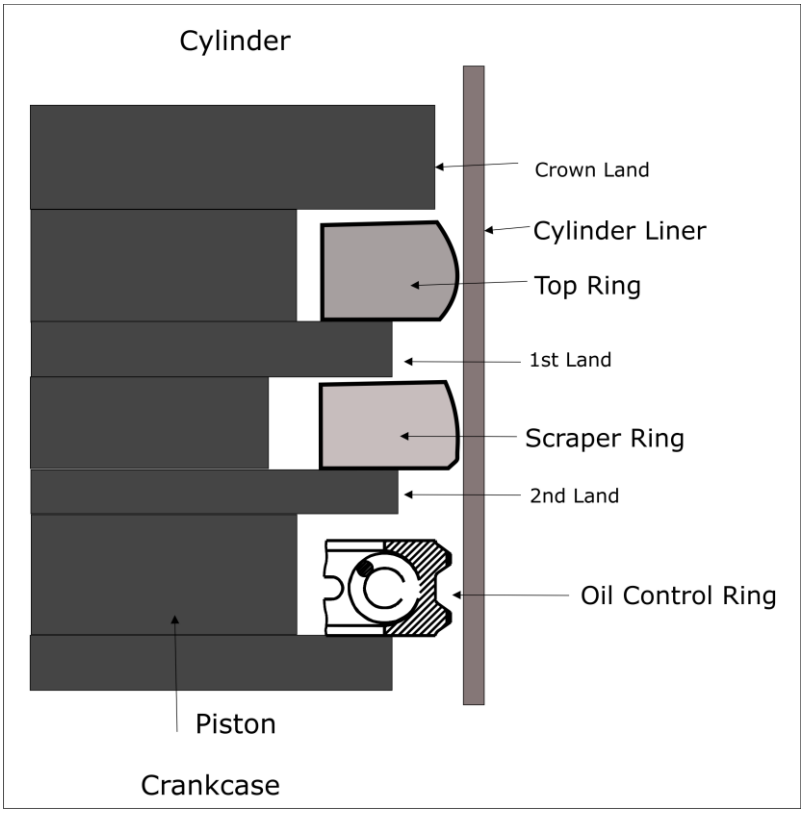

Figure 2.1: Piston ringpack schematic diagram

The top ring seals the interface between the combustion chamber above the piston to the crankcase below the piston. This tight seal prevents the escape of combustion gases from above the piston during the operation cycle of the engine. A second ring, also known as a Scraper ring is also installed on the Volvo engine, and in most other diesel engines. This ring has a sharp face and it scrapes the oil that may have been deposited on the surface of the liner during the up and downstrokes of the piston. Although the main purpose of the second ring is to scrape the excess oil off the surface of the liner, it also prevents further leakage of the blow by gas which leaks through the seal of the top ring from the cylinder. In order to maintain this tight seal, the piston rings are always manufactured to a size larger than the bore of the cylinder and then fit into the cylinder by means of applying a ring tension or tangential force due to the radial compression of the liner. Typically, both the top and the second ring are single piece, slotted, solid rings made of hardened material and are self-tightening. In some applications the running surface of the rings may be coated with a special coating that helps lower friction. (Specialized coatings and DLC material are discussed in Appendix B). [13]. Piston ring coatings and construction materials require,

- Good running and boundary lubrication capabilities
- Elastic behaviour
- Mechanical strength
- High strength at elevated temperatures
- High heat conductivity
- High wear resistance
- Good machinability [13]

The third ring is the OCR – Oil Control Ring, its design is different from the other two rings. The OCR may be comprised of two or three piece assemblies, in most cases the ring is made of steel or nodular cast iron and is supported by a radial spring as shown in cross section of the OCR in Figure 2.2.

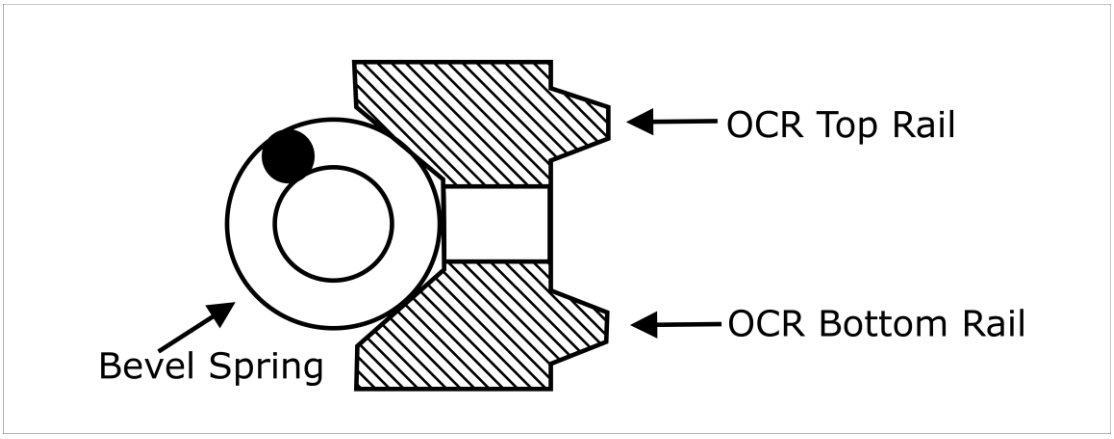

Figure 2.2: Oil Control Ring, Cross Section schematic

The ring is manufactured to a dimension much larger than the bore and is slotted. Unlike the other two rings, the tangential force of the oil control ring is determined by the circumferential length of the spring that is assembled with the ring. The OCR is the one which has the highest ring tension and this is necessary for the ring to maintain conformability with the cylinder bore even in conditions of high thermal and mechanical deformation. An additional advantage of the high tension force is the

possibility of maintaining a high oil pressure between the relatively small running surface of the ring and the liner. The running surface or the 'land' of the OCR is also different from the other two rings. The OCR in the Volvo engines is a twin land OCR. This means that there are two contact surfaces on the rings. The small contact surfaces coupled with the high tangential force provide the necessary pressure to the oil film. Also, the twin land design ensures that at least one of the lands of the OCR is in contact with the cylinder liner even under adverse twist or tilt conditions. The lands of the oil control ring are almost flat, but possess a sharp profile as shown in this diagram. [13]

It is evident from the diagram that the running surfaces or 'lands' of the three rings are not the same. Since the three rings perform different functions, the lands of the rings are designed accordingly. The Top Ring land is generally designed with a smooth profile, such as to allow the ring to develop a pressure gradient for the motion of the oil film through the ring, but also the ring face is designed in order to seal the combustion gases from the lower crankcase. The top ring usually does not have any additional chamfers or grooves, and is constructed as shown in Figure 2.3.

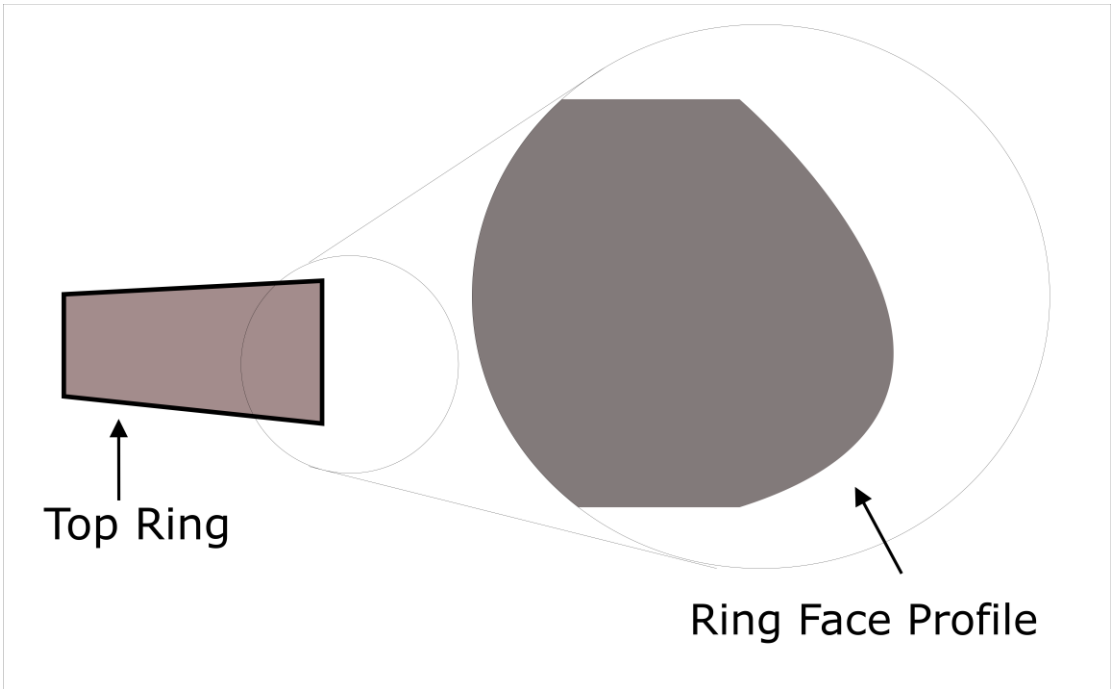

Figure 2.3: Top Ring Face Profile schematic

The scraper ring is designed with a static twist as shown in figure 2.4. This is required to enable the ring to scrape the surface of the liner to remove any excess oil that is retained upon the liner surface. The 2nd ring has a sharp ring face profile as shown in the Figure.

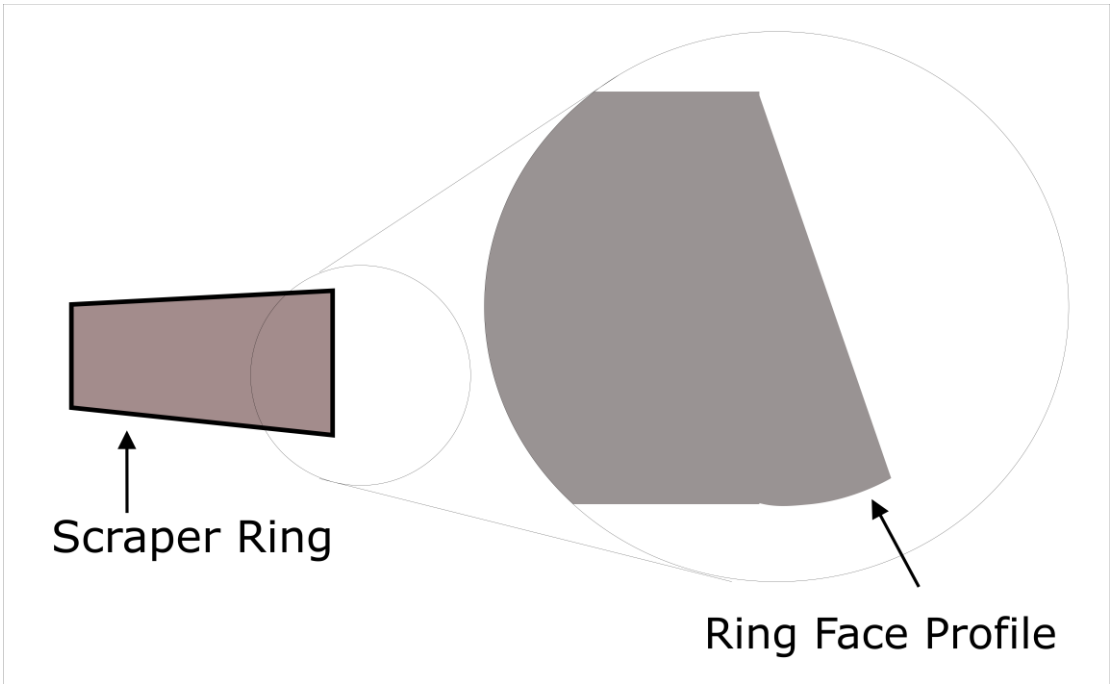

Figure 2.4: Scraper Ring Face Profile.

Modern advancements in ring design by popular piston cylinder unit component manufacturers such as Mahle and Federal Mogul have brought about many improvements in the design of the face profile of the piston rings.

2.1.2 Piston Skirt

The piston skirt is the lower part of the piston that is not in direct contact with the combustion gases, as shown in Figure 2.5.

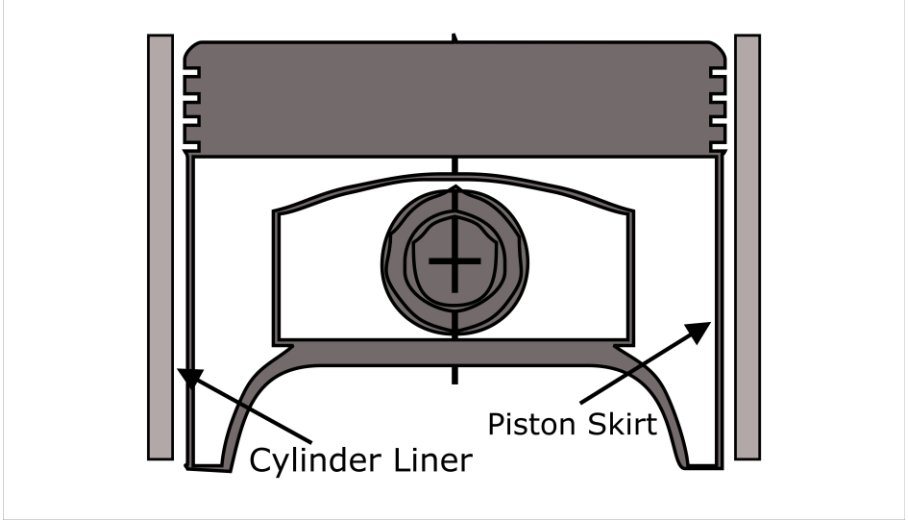

Figure 2.5: Piston Skirt schematic diagram

The main task of the skirt is to guide the piston through the cylinder and to maintain the piston in an appropriate position and to withstand the inertial tilt forces generated by the combustion gas above the Piston crown [13].

The skirt also accommodates the piston during the piston tilt or piston slap conditions, which occur around the TDC or BDC positions of the piston due to the concomitant change in direction. In order to allow the skirt to guide the piston by maintaining an oil film between the skirt face and the cylinder wall, the skirt is always designed with a suitable clearance. Optimized skirt clearance and appropriate skirt length can ensure minimal piston contact as the piston alternates from an upstroke to a downstroke.

In the past, diesel pistons were designed with full 260 deg. skirts and the skirt was modified to accommodate the piston pin boss. But, with the evolution of piston design, modern pistons range between 90 – 140 deg. symmetric skirts extending only on the Thrust and the Anti-Thrust sides of the piston – which are the sides that are susceptible to contact with the liner due to the piston tilt [13].

The requirements on the piston skirt are

- Must bear heavy lateral loads without major deformations
- Elastic adaptation to the deformations of the cylinder
- As the piston crown deflects under the elevated thermal loading, it causes the piston skirt to deform both circumferentially and axially, therefore the piston skirt must be designed to operate under extreme thermal stress.

2.1.3 Piston Ring Liner dynamics

The dynamic phenomena of the PCU can be broadly classified into two sections - Piston motion and Ring dynamics. The piston motion involves the reciprocatory movement of the piston from TDC to BDC through the 4 stroke cycle and also, the secondary motion of the piston within the cylinder due to the tilt and slap because of the high pressure gas forces.

The primary motion of the piston can be shown by the equations of motion as

$$x = r\cos\theta + \sqrt{l^2 - r^2\sin\theta}$$

x = Piston position
l = Connecting rod length
r = Crank radius
θ = Crank angle

The secondary motion of the piston involves the sideward motion of the piston induced by the change in direction at the end of strokes and by the high pressure combustion gases acting on the piston crown. The secondary motion of the piston is presented in section 5.3.1. All the other equations such as the lubricant oil properties and the hydraulic stresses have to be integrated in order to provide the coefficients to the force equations in the secondary motion of the piston. [13]

2.2 Cranktrain

The Friction contribution from the Cranktrain assembly is dominated by the plain/journal bearings on the crankshaft. The journal bearings allow the crankshaft to rotate in the engine block and also provide the joint between the crankshaft and the connecting rods. Journal bearings are also present on the small end between the

connecting rod and the piston pin. Some details of the bearings, the materials used and the requirements are presented below.

2.2.1 Journal Bearings

The list of journal bearing parts on the inline 6 cylinder diesel engine such as the Volvo MD 13 is

- Main bearings
- Thrust bearings
- Big End Bearings
- Small End Pin bore bearings

The construction of the bearing assembly is shown below.

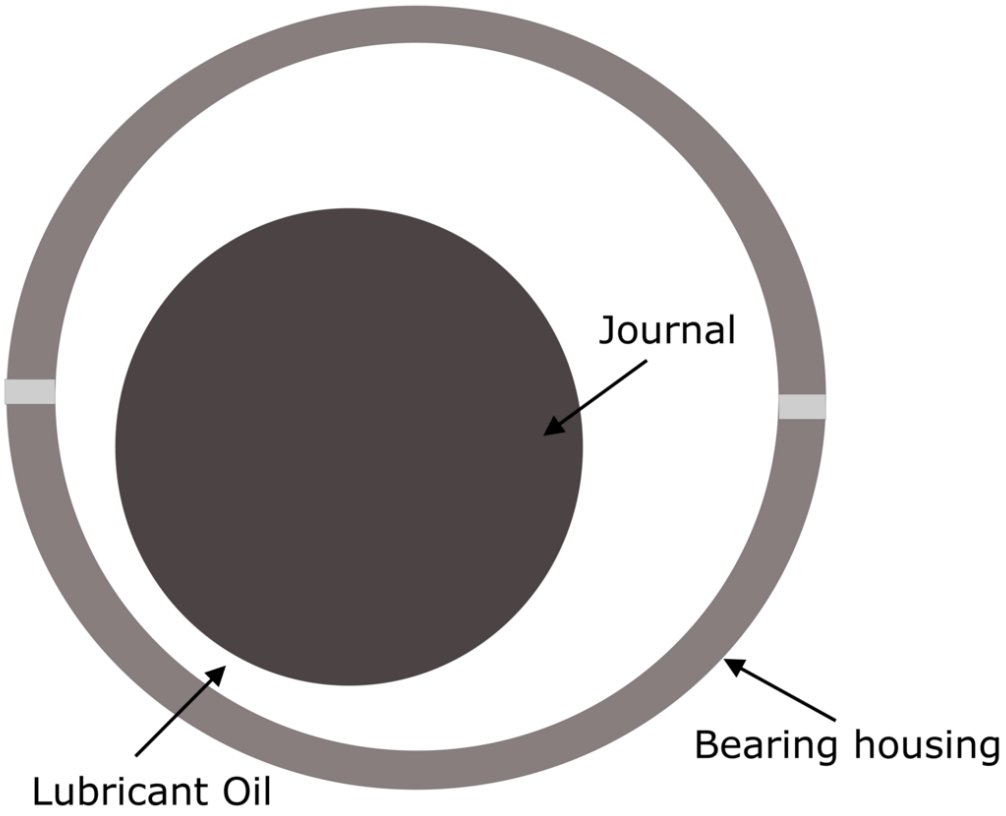

The rotating unit (Journal) is a part of the crankshaft on the Big End bearings and the Main bearings. The piston pin / gudgeon pin behaves as the journal in the Small End bearings. The Bearing unit on the main bearing is installed into the bearings housing which is machined into the engine block, on the connecting rod, the bearing unit is machined on to the inner surface of the big end and the small end eye. An oil film is maintained between the Journal and the bearing surfaces. This oil is constantly churned through by the journal and is expelled from the side of the bearing unit, while a fresh supply of lubricant is supplied to the bearing clearance from the oil pump usually through oil galleries which are drilled through the crankshaft and the connecting rods. The positions of these holes or grooves also influence the performance of the bearing [14].

Two major definitive characteristics of a bearing are the Peak Oil Film Pressure (POFP) and the Minimum Oil Film Thickness (MOFT) between the journal and the bearing. Both these characteristics are influenced by the width and diameter of the bearing, which are the two most important parameters of the journal bearing. A larger bearing width reduces the POFP and increases the MOFT, a larger bearing diameter also has the same effect, due to the fluid properties of the steady state volume of oil maintained in the clearance. Apart from the width/diameter ratio, the design clearance of the bearing, which is the difference between the outer diameter of the journal and the inner diameter of the bearing, also as an effect on the oil film and therefore the friction performance of the bearing. With less clearance the loads are distributed evenly and because the journal curvature is almost nearly identical to the bearing surface, the motion of the journal in the bearing generates lower POFP. Although, a lower clearance increases the operating temperate of the oil within the bearing, this increases the oil viscosity and therefore influences the MOFT and the POFP through the oil shear phenomenon [14].

Another distinction between bearings can be made based on the materials used on the bearing running surface. Bearing materials are generally bi-metal or tri-metal assembly alloys, which generally consist of a steel back with aluminium or a bronze alloy. The selection criteria for the bearing materials include the load and the permissible stress of the material; the capacity limits are determined for each material on the basis of simulations and testing. Materials range from Cast iron, sintered steel to bronze, aluminium and white metal. These bearing surfaces may then have galvanic or sputter overlays for wear protection.

3 Friction Analysis

Friction, in general, is the resistive property that opposes the motion between two surfaces. Modern developments in engine design are targeted towards minimizing friction, and thereby improving the efficiency of the engine and realizing an improvement in fuel economy.

Due to the presence of a lubricant such as the engine oil, between the contact surfaces on the bearings, piston rings and other components such as gears, cams or valves, three modes of lubrication are plausible. The contact phenomenon and thereby, the resulting friction losses from these modes are different and are discussed below.

3.1 Modes of Lubrication

In principle, the three modes of lubrication are applicable to the lubrication of surfaces in the piston ringpack, skirt and bearings. The modelling of these friction phenomena is discussed in Chapter 5.

A schematic diagram of a friction phenomenon similar to the conditions in the running engine is shown below. Although there is a thin layer of oil that separates the moving surface such as the ring or the skirt from the cylinder liner surface, the roughness of the surface due toi the presence of asperities provides a possibility for certain parts of the surface to have asperity (metal-to-metal) contact.

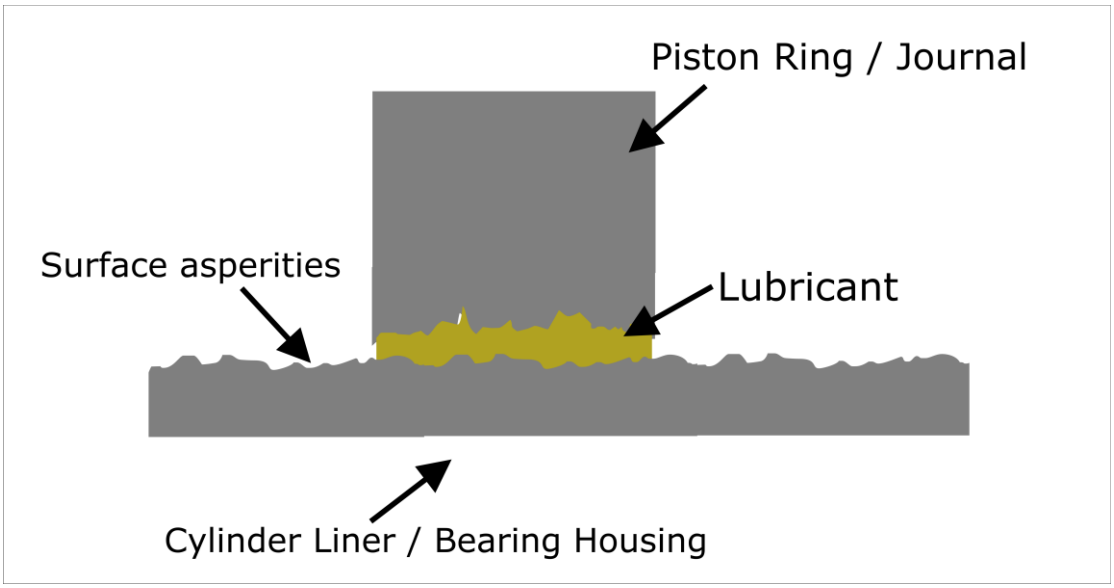

Figure 3.1: Surface Friction schematic

Depending on the distance between the nominal lines of the surfaces, three modes of lubrication can be observed.

i) Hydrodynamic lubrication
ii) Boundary lubrication
iii) Mixed Lubrication

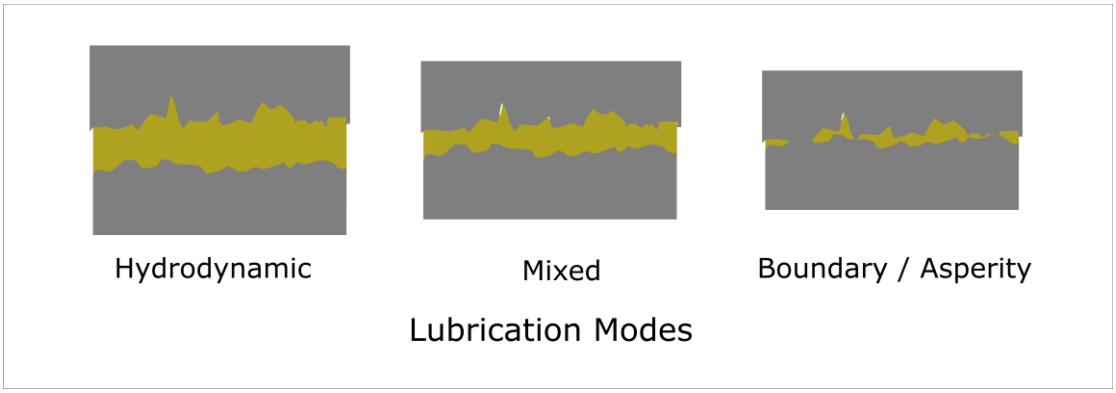

Figure 3.2: Lubrication modes

3.1.1 Hydrodynamic Lubrication

Pure hydrodynamic lubrication is the mode that is characterised by a significant oil film that separates the two surfaces completely, hence the oil supports the load from the moving units, without any surface contact. A schematic of the piston rings in full hydrodynamic lubrication is shown below.

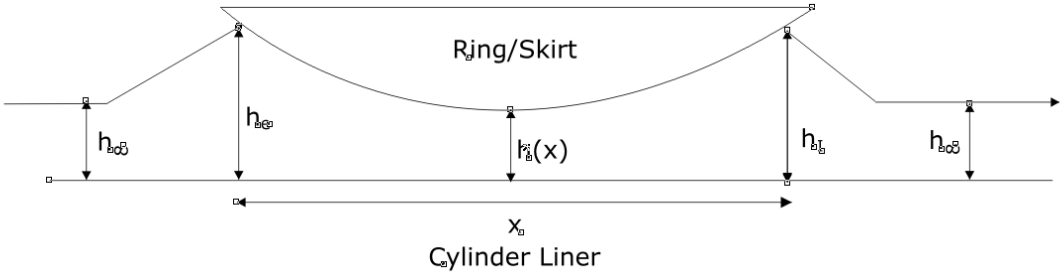

Figure 3.3: Surface Lubrication diagram

'h' is the thickness of the oil film that is maintained on the liner. This film thickness is called as the supply thickness to the ring. Due to the fluid capillary characteristics, the oil film thickness changes as the ring approaches. As explained earlier, the piston ring, is not a flat surface, but has a curved profile. This enables the ring to have a different film thickness across the ring running surface. The entering film thickness is called h_1 and the exit film thickness is called h_2. At any point x, the film thickness of the oil can be calculated as h(x). The system remains in pure hydrodynamic lubrication only until the film thickness h(x) remains above a certain critical value. In case the film thickness drops below the critical value then the particular system enters into a mixed lubrication regime or into a boundary condition based on the extent of the roughness of the two surfaces.

In the most general case, a minimum of three equations are required to solve the characteristics of the lubrication condition between the ring or the skirt and the liner, or between the journal and the bearing. The equations are

i) Consideration of the conservation of mass and the conservation of momentum on the oil film under the surface.
ii) Radial force balance on the system. (i.e radially over the complete circumference of the cylinder.)

iii) Using appropriate boundary conditions and assuming that the oil is incompressible, the system can be reduced into a solution of the 2D Reynold's equation.

With these three governing equations, the number of unknowns may depend on the possible wetting conditions between the surfaces. The wetting condition refers to the schematic representation of the volume of oil between the running surfaces. For the translational components (rings, skirt) there are four wetting conditions possible in the hydrodynamic lubrication regimes.

a) Fully flooded inlet and outlet
b) Fully flooded inlet and partially flooded outlet
c) Partially flooded inlet and fully flooded outlet
d) Partially flooded inlet and outlet

The solution of the governing equations for all these cases is which are explained in detail in the forthcoming Modelling Approach chapter of this report. The derivation of the Reynold's equations used in this study is shown in [4], [5].

In the common condition, where the oil is available between the running surfaces both at the inlet and the outlet, the Reynolds equation reduced from the Navier Stokes equation can be expressed in a simple form by making the following assumptions.

- Height of fluid film - y << x - sliding distance. Therefore the film curvature is ignored.
- Laminar flow
- No pressure variation across the length of the fluid film between the surfaces
- No fluid inertial effects
- No external forces act on the fluid film
- All velocity gradients are negligible compared to rates in x and y.

Hence, the Reynold's equation relates pressure, to the oil film thickness and the piston speed and oil viscosity as,

$$\frac{d}{dx}\left(\lambda_p h^3 \frac{dP}{dx}\right) = 6U\mu\left(\frac{dh}{dx}\right) + 12\mu\frac{dh}{dt}$$

Where:
x = Direction of Ring motion
h = Instantaneous local film thickness
P_0 = Oil film pressure
U = Piston Speed
σ = Composite Roughness mean asperity height
μ = Oil viscosity
T_{oil} = Average oil film temperature =
$\lambda_p(h_T/\sigma,\gamma)$ = Patir-Cheng pressure flow factor
$\lambda_s(h_T/\sigma,\gamma)$ = Patir-Cheng shear flow factor [7].

Using this equation the hydrodynamic friction force can be expressed as,

$$F_f = \int (\frac{\mu U}{h} - \frac{h}{2}\frac{dP}{dx})dx$$

Therefore, once the oil film height and the viscosity of the oil are determined, the hydrodynamic friction force can be estimated.

3.1.2 Boundary Lubrication

Boundary lubrication is the condition that arises when there is no oil film that supports the running surface from the other. In the pure boundary condition, the two surfaces have metal to metal contact. The boundary lubrication may be caused due to the dynamic phenomenon of the motion of the engine components or by microscopic asperities which are present on the surfaces of all the friction components including the liner, rings, skirt and the bearing surfaces. Since, it is not possible to discretely model all the asperities and to solve the asperity contact phenomenon; a stochastic simplification such as the greenwood Trip model coupled with the flow factor model by Patir and Chang is used. [6], [7], [8].

In these models, the asperities are treated as a Gaussian statistical distribution, further explanation of the models is provided in the Chapter 4 on Modelling approach.

Since the oil film is absent, the friction force is calculated by using the asperity contact pressure.

$$F_f = \int (a_{asp} P_{asp})dx$$

Where a_{asp} is the friction coefficient governed by the surface properties of both the contact surfaces, and P_{asp} is the contact pressure, According to the Greenwood-Tripp model, the contact pressure can be calculated using [6].

$$P_{asp} = \left(\frac{16\sqrt{2}}{15}\right)\pi(\sigma\beta\eta)^2 E\sqrt{\frac{\sigma}{\beta}}F\left(\frac{h}{\sigma}\right)$$

h = local film thickness

σ = Composite roughness (mean asperity height standard deviation) = $(\sigma_1^2 + \sigma_2^2)^{½}$

β = Composite mean radius of curvature of asperity tops

η = Composite asperity density

E = Composite Young's modulus of elasticity of surfaces

v=Poisson ratio

By determining these characteristics of the surfaces, the friction forces for the boundary lubrication conditions can be determined.

3.1.3 Mixed Lubrication

As implied, the mixed lubrication condition is the regime in which the hydrodynamic condition and the boundary lubrication are present. Although the support from the oil

film between the running surfaces is available, but the pressure is not sufficient to avoid the asperity contact. In many operational cases, it has been observed that the lowest friction force contribution is from the mixed lubrication condition. This can be accounted to the optimization of the oil pressure and the asperity contact pressure contributions to the support of the running surface. So, mixed friction is calculated as an integral sum of contributions from both hydrodynamic and boundary conditions.

$$F_f = k_1 \int \left(\frac{\mu U}{h} - \frac{h}{2}\frac{dp}{dx}\right) dx + k_2 \int (a_{asp} P_{asp}) dx$$

Where k_1 and k_2 are influence factors for mixed lubrication.

3.2 Stribeck Curve

The three lubrication regimes can be presented schematically by using the Stribeck curve. The Stribeck curve represents the change in coefficient of friction of the surface pair, against μN/σ – (Viscosity X Sliding speed / Surface Roughness) as shown below.

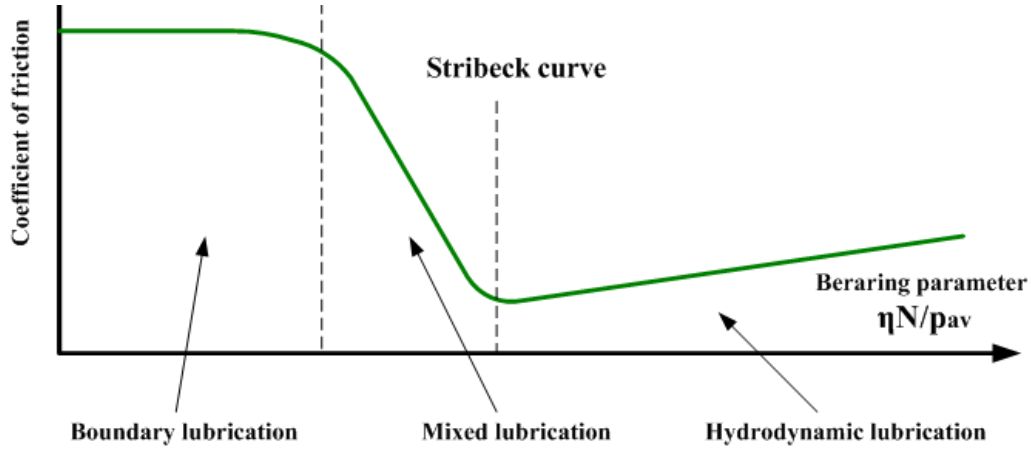

Figure 3.4: Stribeck curve

The x-axis represents the variation in other parameters, of which the most influential is the speed. From the graph, it is evident that the boundary friction reduces with increasing speed, and the hydrodynamic friction dominates. Also, the region of optimum sliding speed for minimum friction is provided, assuming a fixed viscosity and surface roughness. But, in the engine operation, although the surface parameters are constant through the cycle, the viscosity of the oil changes constantly due to the temperature and pressure variations and also due to the shear thinning effects of the oil between the running surfaces.

But the observed trends in common engine operation, as the piston moves towards the TDC and the BDC and approaches the end of a stroke, the low velocity boundary lubrication dominates the friction, and in the middle of the stroke, high velocity, hydrodynamic lubrication is observed. The passage through the mixed lubrication regime occurs many times over the cycle, based on the parameters and the operating conditions.

4 Modelling approach

The modelling of the engine strip down simulation is performed on GT Suite. The bearings have also been modelled using AVL Excite, in order to provide a comparison between the modelling techniques between the two tools.

4.1 Correlation modelling or empirical modelling

The most common way of handling friction losses in system simulations is by using simple correlations or empirical fits which have been designed to suit certain engine types and volumes. These correlations prove to be ineffective when simulating engines which are different in construction as well as operation. Some of the popular empirical correlations are discussed in this section.

4.1.1 Chen Flynn Model

The Chen Flynn friction model is an empirical model based on engine experiments based on engine tests. The model is empirical and shows a simple correlation between FMEP and the inputs. There are only three parameters in the model and then require three coefficients to tune the curves in order to fit the model results to the test results. The two variables used are the mean piston speed and the maximum cylinder pressure, which are fairly easy to measure.

The correlation between the FMEP and the parameters is shown in the following equation.

$$FMEP = FMEP_{const} + C_1\, PCP + C_2\, c_p + C_3\, c_p^2$$

$$C_i = constants$$

$$PCP = peak\ cylinder\ pressure$$

$$c_p = mean\ piston\ speed$$

4.1.2 Schwarzreimer Reulein Model

This empirical model was introduced in 2006 and provides a more detailed version of the engine friction than the Chen Flynn model. The model requires a few more inputs and also a reference point which is ambiguous with physical engine data. Although the number of inputs is higher than the Chen Flynn model, the accuracy trend of this model is still not comparatively higher.

This model is similar to the Chen Flynn in terms of being an empirical relation. But the friction contribution is split between different components. The individual friction coefficients are calculated using tests on various engines. Another restriction is that the model only is valid for oil and coolant temperatures from 293 – 400 K. It also requires a reference point with measurement data, and one reference FMEP. One way to evaluate this is to calculate the corresponding IMEP from a pressure trace that has been measured. Although the mathematical model behind the Schwarzreimer Reulein model is more complicated than the Chen Flynn, the FMEP calculations are expressed using one equation.

$$fmep = fmep_x + C_1\left(\frac{c_m}{T_{cyl}^{1.68}} - \frac{c_{mx}}{T_{cylx}^{1.68}}\right) + C_2\left(\frac{mep}{T_{cyl}^{1.68}} - \frac{mep_x}{T_{cylx}^{1.68}}\right) +$$

$$+ C_3\left(\frac{(d\,n)^2}{T_{oil}^{1.49}} - \frac{(dn_x)^2}{T_{oilx}^{1.49}}\right)$$

$$+ C_4[(1 + 0.012\,c_m)mep^{1.35} - (1 + 0.0012\,c_{mx})mep_x^{1.35}]$$

$$+ C_{5(n^2 - n_x^2)} + C_6\left(\frac{mep}{T_{oil}^{1.49}} - \frac{mep_x}{T_{oilx}^{1.49}}\right)$$

The first term after $fmep_x$ considers the friction of the piston. It takes into account the oil temperature between the piston and the cylinder wall and the mean piston speedc_m. The second term reflects the friction amount due to engine load and again oil temperature between piston and cylinder. The third considers friction from main and Connecting rod bearing as a function of bearing geometry - d, engine speed n and the oil temperature- dependent oil pump work - T_{oil}. The fourth term is for how the speed influences the injection pump and the fifth part is for ancillary components, coolant pump and cooling air fan as a function of speed and fan geometry. The index x stands for a reference point. They have decided only to include the first term, perhaps because the auxiliary loads can differ between different engines.

4.2 Modeling approaches

The differences between 0 dimensional modelling, 1 dimensional modelling and 3 dimensional modelling are presented in the form of this table.

Table 1: Properties of 0D, 1D and 3D modelling

	OD	**1D**	**3D**
Behavior	System dynamics as a function of time	System dynamics as a function of time and one dimension	System dynamics as a function of time and space
Type of model	Lumped parameter ordinary differential equations or differential-algebraic equations	Ordinary differential equations or differential-algebraic equations	Partial differential equations
Inputs	Component-connectivity model; Component behavior models;	Component-connectivity model; Component behavior models;	3D CAD configuration; material properties;
Critical expertise	Model abstraction	Model abstraction	Grid generation
Typical use	Component sizing; design space exploration; preliminary verification of performance and function	Component sizing; design space exploration; preliminary verification of performance and function	Detailed analysis and verification of performance, risks, and failure modes
Common tools	MATLAB/Simulink, Java, Excel	GT Suite, MIT lc2dm, MATLAB, Simulink, C, Java, AVL Fire, Ricardo Wave, PisDyn, RingPAK	Various open and proprietary CFD and FEA solvers

In order to study friction, simulations are carried out in the 1 dimensional domain, although inputs for these 1-dimensional simulations may be generated using full 3D CAD based simulations.

4.3 Modelling using GT Suite

Gamma Technologies' GT Suite 7.4 is designed to allow the simulation of engines and vehicles using a modular approach. Physical models of components can be modelled individually and then connected in order to transfer forces and energy

between them. This approach provides an excellent improvement to the current modelling approach used with engine friction.

The need for a robust 1-dimensional simulation platform for engine thermodynamics and mechanics is driven by the automotive and the energy industry.

- In order to predict the effects of design and operating conditions, desin trade-off and optimization studies in support of friction reduction and development of minimum friction engines.
- To be able to simulate in-cylinder friction on a timestep basis for steady state and transient simulation events.
- Estimation of friction for engine Strip Down measurements.

One dimensional modelling approach combines the advantages of the 3D CAD based simulations, but provides faster computational runs than full 3D simulations. Also, 1D simulation can be run using lower CPU resources.

The major advantages of predictive physical models over the empirical and correlative models are

- Separate modelling of each engine friction element.
- Physical models, close to first principles can be developed.
- Transient simulations marching in timestep or CAD can be run.
- Measurement lab data for surface roughness, lubricant properties and friction data can be entered. Sensitivity analysis to measurements can be compared.

In order to be an effective tool for engine development work, the challenges for the 1 dimensional simulation are to

- Develop models that are robust and provide consistent results.
- Models should have a high fidelity, and repeatability
- Models should be capable of accommodating various designs, surface treatment, lubricants and materials
- Models should be fairly fast, so that they are suitable for optimization and day to day simulation runs
- CPU requirements should be reasonable such that it is possible to use these models on normal simulation computers.

An example of the GUI for the model built using GT-Suite is shown below.

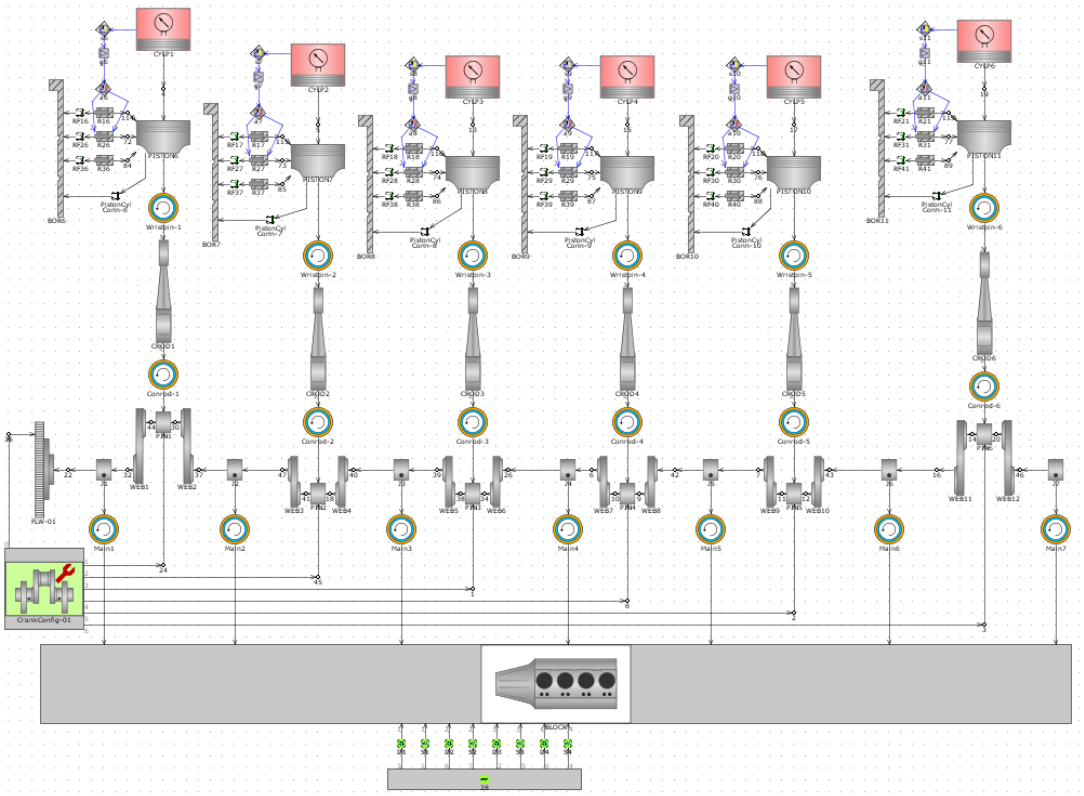

Figure 4.1: GT-Suite model GUI

4.4 Modelling using MIT lc2dm

The MIT psim simulation tool is a Matlab based tool that also works on the same principles as the GT Suite tool. Although the MIT tool has some differences on the type of theoretical simplifications to the physics, the structure of the 1-dimensional simulations are similar to the GT Suite models.

The MIT simulation tool divides the simulation model into three solution sections.

- Ringpack – Solves Ring dynamics of Top and second ring
- Friction – Solves friction forces and friction power loss of top and second ring
- TLOCR (Twin Land Oil Control Ring) model – Solves dynamics and forces for the Oil Control Ring

A combined output of all the three solution modules is presented in the post processing charts.

The MIT tool considers the Oil Control ring to have different dynamics compared to the top and the scraper ring, and this means that the solution for the oil control ring is calculated separately.

Advantages of the MIT lc2dm over the GT Suite tool

- Integrated blow-by calculations to the axial dynamics solution.
- Advanced Ring groove dynamics model, including calculations for ring groove friction losses.

- Advanced Oil Control model to calculate coupled oil consumption for complete ringpack, without the use of reduction techniques such as Martin's equation.
- Deterministic solution for the Asperity contact pressures and realistic calculation of the Patir and Cheng flow factors.
- Variable observation of the wetting conditions of the three rings and continuous solution update for the changes in lubrication regimes.

Disadvantages of the MIT lc2dm compared to the GT Suite tool

- Does not allow variations in ringpack configuration or ring design.
- Absence of a modular solution does not allow sensitivity studies and parameter identification.
- Complicated solution system and a large number of input parameters required.
- No ODE control or explicit solution methods available.
- No clear post processing capabilities or ability to run batch simulations, DOE or optimization trials.

Due to the limited scope of this report, it is not feasible to explain the complete MIT axial dynamics and blow-by modelling calculations in detail. Due to the extensive calculations performed within the solution model of the program, understanding the problem flow path is not as simple as the GT-Suite solution.

The fundamentals of the MIT psim simulation for the axial dynamics, piston dynamics and the blow-by are presented in the papers by Wong et. al, and Tian et. al. and others from the Sloan Automotive Laboratory at MIT. These papers are listed in the References section as [15], [16], [17], [18].

The MIT *psim* simulation tool, part of the lc2dm program is used as a verification in order to check the design changes which have been made with respect to the Piston Rings and the Skirt to study the effects caused to the Blow-by gas flow, since the GT model does not contain an accurate gas flow model.

Also, comparisons on Piston Ring friction estimates between the MIT program and the GT Suite simulations are analysed in the Results section.

5 Modelling Theory

This Chapter examines the theoretical physics that underlines both the GT-Suite and the MIT lc2dm simulation platforms used in this study. The section is divided on the basis of the friction component that is modelled. Due to a large number of physical models reductions used to accommodate the simulations, a number of reference papers are addressed in this section. These papers provide a thoroughly detailed explanation of the physics involved in the calculations.

5.1 Journal Bearings

As it was mentioned earlier, the Journal Bearing models in GT Suite can be modelled in three levels. The differences between the three modelling approaches available in GT-Suite for the journal bearings are shown in this table.
For the purpose of this study, the 'Journal Bearing' model is used.

Table 2: Journal Bearing models in GT-Suite

	Revolute Joint	**Journal Bearing**	**Journal Bearing HD**
Geometry	Only diameter and width defined.	System dynamics as a function of time and one dimension	System dynamics as a function of time and space
Lubricant	Oil properties absent. Only coefficient of Friction.	Full oil properties.	Full Oil properties.
Fluid film model	No fluid film model	Map based modeling. Calculated states journal and forces.	Squeeze film effects and film shear effects modeled.
Journal dynamics	No dynamics model	Only planar kinematics of Journal.	Full dynamics modeled. Including torsional and shaft bending effects.
Bearing deformation	No bearing deformations modeled.	No bearing deformations modeled.	Bearing deformation purely based on contact physics.
Reynold's Equation solution	No Reynold's equation	1 D reduced Reynold's equation. No mesh integration	Mesh integration. 1 D Reynold's equation
Runtime	Extremely fast	Reasonably fast	Slow
Memory requirement	None.	Few MB	Depends on mesh density.

The theory for the modelling of the bearings using these templates is explained in this section.

The most important functionality of the Journal Bearing model is to utilize the magnitude and the direction of the forces that are applied on the Journal or the bearing housing in order to obtain the magnitude and direction of the motions, both transient and planar, of the journal within the bearing due to hydrodynamic action and asperity contact. This model presents these relationships between the forces and the motions in the form of maps or fits which are based on the integration results of the 1 dimensional Reynold's equation reduction from the Navier Stokes equation. Some assumptions which are made in order to allow the solution of the Reynold's equation,

- The fluid film is considered to be a thin film, hydrodynamic operation.
- The annular oil film exists through the complete bearing, i.e No cavitation.
- Bearing is modeled without any misalignment.

Two methods of solving the simplified Reynold's equation are presented. And based on the type of application, the user may choose one of the two. They are called the Mobility approach and the Impendence approach.
For this application, the Mobility approach is more appropriate due to the availability of the necessary inputs top solve the Reynold's PDE. A brief description of the Impedance approach is presented, followed by a detailed description of the mobility approach.

5.1.1 Impedance approach

The Impedance solution approach solves the Reynold's equations and models the oil film as a function of the states of the journal within the bearing. This means that, the forces and the torques exerted by the journal on the oil film are the unknowns, and are determined from the model solution.[8] The forces and the torque are expressed as functions of the oil shear stress and the hydrodynamic pressure and the distribution of the oil film through the bearing. And these pressures and shear stress levels are determined by solving the equations of motion of the journal within the bearing housing. The oil film pressure between the journal and the bearing is governed by the Reynolds Equation, expressed as a partial differential equation which is derived from the Navier-Stokes equations as shown in [4], [5].
The solution procedure for the Impedance approach is

- Application of Boundary conditions – Timestep, Temperatures of the oil, pressure of the lubricant.
- Solve equations of motion for the journal shaft within the bearing, to determine shaft position.
- Solve the Reynold's equation PDE at every time step for the predetermined shaft position integrate the oil film pressure and shear stress over the solution domain.
- Calculate hydrodynamic force and torque.

The calculated forces are then used to determine the friction force, the calculated friction force can then be converted into Friction power and eventually into a n FMEP for the bearing.

5.1.2 Mobility approach

The mobility approach used by the GT Suite model mirrors some solution procedure from the Impedance method described above. It is also a map based solution, where the map of the journal motion and the forces and torques is prepared with respect to the planar states or positions of the journal [9].

Note: The instantaneous planar state and the Force are expressed as vectors as shown in [9].

To simplify the cumbersome task of solving the Reynold's equation in terms of independent variables, the solution can be rewritten to express the vectors for varying eccentricity, e ad for angle β, of the eccentricity normal and the velocity vector as shown in the diagram below.

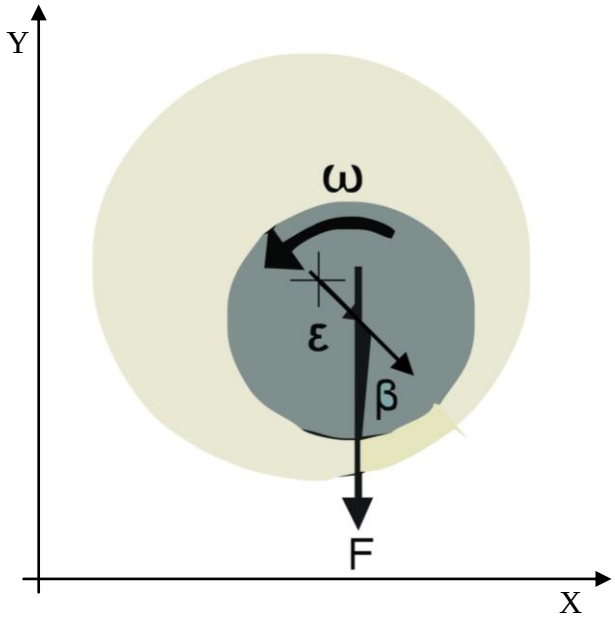

Figure 5.1: Bearing schematic: Mobility approach

The variation between the velocity and the Force can be shown to be linear and te dependence of the vectors on the eccentricity and β can be expressed in the form of a Mobility vector M, which is defined below.

$$de/dt = |F|(C/R^2)/(WD/\mu/C).M(e,\beta) + \omega xe$$

Where,
ω = angular velocity
e = eccentricity
$|F|$ = Force vector, acting from Journal centre to bearing housing surface.
C = bearing radial clearance
R = Bearing radius
W = Bearing width
M = Mobility vector
μ = oil viscosity
β = angle between eccentricity normal and velocity vector

Also, the pressure from the Reynold's equation is related to the average load by a dimensionless pressure factor P, which can be expressed as the dot product of the load vector and the Pressure.

$$P_{\max} = |F|/(WD).P((e,\beta))$$

The volume flow rate of the oil can also be related to the Mobility vector as shown below.

$$Q = 4M(e,\beta).(W/D).(C^3|F|/(WD))/\mu$$

Using these vector equations, maps of the M and the P vectors with respect to the eccentricity and the β can be created once the input data is available.
Therefore the force vector can be expressed as two dimensionless Forces acting along the eccentricity normal and the Force acting perpendicular to the eccentricity normal, along with a dimensionless torque.

$$F_1'(e,\beta) = along, e$$
$$F_2'(e,\beta) = perpendicualr, e$$
$$T'(e,\beta) = Torque$$

And the then the generated maps can be used for fits of the load F, torque T from solving the simple Reynold's equation for all the points of the journal using the e,β. [9].

Now the equations for the actual calculated forces and the Torques can be expressed as

$$F_1 = \mu VRF_1'(e,\beta)$$
$$F_2 = \mu VRF_2'(e,\beta) + ER^2\mu F_c$$
$$T = \mu VRT'(e,\beta) + ER^2F_c + T_{sq} + T_{shear}$$

Where,
T = Effective Torque
F_1 = Force acting along the eccentricity normal
F_2 = Force acting perpendicular to eccentricity normal
F_c = Asperity contact Force
T_{sq} = Squeeze Torque
T_{shear} = Shear Torque

With the appropriate input data, the fits for the hydrodynamic lubrication can be generated. These maps and fits are only valid when the eccentricity *e* remains with 99% of the maximum eccentricity of the journal bearing assembly. Beyond which the surface roughness effects causes a certain part of the load to be 'carried' by asperity contact. The load distribution between the hydrodynamic oil film support and the asperity contact is modelled according to the Greenwood Tripp model, which is described in [6].

From this model, the load vector can be expressed as a vectoral sum of the hydrodynamic and the asperity contact load at these points.

$$F = F_h + F_c$$

These non-linear fits of the Force vector and the maximum pressure can be handled by the method proposed by Goenka in [10].

The Torque from the squeeze and the shear effects are detailed below. With these calculated Forces and torques for every timestep through the engine cycle, the further calculation of the Friction Torque and power loss can be carried out.
In order to use the Forces calculated in terms of the parent coordinate system of the Crankshaft, the forces F_1 and F_2 can be expressed in terms of the Cartesian coordinate axes F_x and F_y as shown below, where α = angle at a particular timestep with respect to coordinate axis.

$$F_x = F_1 \cos\alpha - F_2 \sin\alpha VRF_1'(e,\beta)$$
$$F_y = F_1 \sin\alpha + F_2 \cos\alpha$$

5.1.3 Friction Torque and Power Loss Calculations

There are three components that contribute to the total friction power loss in the Journal bearings: Shear, Squeeze and Contact.

The shear part of the power loss arises from the power required to shear the oil due to the relative rotation of the journal with respect to the earing housing. The shear torque can be calculated using the equation shown below. The negative sign at the shear torque indicates that the torque always acts in the direction opposite to the direction of the journal motion. The shear power loss is the simple product of the shear torque and the operating speed.

$$T_{shear} = \frac{2\pi R3W\mu\omega}{(c^2 - e^2)^{1/2}}$$

Due to the 100% squeeze film modelling of the oil film in the bearing, the squeeze torque is expressed as

$$T_{squeeze} = \frac{e*F}{2} = \frac{(e_x F_y - e_y F_x)}{2}$$

e_x = eccentricity in x-direction
e_y = eccentricity in y-direction

But the squeeze power is not the same as the Shear power and cannot be calculated by simply multiplying the Torque with the operating speed. The squeeze power is divided into two elements. The first part is the direct power from the squeeze torque generated from the translational motion of the journal within the bearing housing, and this is given by

$$P_{squeeze} = -2T_{squeeze}\omega$$

The negative sign for the torque indicates that the torque acts against the journal and not on the oil. The other part of the power is due to the force generated by the journal moving with a certain velocity. The pure mass of the journal presents the power loss, and this does not exhibit any torque. Also, this squeeze power may behave like a

viscoelastic damper for the oil film thereby allowing the journal to use the kinetic energy of the fluid.

$$P_{squeeze2} = \frac{de}{dt} F = \frac{de_x}{dt} F_x + \frac{de_y}{dt} F_y$$

The total squeeze power is defined as

$$P_{tot.sqeeze} = P_{squeeze} + P_{squeeze2}$$

The contact term is active only when the metal-to-metal contact is predicted. The torque due to the contact can be represented as

$$T_{contact} = -C_f F_c R$$

The contact forces and the effective coefficient of friction are predicted from the Greenwood Tripp asperity contact model [6], which is also presented in the section.

5.1.4 Other sub model calculations in the Journal Bearing model

The other constituent calculations which provide an increased accuracy to the results from the Journal Bearing calculations are,

Oil Film supply calculations: The oil supply in the journal bearing is calculated using the modified Martin-Xu equation. By splitting the oil supply into the hydrodynamic oil pressure generation and the Oil supply pressure effect, the Oil supply is evaluated in each journal bearing separately.

Oil Thermal Balance: The thermal balance of the oil film is an important parameter, since this influences the steady state temperature of the oil every timestep and can influence the viscosity of the oil.
The thermal balance calculations are divided into

- Power generated from shearing the oil.
- Fraction of power lost to the surrounding surface.
- Power transferred as enthalpy.
- Heat transferred to bearing housing structure.
- Power transferred to the thermal inertia of the oil film and the bearing.

Effects of pressurized grooves and holes: The grooves and holes which might have an influence on the bearing operation and contribute to a hydrostatic pressure are solved by splitting the bearing solution at the region of the groove into two bearing solutions and thereby solving the load bearing of the oil film between the individual bearing housing and the journal surfaces only. Holes having an effect on the hydrodynamic pressure of the oil film are modelled in a way so as to provide a pressure loss to the flow component of the oil directly above the hole at every timestep.

5.2 Piston Rings

The piston rings are the most complicated sub model with respect to the friction modelling. The piston ring model requires an advanced multi body dynamic simulation of several interdependent bodies. Resolution of gas dynamics to evaluate effects of the gas pressures on the ring friction, and a full-fledged model of the hydrodynamics of the oil film between the rings and the liner. Therefore a physical model based on first principles is implied.
The level of fidelity of the models has been optimized to maintain the results to be close to the results from the first principle models while accounting for various speeds, loads, surface roughness, material properties and design configurations without any major tuning or calibration required [10],[11]. The simplifications on the 1-dimensional models are,

- 3-D motions of the rings are not accounted. i.e the motions of the ring around the groove as the piston runs through the cycles are not modelled.
- Ring-groove dynamics are not modelled as part of the Friction model. i.e The axial dynamics of the ring within its groove due to the ring inertia and the piston acceleration are not modelled. The rings are assumed to be seated on the bottom of the groove. Although, a separate model for the ringpack blow-by calculation is present, in which the axial dynamics of the rings are considered. The twisting of the ring due to the interaction with the liner surface is modelled for all the rings. The complete axial dynamics models for the piston rings will be included in upcoming future models.
- 3-D elastic deformations and twisting of the rings is not modelled. The rings are considered to be axisymmetric with respect to the friction losses and gas forces.
- The discretization of the rings is considered based upon the accuracy of the surface measurement and the profile data of the ring.

In order to predict the ring friction to a sufficient fidelity, the following elements of the calculation are mathematically modelled as part of the piston Rings sub model. [10], [11]

- The radial force equations and the moment of the ring twist is calculated for each timestep, based on the piston motion, and tilt, the instantaneous oil film thickness characteristic and the ring profile and roughness inputs.
- The 1-dimensional Reynolds equations, which govern the hydrodynamics of the oil film is solved to obtain the distribution of the oil film pressure through the face of the ring. By integrating the oil film pressure over the ring face oil film pressure distribution, force and moment on the ring cross-section due to the oil film pressure
- The Greenwood-Tripp model for asperity contact is solved with the same resolution as the Reynold's Equation. By integrating the asperity contact pressures derived from the Greenwood Tripp model, the contact forces and the power losses are determined [6].
- The effect of surface roughness on the oil film hydrodynamics calculated by using the Patir-Cheng pressure and shear flow factors in the Reynolds equation [7].

- A very minor, fast-running, simplified bore conformability analysis is available to estimate the fraction of bore circumference which contacts the ring load and this is used as an "attenuation" factor for the cylinder load reactions in the force and the moment balance equations.

The calculations for the steps described above are presented in a concise form below.

5.2.1 Ring Radial Force Balance

The Forces on the Ring are solved by using the known characteristic properties of the instantaneous oil film. The circumferential motion of the film is omitted in the model; hence those effects on the film are also not included. The Radial Force balance can be expressed as

$$\frac{d^2 M_r}{dr^2} = F_p + F_t - F_{oil}\left(\frac{dh}{dt}\right) - F_{asp} = 0$$

F_p = Ring gas pressure Force (From gas pressure trace)
F_t = Ring Tangential force (From kinematics and Initial Ring Tension)
F_{oil} = Oil film pressure (From Reynold's equation)
F_{asp} = Asperity contact pressure force (from Greenwood Tripp model)

5.2.2 Twist Motion solution for the Piston Rings

During operation, the rings undergo a twist due to the interaction with the liner and also due to the influence of the gas pressures. This motion causes a change in the effective face profile of the ring and also results in a change in the operating characteristics of the rings.
The twist is solved by calculating the effective moment balance on the ring cross section. [11].

$$I_{ring}\frac{d^2\theta}{dt^2} = F_g\,(R_g - R_r) + F_p\,(R_g - R_r) + F_{cf}\,(R_c - R_r) + M_{cn} - K_T\theta = 0$$

$F_g\,(R_g - R_r)$ = Moment due to groove load

$F_p\,(R_g - R_r)$ = Moment due to bottom pressure

$F_{cf}\,(R_c - R_r)$ = Moment due to Cylinder Friction

M_{cn} = Moment due to Cylinder Normal Load

$K_T\theta$ = Internal Ring stiffness

5.2.3 Hydrodynamic Load solution using Patir and Cheng flow factors

Similar to the journal bearing characteristics, the film are modelled along with the additional influence of the Patir and Cheng Roughness pressure and shear flow factors.

$$\frac{d}{dx}\left(\lambda_p h^3 \frac{dP}{dx}\right) = 6U\mu\left(\frac{dh}{dx} + \sigma\frac{d\lambda_s}{dx}\right) + 12\mu\frac{dh}{dt}$$

Where:
x = Direction of Ring motion
h = Instantaneous local film thickness
P_0 = Oil film pressure
U = Piston Speed
σ = Composite Roughness mean asperity height
μ = Oil viscosity
T_{oil} = Average oil film temperature
$\lambda_p(h_T/\sigma,\gamma)$ =Patir-Cheng pressure flow factor
$\lambda_s(h_T/\sigma,\gamma)$ =Patir-Cheng shear flow factor

5.2.4 Patir and Cheng Flow Factors

The Reynold's Equation assumes that surfaces are perfectly smooth. The actual Piston liner surfaces consist of a varying degree of asperities and this causes a variation in the calculations of the Fluid pressures. But, measurement of these fluid pressures is not practical, hence a method of Flow factors developed by Patir and Cheng [7] is used. The factors λ_x and λ_y modify the shear stress formation in the film, and these are dependent on the roughness of the surface and the film thickness. This formulates a simple way to solve many different kind of surfaces. The only disadvantage is that the Patir and Cheng model is valid only for Gaussian Surfaces and is not valid for Non-Gaussian surfaces with high skew or kurtosis.

5.2.5 Asperity Contact Model: Greenwood Tripp

The asperity contact between the rings and the liner, also the skirt and the liner, is solved using the Greenwood and Tripp models. Due the nature of the inputs to the Greenwood Tripp model, which are impossible to measure, a mathematical simplification of the surface measurements is required in order to use the Greenwood Tripp model in order to solve the contact asperity pressures [6].

The simplification used in this Thesis project is the McCool modification to the Greenwood Tripp model [20][21], which allows the model to estimate the composite sigma, beta and eta values for the Greenwood Tripp equation shown below from a measurement of the rough surfaces of the liner, the rings and the skirt, made by using a topography measurement tool. A sample measured surface for the Volvo MD13 engine along with the simplification obtained by the McCool model are presented in Appendix B.

From the results for the surface characteristics obtained from the McCool simplification, the values of sigma, eta and beta are used as inputs in the Greenwood Tripp model. The final equations of the model, which present the asperity contact pressure and the equivalent asperity contact force is given as,

$$Pasp = \left(\frac{16\sqrt{2}}{15}\right)\pi(\sigma\beta\eta)^2 E\sqrt{\frac{\sigma}{\beta}}F\left(\frac{h}{\sigma}\right)$$

$$Fasp = \left(\frac{2}{\sqrt{\pi}}\right)\int_x^\infty (s-x)^{5/2} e^{\left(\frac{-s^2}{2}\right)ds}$$

h = local film thickness
σ = Composite roughness (mean asperity height standard deviation) = $(\sigma_1^2 + \sigma_2^2)^{½}$
β = Composite mean radius of curvature of asperity tops
η = Composite asperity density
E = Composite Young's modulus of elasticity of surfaces
v = Poisson ratio

5.2.6 Ring Tension Force Calculation

The tension force for the rings is calculated as

$$T = T_o + K_T(R_o + \Delta R_{tex} - R_b - \Delta R_{bd} + h_o t$$

T = Instantaneous Ring Tension force
T_o = Prescribed Ring Tension
K_T = Ring Stiffness
R_o = Ring Radius
R_{tex} = Change in Radius due to thermal expansion
R_b = Bore Radius
R_{bd} = Change in bore radius due to bore distortion,
$h_o t$ = Instantaneous film thickness

The calculated ring tension can be reduced into ring tension Force which is plugged into the Radial Force balance shown in section 5.2.1.

5.2.7 Ring Bore Conformability calculation

A simple fast running bore conformability model is used in the model. Based on the work by Tomanik [19], the Bore conformability model calculates the non-conformance of all the rings with the prescribed bore data. The Bore Distortion data is presented in the form of Fourier Harmonics for the orders of distortion with the phase differences.
Based on this conformability check, the coefficient of the conformability for the part of the liner which 'carries' the load is predicted.
A result of non-conformance with the bore significantly increases the ring-bore friction force.

5.3 Piston Skirts

Similar to the piston rings, the piston skirt is also modelled using the physical models based on first principles, for the modelling of hydrodynamic oil film lubrication between the skirt surface and the liner, and also for the modelling of mixed and asperity contact conditions. The method of solution of the skirt friction characteristics are the same as that of the rings as explained in section 5.2.

The major addition to the skirt simulation is the simulation of the secondary motion of the piston. This is the 'piston slap' or the 'piston tilt' phenomenon caused due to the sudden pressure impounded upon the piston crown due to the combustion gases.

5.3.1 Piston Secondary Motion simulation

Consider a free body diagram of the skirt as shown in Figure 5.2, which represents the secondary motion of the piston.

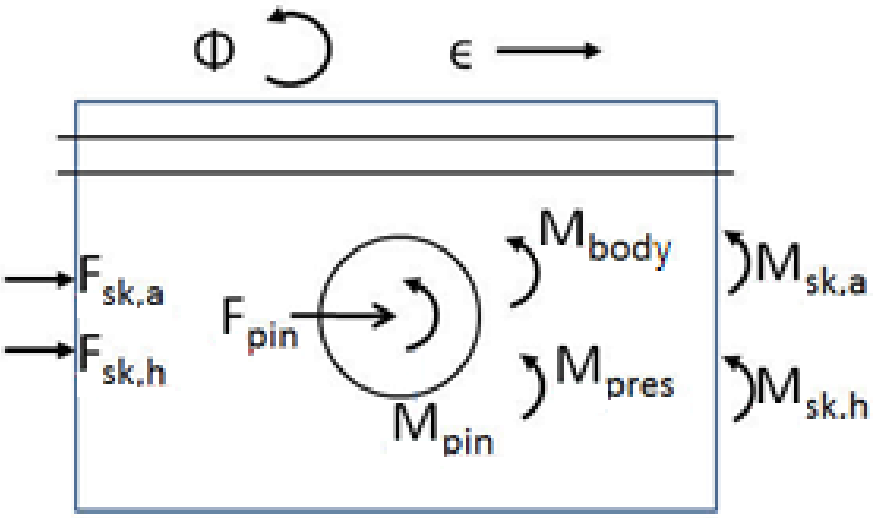

Figure 5.2: Skirt Free Body Diagram [10]

The lateral acceleration of the piston caused due to the gas pressure can be expressed using a force and moment equilibrium as

$$M_p\left(\frac{d^2\phi}{dt^2}\right) \approx 0 = F_{pin} + F_h + F_a$$

$$I_p\left(\frac{d^2\phi}{dt^2}\right) \approx 0 = M_{piston} + M_{pressure} + M_h + M_a$$

Where,

M_p= Piston mass
I_p= Piston Inertia
F_h, M_h= Hydrodynamic Force
F_a, M_a= Asperity Force and Moment

This equation is solved quasistatically, and the forces and moments are input to the Greenwood Tripp model and the Reynold's equation which is then solved using the secant method in order to generate the oil film pressure and the asperity contact pressure.

On translation, the pressures are converted into forces, and thereby the Friction Torque and the Friction power and also the FMEP can be expressed.

5.3.2 Hydrodynamic Reynold's Equation solution

The Reynold's Equation is solved using a quasi-static Finite Element or a Finite Difference based solver, over a grid as shown in the diagram below.

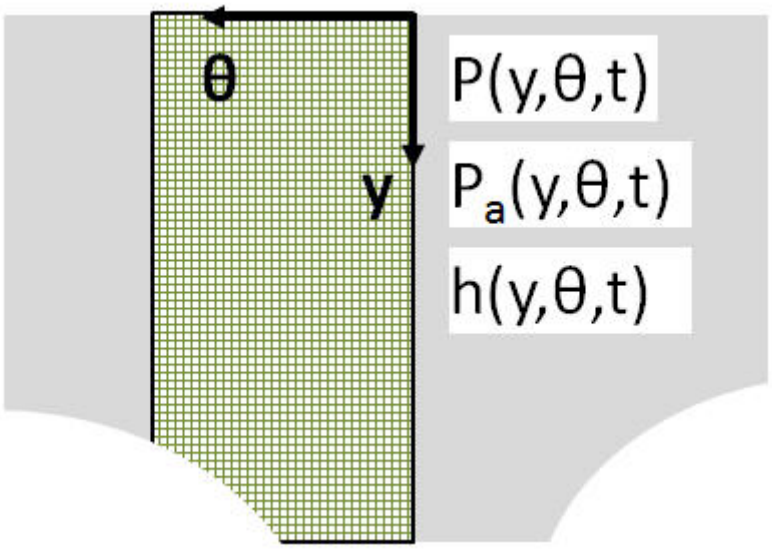

Figure 5.3: Piston Skirt Finite Element Grid [10]

$$\frac{d}{dx}\left(\lambda_p h^3 \frac{dP}{dx}\right) = 6U\mu\left(\frac{dh}{dx} + \sigma\frac{d\lambda_s}{dx}\right) + 12\mu\frac{dh}{dt}$$

Where:
x = Direction of Ring motion
h = Instantaneous local film thickness
P_0 = Oil film pressure
U = Piston Speed
σ = Composite Roughness mean asperity height
μ = Oil viscosity
T_{oil}= Average oil film temperature =
$\lambda_p(h_T/\sigma,\gamma)$ = Patir-Cheng pressure flow factor
$\lambda_s(h_T/\sigma,\gamma)$ = Patir-Cheng shear flow factor

The estimation of the Patir and Cheng flow factors is similar to the method shown in Section 5.2.4.

6 Friction Measurement and Test results

This section provides an overview of the common engine friction measurement tests performed, and also presents the results and recommendations from the two tests performed on the Volvo MD13 engine.

A few methods to determine the engine friction power loss in the form of FMEP are shown below. These methods require high technical expertise, expensive measuring equipment and most paramount, is the accuracy in the tests.

6.1 Willan's Line method

This is a simple method that is based on the extrapolation of the Fuel Consumption vs. BMEP curve for an engine.

In order to determine the FMEP for a certain operating speed, the engine is operated at the particular rpm at different load conditions. The BMEP is calculates and plotted. The line is then extrapolated towards the origin, as shown in the Figure 6.1. The intersection with the x-axis yields the net fuel consumption of the engine that is lost as friction power.

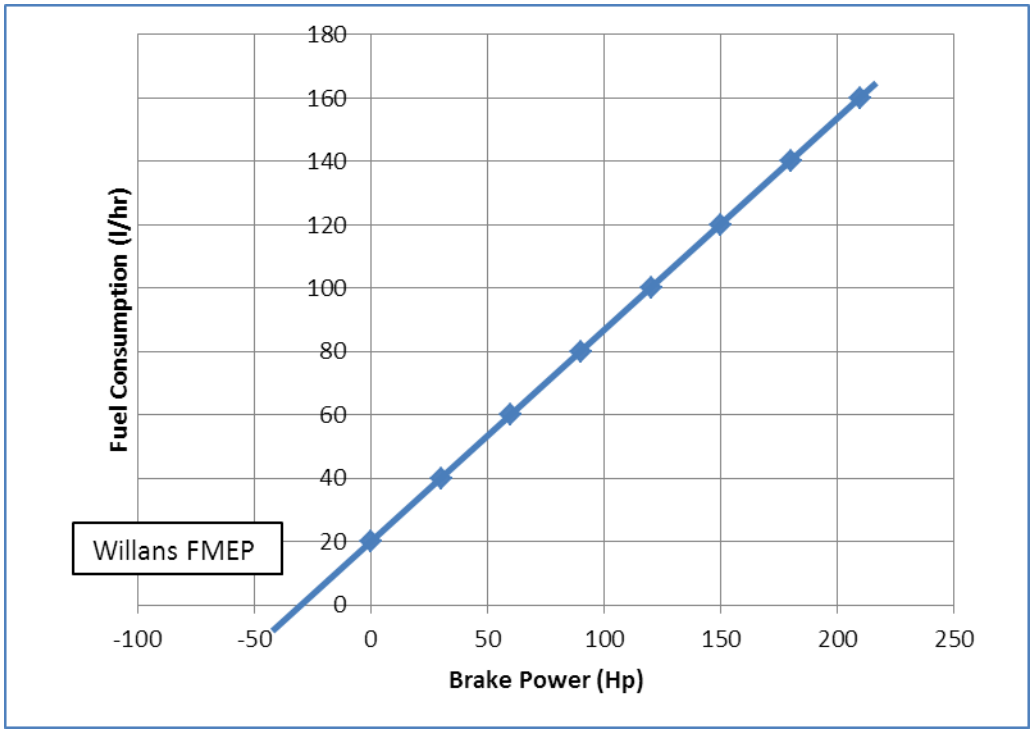

Figure 6.1: Willan's Line

This graphical method of estimating the FMEP is a primitive method that only provides the friction power loss of the complete engine at a single operating speed.

6.2 Floating Liner Test Rig

In a floating liner test rig, the friction forces from the Piston Cylinder Unit can be measures directly by using sensitive equipment in order to measure the loads on the liner from the ringpack and the skirt. By using highly sensitive instrumentation, only single cylinder floating liner rigs are reasonable to build and operate. Along with the load-pickup piezoresistive sensors, additional sensors such as thermocouples etc. may be used in order to obtain thermal loading and oil temperature measurements from these tests.

The glaring issue regarding the floating liner tests is the maximum achievable engine speeds and loads, which are limited by the equipment and the cost of instrumentation and operation of a rig. Another problem is the presence of certain cylinder distortion effects which arise due to the floating liner and influence the performance and conformability of the rings to the liner, but which are absent in actual engine operation.

6.3 Fired engine tests

Fired engine tests provide some knowledge regarding the friction performance. Often certain conditions such as the top ring loading, or true bearing performance and piston slap losses from the skirts are observable only under firing engine tests. Although, it is impossible to make any useful measurements from a firing test on a multi cylinder engine, the inputs and the tuning provided by these tests for simulation model calibration and for the calibration of the test equipment for motored engine testing is commendable.

Certain test methods such as cylinder deactivation or coast down tests may be used as part of the fired engine test cycle to provide an overview of the complete engine firing FMEP values.

6.4 Motored engine tests

In a motored engine test, the engine is driven using an electric machine and the ignition and the fuel supply are disconnected. The temperature of the engine, in terms of the coolant and the lubricating oil are maintained at similar operating temperatures as the running engine in order to produce comparable operating conditions. The FMEP losses of the engine and the individual component losses can then be calculated based on a difference of the power required to operate the engine

Strip Tests – The Strip Tests are a type of motored test, wherein the individual engine components are disassembled or stripped step by step. Initially the complete engine is motored at different rpm values and the power losses are calculated. Then on, components are stripped one after another. Turbochargers, valvetrain, Cylinder head, manifolds, Piston assembly, gear drives etc. are removed individually and the continuous measurements at the same operating points are made. Using the differences in measurements between the tests, a conclusion on the friction power consumption of the particular component can be determined.

Special modifications to the rig are made to include mass and inertial effects of the removed components so as to allow the remaining components on the engine to operate normally. For example, in the test for the removed valvetrain mechanism and removed head test, the head of the cylinder is replaced by a plate of steel with circular pockets above the cylinders. This plate is mounted on the cylinder block in order to duplicate bolt loads from the Head bolts on to the liners of the engine, so that they operate in a similar condition. Or, the removal of the connecting rods and the piston assembly requires the addition of another rotating mass on to the crank pins of the crankshafts in order to allow an even and balanced rotation of the Crankshaft, in the bearing friction measurement tests.

6.5 Volvo Engine Strip Down Tests

The Volvo MD13 DST Euro 4 engines have been subjected to a complete engine strip test by FEV in 2005. Further tests on the MD13 Euro 5 engine were conducted internally by Volvo in 2009. A detailed description of the engine and the test methods are presented in this section.

The testes made by FEV in 2005, involved the measurement of fired and motored friction of the engine at various load and rpm points, as well as a standard strip test. Two test benches were used, one with an eddy current brake for the fired engine tests, and another with an electrical dynamometer.

In all the tests the engine was operated directly by the brake or the dyno, without a gearbox. The oil and the coolant used were conditioned to a fixed temperature of 90 deg. C through the galleries. This is done by maintaining a closed loop sump oil temperature sensor and an oil cooler unit, although, it is unrealistic to maintain a temperature of 90 deg. in the oil and coolant galleries during firing.

6.5.1 Fired Tests

The fired tests were conducted to analyse variations in load and speed over the complete engine.

The Fired tests are conducted on an FEV equipped test bench, through a complete RPM sweep from 800-2000. Load conditions ranging from 25% to Full Load were tested as well. The friction prediction is carried out on the fired engine by claulcating a difference between the IMEP of the engine and the Shaft power produced from the dynamometer. The accuracy of the friction prediction for the fired condition cases is +/- 0.1 bar.

6.5.2 Motored tests

The motored engine tests were conducted using an FEV equipped engine test cell and an electric dynamometer. For the engine, the tests were conducted between 600-2400 RPM at points of 200 rpm. Variations in the oil/coolant temperature was tested between 35/35 deg. C, 90/90 deg. C, 90/110 deg. C, 135/135 deg. C.

Two different oil combinations were tested. The Volvo standard Mobil DELVAC MX 15W40 and the Total D4243/60 10W30 oil were used on the Strip Tests.

The tests which will be investigated as a part of this thesis study are

- Full Engine (Stripped) without generator
- Cranktrain (Open Cylinder) - Valvetrain removed
- Crankshaft only (with Master weights)
- Crankshaft (without Master weights)

The data of the Engine which was tested by the Strip tests is presented below.

Table 3: Engine Data

Specification	**Description**
Engine	Volvo MD13 – Euro 4
Number of Cylinders	6
Displacement	12.77 l
Rated power	530 HP @ 1800RPM
Rated Torque	2550 Nm @ 1300 RPM
Specific Power	25.4 kW/l
Aftertreatment	DOC + DPF + SCR, EGR
Turbocharger	Garrett VGT
Bore	131 mm
Stroke	158 mm
Oil Pump	Gear Driven (Ratio 2,03)
Water Pump	Gear Driven (Ratio 1,47)
Valvetrain	Single Camshaft, Gear Drive, Unit injector drivers

6.5.3 Results and recommendations from the FEV Strip tests

- Under full load conditions the engine exhibits low friction in the low speed range and average friction in the high speed operating range.
- No influence of the FME due to the change in oil level is seen. Therefore, FMEP losses due to Crankshaft windage losses are not present. .
- Motored tests show a variation in friction levels between the two oils A major share of the Cranktrain friction is contributed by the Main and the Big End bearings at increased speeds. This is reasoned to be due t the balancing and design of the Crankshaft weights, and due to the super finishing of the bearings. The large main bearing diameter also contributes to the high friction.
- Significant improvement of the contribution from the bearings as the speed is increased.
- Crankshaft measured without master weights show a massive change in friction characteristics; this is either due to a weak crankshaft or due to improper balancing techniques. Optimization of Crankshaft design is imminent.
- Contributions from the oil control ring are steady with an increase in speed.

7 Results and Discussions

This section presents the results from the simulation models that have been developed as a part of this thesis project. The Results are divided into three sections – Model Validation, Detailed Analysis, and Friction Reduction Strategies.

As explained in the section above, physical models based on first principles are extremely sensitive to input data – geometries, surface roughness, material and lubricant properties and temperatures. The input data used on these models is monitored with precision and as per the desired degree of fidelity. Also, due to the large number of interlinked partial differential equations which are integrated in a quasi-static format, the choice of the ODE solver and the explicit time step conditions can cause a variation in results.

7.1 Model Validation

The models that have been developed using the Gamma Technologies GT Suite simulation platform have to be validated against actual test results in order to establish their fidelity. Hence, these models are compared to the results obtained from the Strip tests. The testing conditions and the part of the Cranktrain tested are mentioned with each graph.

All the results from the FEV Strip tests are normalized against an undisclosed FMEP value, in accordance with the Volvo Confidentiality Policy on the actual strip test results for the MD13 engine. The results from simulations are also expressed using the same fraction.

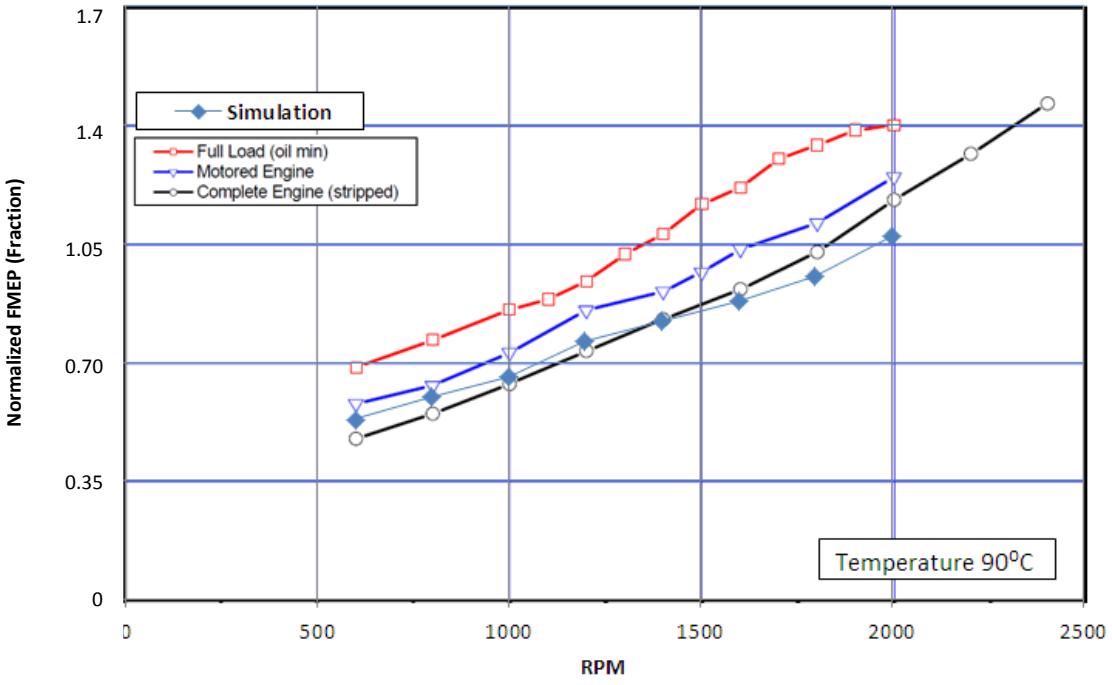

Figure 7.1 - Fired Engine Friction Tests vs. Simulation

Figure 7.1 shows the results between the Fired Engine, Motored Engine, and the Stripped Engine test from FEV compared to the simulation plot.

The variation in the FMEP between the simulation plot and the other graphs is due to the absence of the Valvetrain, Oil pump, Water pump, and the Turbo and Compressor assembly from the Simulation model. Unfortunately, Graphs indicating only Cranktrain Friction are not available for the Fired Engine, and therefore a reasonable comparison between the model results are the Cranktrain Friction cannot be obtained in the Firing tests. Therefore, motored engine tests are performed.

7.1.1 Motored Engine Comparison

In this test, the Cranktrain – Pistons, Connecting rods, Crankshaft, and Sealing Rings are motored at various speeds with an Open Cylinder setup. Two different oils are tested. The same conditions are also simulated using the model. (Test temperature 90 deg. C.)

The observed variation between the simulation results and the test results at higher RPM values is due to the inaccuracy of the Bearing model to effectively predict the Mass conservation of the oil film. As explained above, the Mobility model is limited to calculating the effects of the Journal motion only with respect to the states of the journal and does not consider the shear acceleration of the oil between the bearing and the journal which increases with higher speeds. This effect is vital in the Large End Bearing of the connecting rod, and the inability to model this phenomenon causes the simulation model to veer away from the test results at higher speeds.

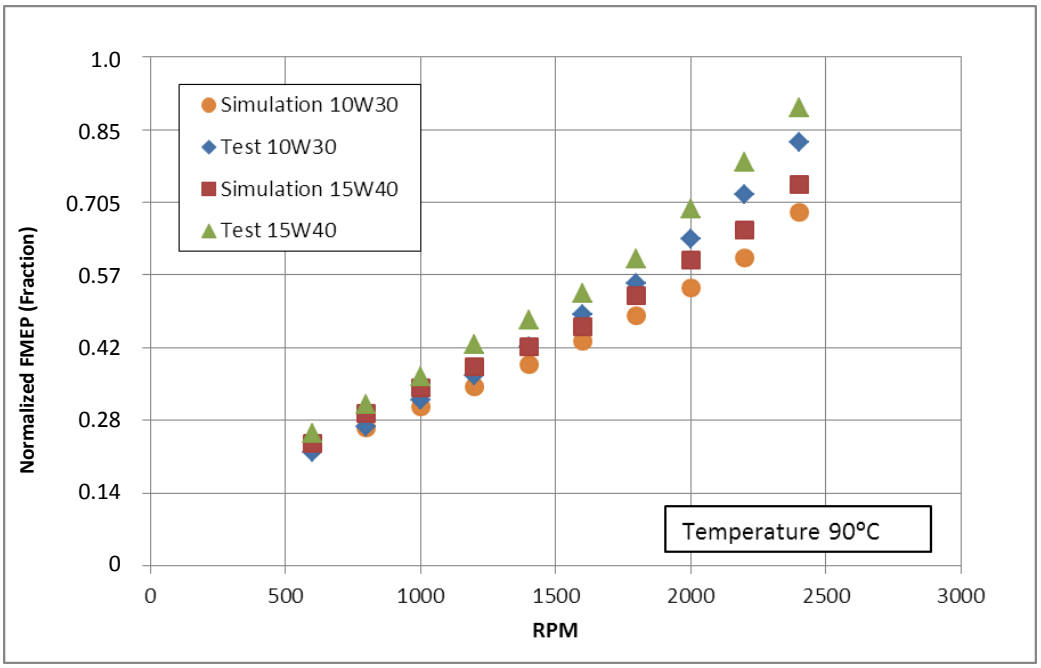

Figure 7.2: Comparison of Oil change between the FEV Strip tests and Simulation results

A further observation of the model, and perhaps a recalculation of the Mobility maps using tuning factors for the velocity "drift" and the displacement "drift" of the bearing

will provide the coincidence with the results for the higher speeds. This tuning has not been performed as part of the thesis study.

7.1.2 Crankshaft Comparison (With Master Weights)

The next step of the Strip Test validation involves the comparison between the Simulation model and the Engine Tests for Only the Crankshaft. This involves the removal of the PCU completely and is replaced with bobweigths which weigh the same as the Rotating mass of the PCU.

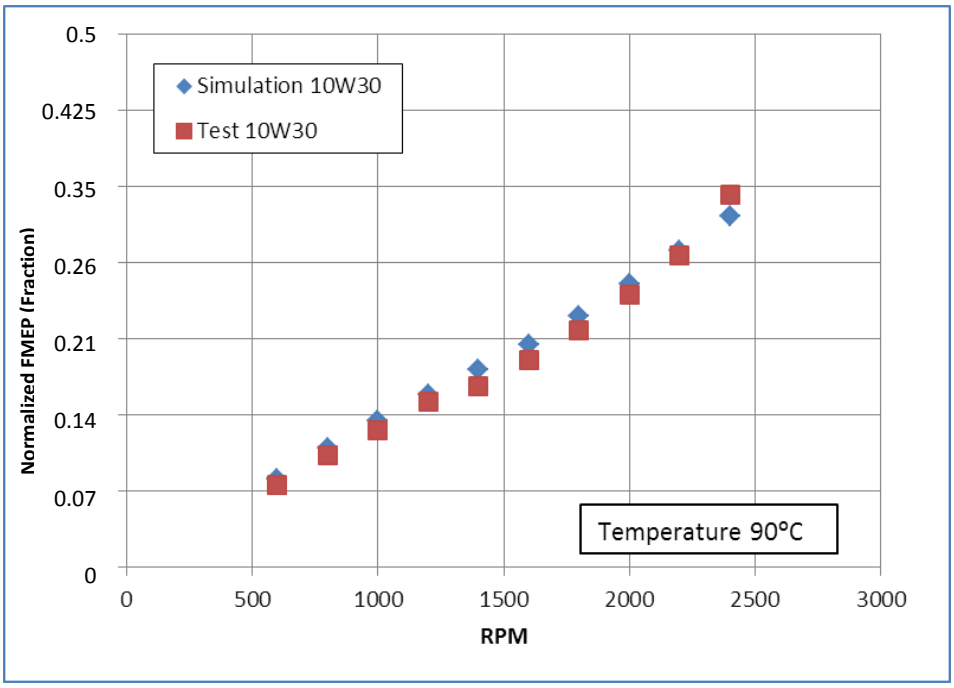

Figure 7.3: Crankshaft simulation vs. Strip Test – 10W30

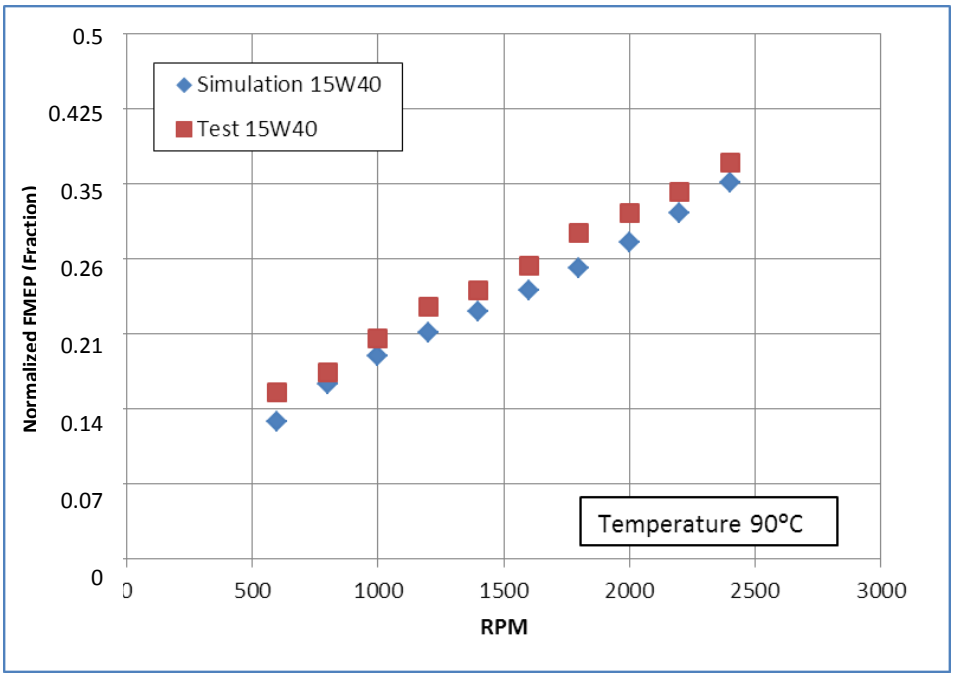

Figure 7.4: Crankshaft simulation vs.Strip Test – 15W40

The coincidence between the Simulation and the Test model for the Main Bearings is excellent in Motored condition. Due to the absence of any asperity contact on the Main bearings when motored, and the Journal orbits are within the hydrodynamic regime which is fairly straightforward to model using the Mobility approach.

7.1.3 Piston Cylinder Unit and Connecting Rod Bearings

These values for the Test friction in this case is calculated by using a difference in measurements from the Full Cranktrain tests and the Crankshaft (With Master weights) tests.

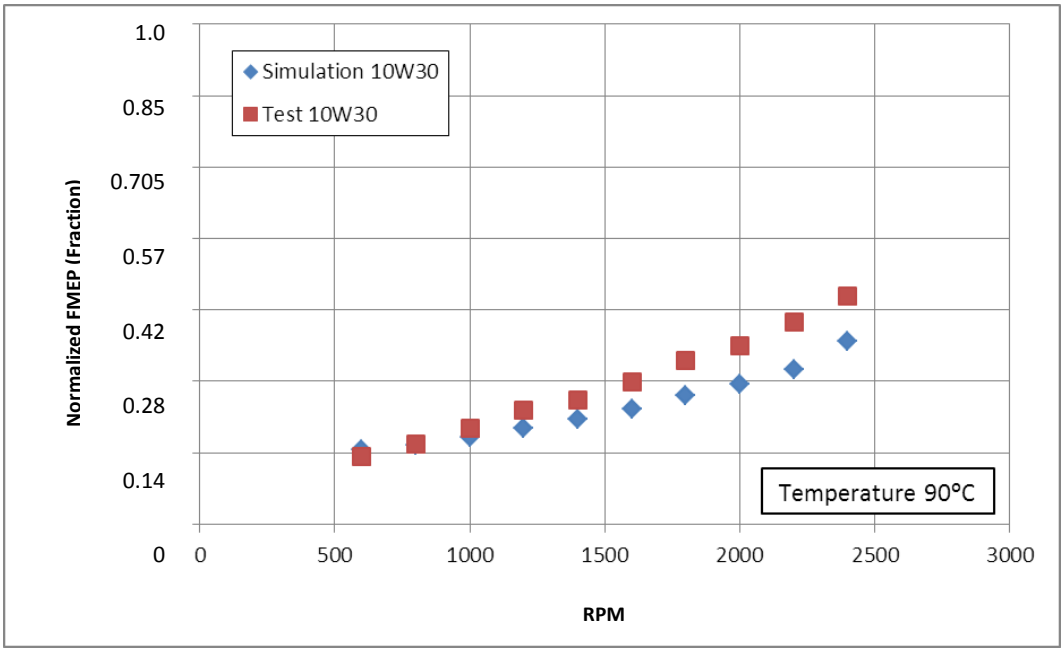

Figure 7.5: PCU simulation vs. Strip Tests 10W30

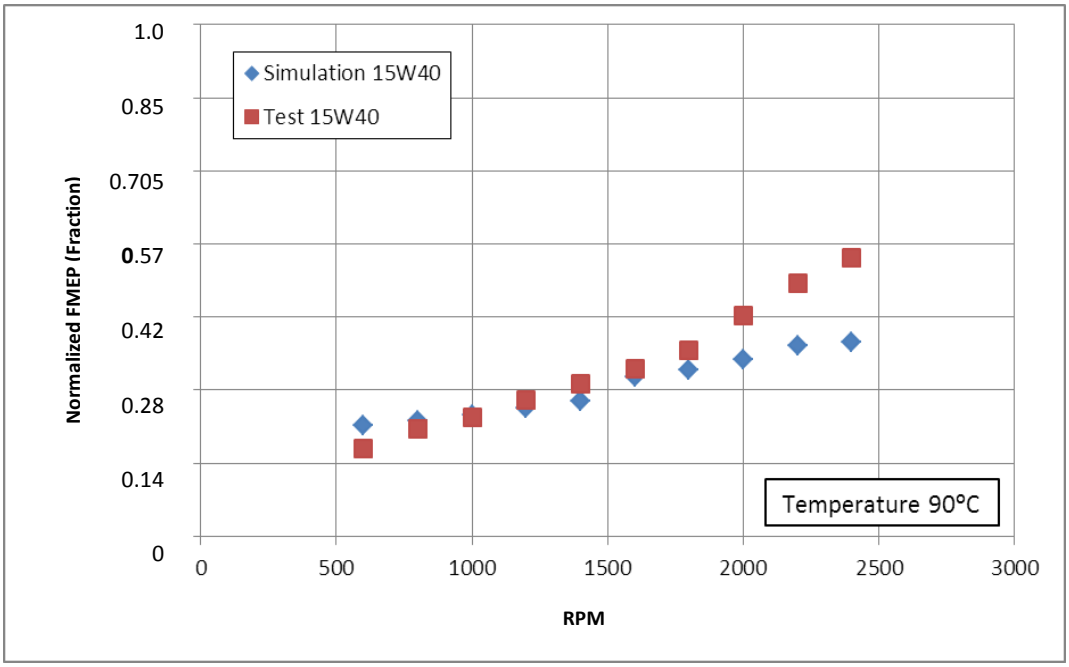

Figure 7.6: PCU Simulations vs. Strip Tests – 15W40

7.1.4 Temperature variation

The variation in temperature is also tested for the same conditions. The variations in the temperature plots between the simulation model and the test results are shown in this section.

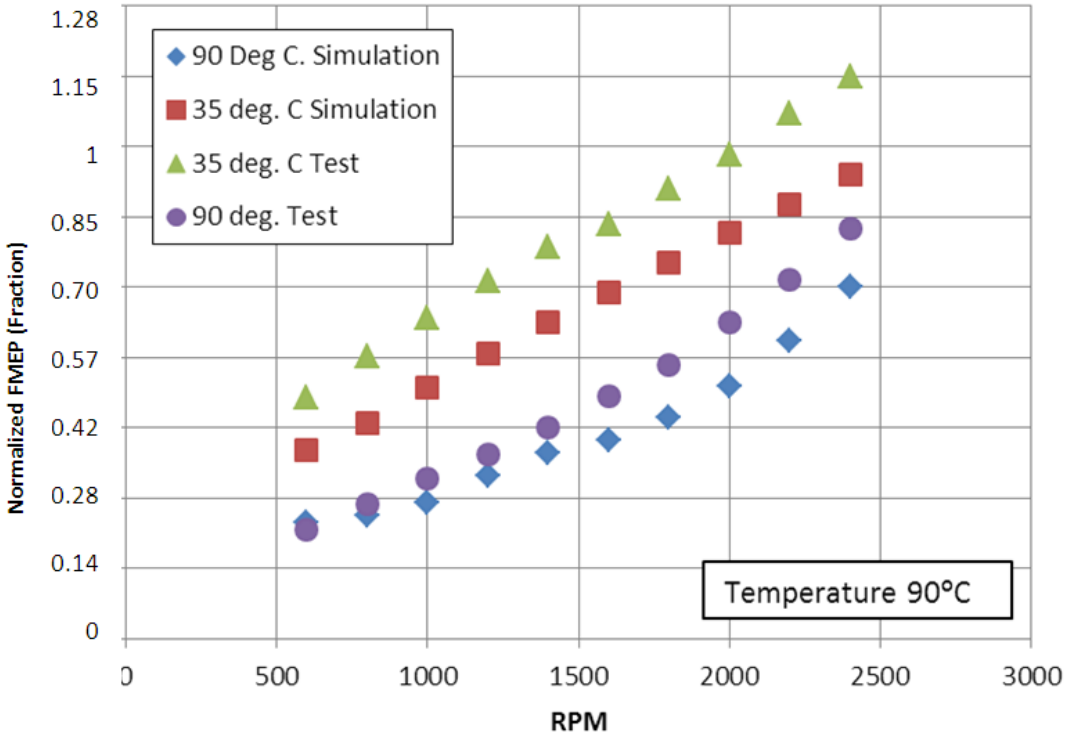

Figure 7.7: Temperature Variation – Simulation vs. Strip Tests – 10W30 and 15W40 oils

The variation in the results between the simulation model and the test results are greater in the case of the 15W40 oil. This is because of inaccurate input data for the shear thinning characteristics of the oil. Due to unavailability of evenly spaced temperature vs. viscosity plots for the high shear and the low shear conditions, the variation in the FMEP is realized with a change in the oil which is used in the simulation models.

7.1.5 Comparison with MIT lc2dm

The results for the friction performance of the ringpack are compared with the results from the MIT simulation tool, fore validation.

All input parameters between the MIT program and GT-Suite are maintained same, except some additional parameters such as groove dimensions, and roughness parameters which are required by the MIT tool.

From the results it is apparent to us that the MIT simulation program results in a superior estimation of the Friction power loss of the Ringpack, due to the contribution of the Ring axial dynamics calculations which are available on the MIT program. Additionally some friction contribution could also be accounted to the friction due to

the groove ring contact, although the effects of the groove-ring friction are dwarfed by the liner-ring contact friction.

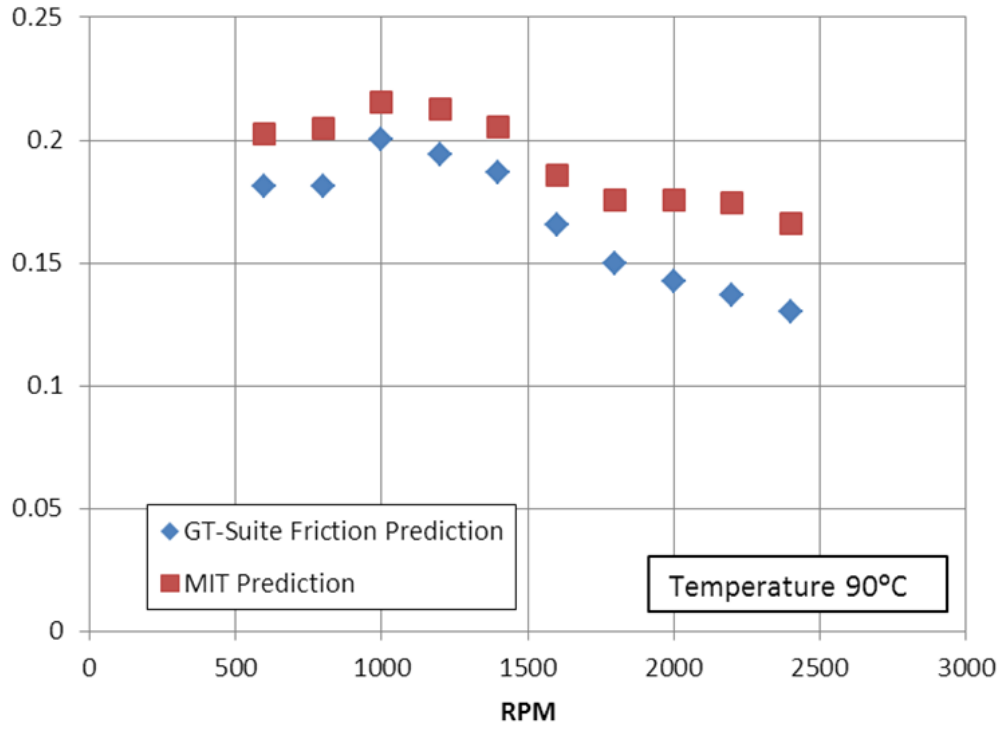

Figure 7.8: MIT simulation vs. GT-Suite comparison – RPM Sweep - Full Load

7.2 Detailed Analysis

This section provides an insight into the friction responses from various Cranktrain components at the level of fundamental physics.

A number of plots featuring characteristics of the friction performance of the various Cranktrain components are presented, several other result outputs such as Instantaneous power losses, Ring-cylinder Normal Loads, Normalized oil extent for bearings and squeeze film and shear force plots are available on GT-Suite, this section provides a short outlook of the ability of the simulation model to analyse friction performance in a detailed manner.

7.2.1 Piston Rings

The Volvo MD13 Engine features a three ring system for the Ringpack. A number of cyclic results varying in CAD and case averaged results are available from the GT-Suite simulations. The results from the individual ring simulations are discussed below.

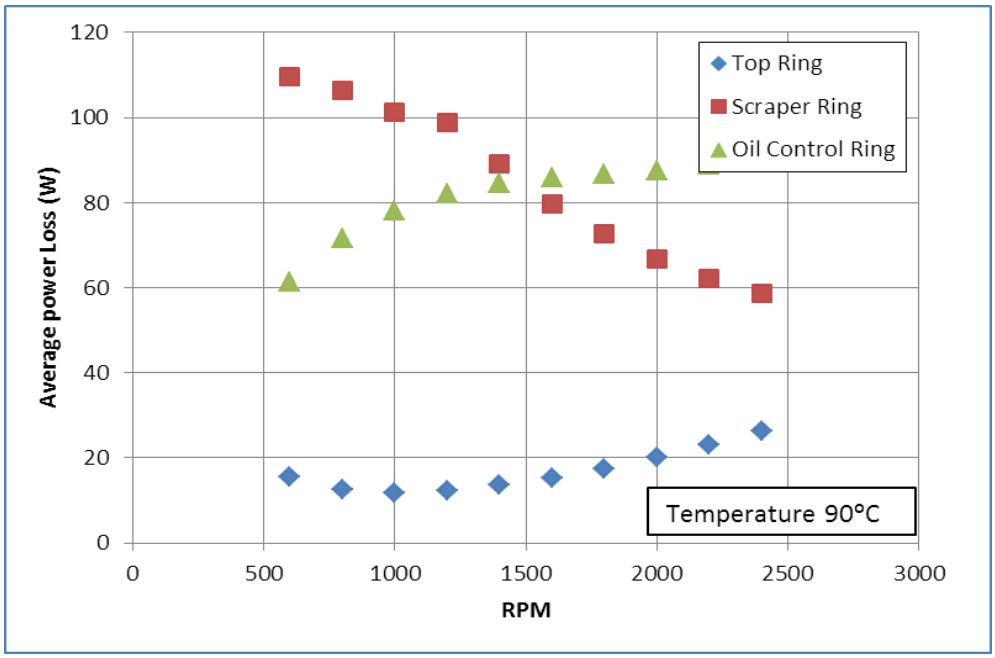

Figure 7.9: Comparison between Ring Power loss - Motored

The Graph above shows the comparison between the friction power losses of the three rings when motored. From this graph, it is observed that the Oil Control Ring contributes the most to the Friction at high speeds and the Scraper Ring contributes at low speeds. This transfer of power between the oil control ring and the scraper ring is due to the change in the starvation condition of the scraper ring as speed increases, and since the oil ring is modelled to be fully flooded at all instances, the Friction power increases steadily in the hydrodynamic regime.

7.2.1.1 Top Ring

The top ring, being a keystone ring with a prominent curved profile, contributes the least to friction when in motored condition. But it has an increased contribution to the friction power loss when in fired condition due to the influence of the combustion gas pressures.

As the engine speed increases, it can be seen from the Piston Rings Modelling theory section that the balance between the hydrodynamic and the asperity contact friction changes favouring the hydrodynamic mode of lubrication. This phenomenon can be observed from the following graphs of the top ring frictional power loss vs. increasing speed for the motored condition.

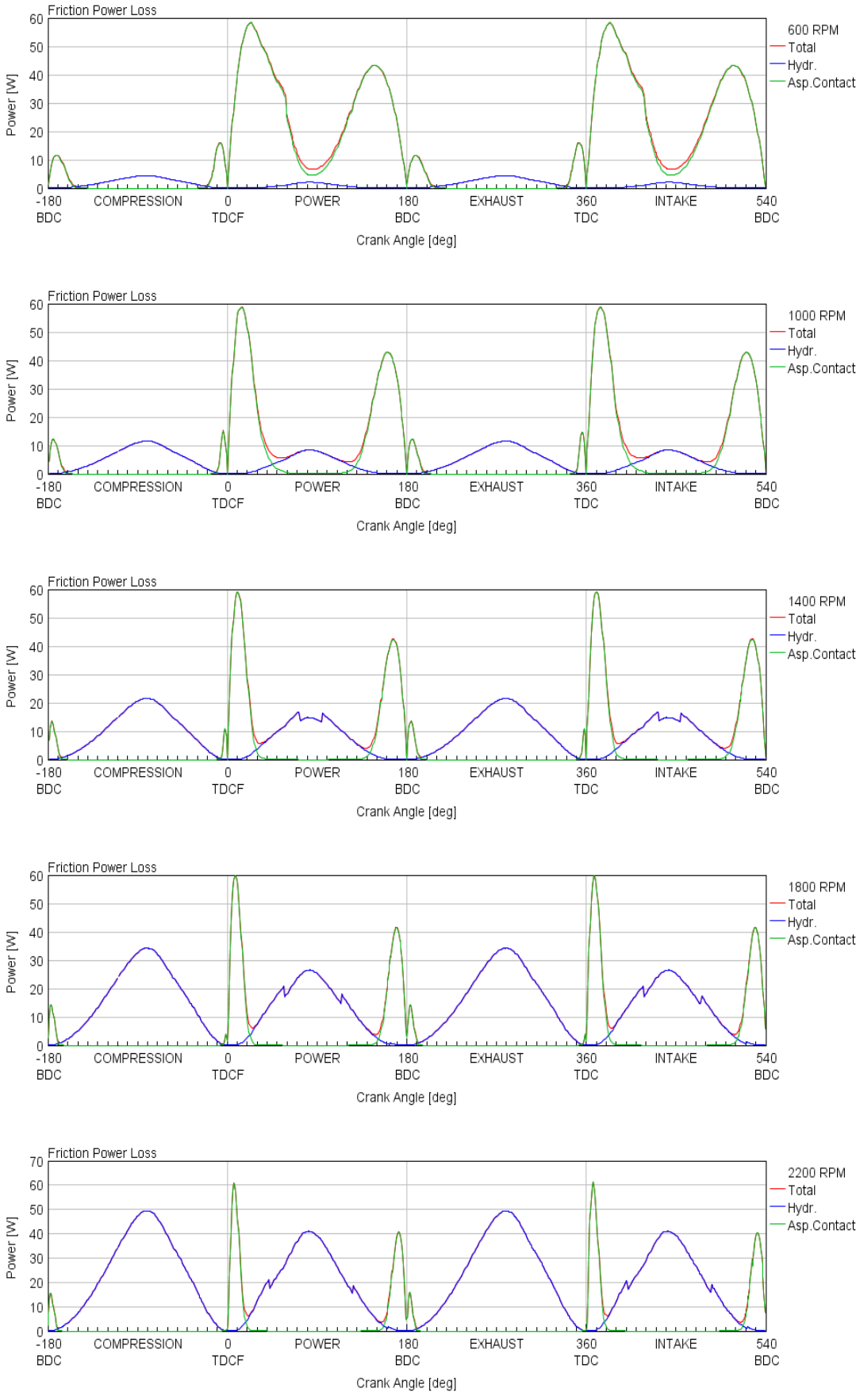

Figure 7.10: Top Ring Friction Power Loss – Motored – 600 – 2200 RPM

As seen from Figure 7.9, an increase in the speed of the ring changes the balance between the asperity friction and the hydrodynamic friction contribution to the overall power loss. This is very similar to the Stribeck phenomenon, wherein, an increased speed leads to an increased hydrodynamic friction power loss, as shown in section 3.2.1.

In the firing phase, the Top Ring contributes to the maximum asperity contact friction due to the high pressure from the combustion gases. Although the asperity contact pressure peak seems high, the overall contribution to the power is averaged through the complete cycle of hydrodynamic lubrication. The friction power loss of the top ring for the firing simulations at full load is shown below. The significant asperity friction spike does not influence the overall FMEP, but influences wear on the top ring, therefore the top rings are manufactured with specialized PVD coatings in order to withstand the high combustion pressures.

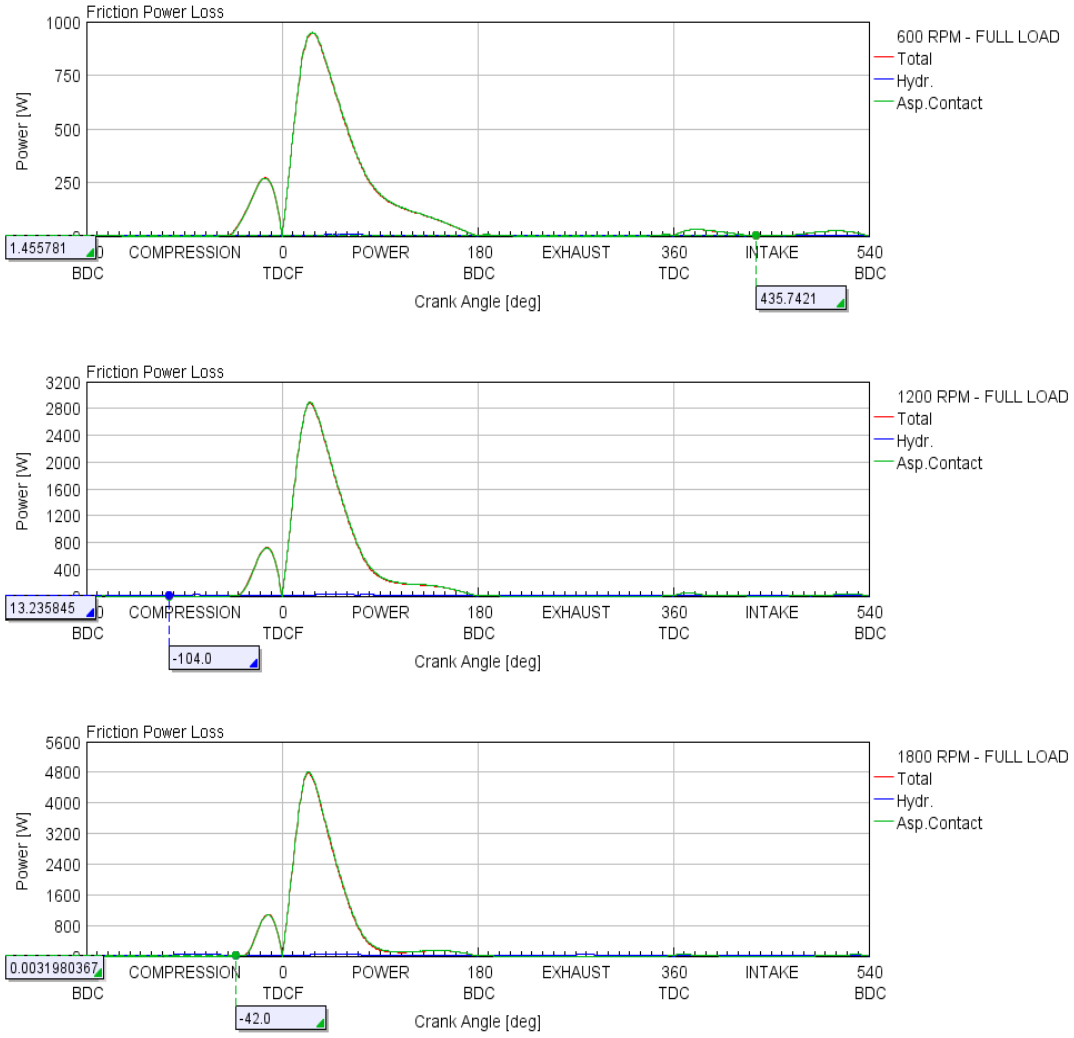

Figure 7.11: Top Ring Fired Friction Power Loss 600 – 1800 RPM

The pressure rise causes a major variation between the cylinder normal loads and the minimum oil film thicknesses on the top ring. These plots show the evident behaviour of the top ring as expected, nevertheless, some of the phenomena which are missing from the results.

- Effect of Bore conformability on the Cylinder Normal Loads
- Waviness effects due to Liner interactions. Not as significant as expected.
- Ring groove dynamics is missing in the model.

These are recommendations for the further improvement of the model for Future Work.

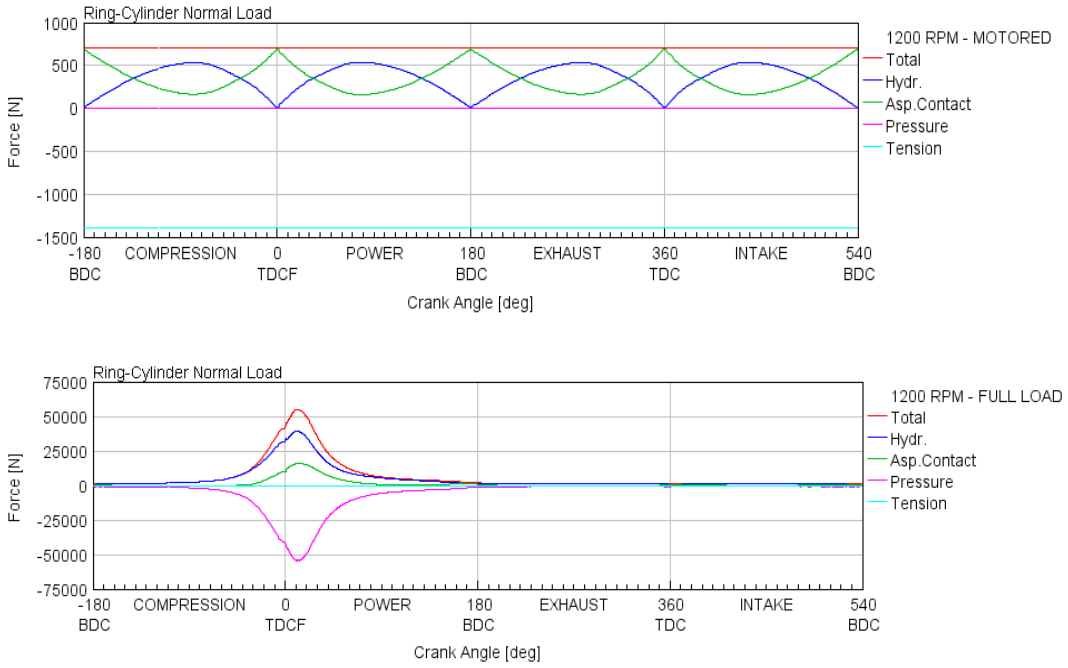

Figure 7.12: Top Ring Variation in Cylinder Normal Load 1200 RPM

The contribution of the TOP ring to the total friction power loss form the rings is seen from the variation in the magnitude of the Ring cylinder normal load between the fired and the motored test conditions. In fired conditions, the additional Gas pressures influence the asperity contact phenomenon of the top ring through the power stroke. This additional loss is seen as a spike in the instantaneous power loss plots of the top ring.

This approximation of the cylinder pressure acting directly on the top ring land and the back pressure of the groove is assumed to be the physical phenomenon that occurs during the combustion process. This is explained in the papers provided in the Reference section [8][10][11].

7.2.1.2 Scraper and Oil Control Ring

Similarly, observations on the blending between the asperity contact lubrication and the Hydrodynamic lubrication can be observed with an increasing speed on the scraper ring as well as the oil control ring.

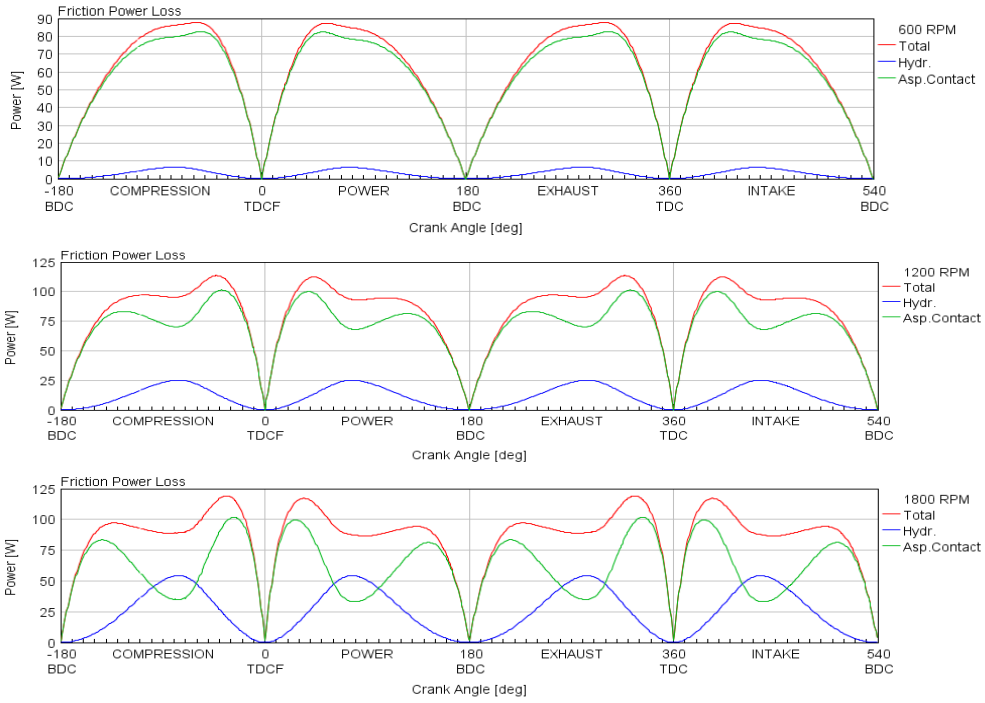

Figure 7.13 : Scraper Ring – Friction power Loss – Motored - 600 -1800 RPM

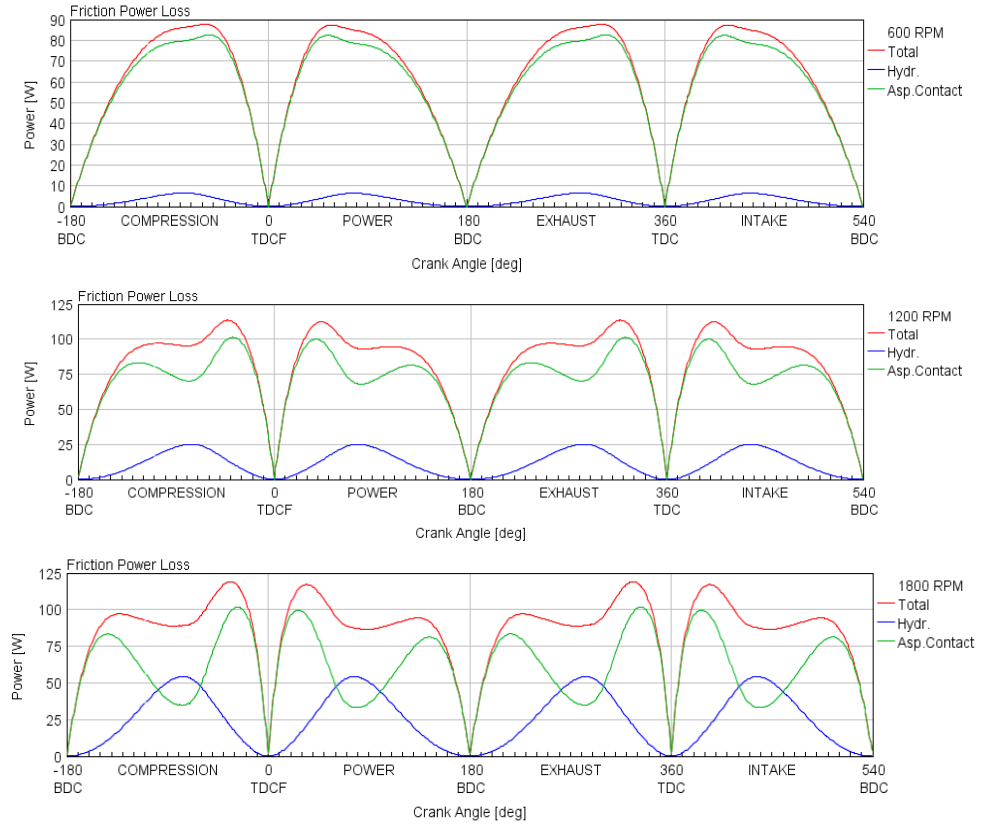

Figure 7.14: Oil Control Ring – Friction Power Loss – Motored – 600 – 1800 RPM

Similar to the Top Ring, as the RPM increases, the hydrodynamic friction increases, and the mixed friction blending between the boundary and hydrodynamic lubrication is clear.

Due to the absence of a blow-by model and a complete axial dynamics model [Refer Modelling Theory Chapter], it is not possible to draw comclusions on the ring dynamics of the oil control ring, which has been observed to be an important focus in friction simulations. This will be present in future versions of the models.

Therefore, this variation is observed on the behaviour of the Ringpack. It is not possible to conlcude on the selection of the Oil Flooding Factor for each of the rings, purely on the basis of assumptions, Floating Liner Rig tests caold provide a better solution to this issue.

7.2.2 Piston skirt

The Piston skirt model featured in the simulation is a full elasto-hydrodynamic lubrication model, capable of modelling the squeeze film between the Skirt and the liner. But, due to unavailability of skirt profile and skirt ovality information for the MD13 piston, the model is not completely accurate. Although the influence of the overall FMEP by the skirt is not significant at lower RPMs, it is observed that this could be a major concern at high rpms beyond 1800.

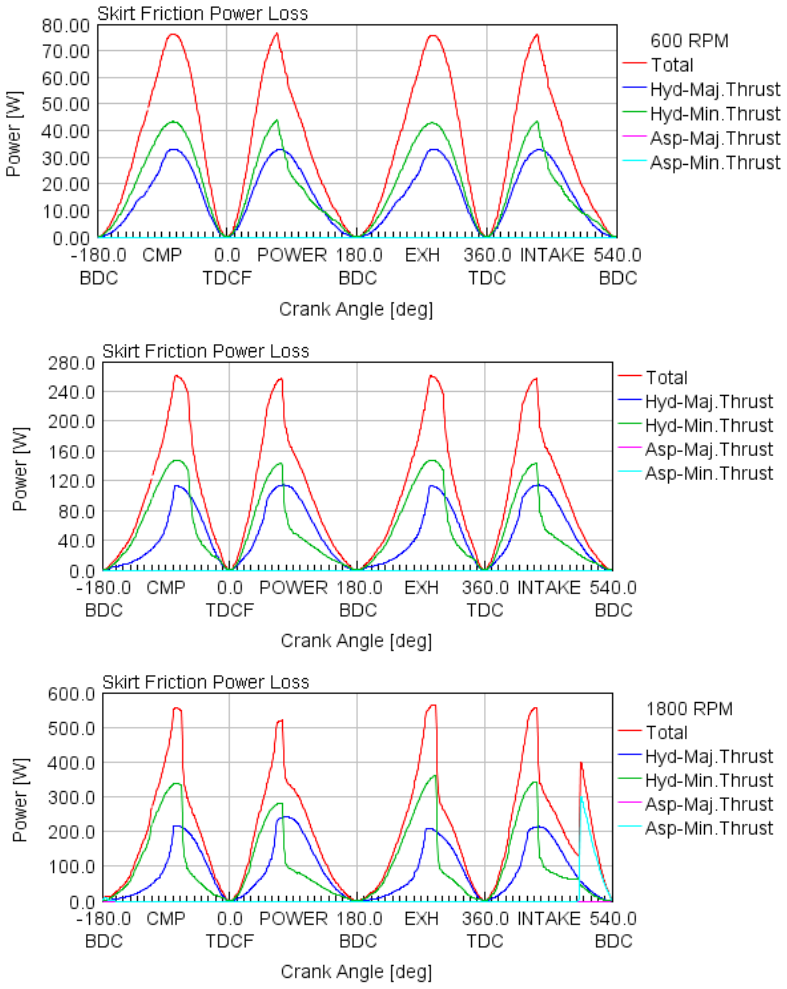

Figure 7.15: Skirt Friction Power Loss – Motored – 600-1800 RPM

Since the secondary motion of the piston is modelled, it is possible to observe variations in Piston tilt, eccentricity and squeeze film effects due to the Skirt lubrication. The major function of the piston skirt is to protect the ring surfaces from adverse wear by contact against the surface of the liner. Therefore the skirt used the squeeze film of the oil to contain the piston tilt during the firing. This condition is not evident from the motored tests.

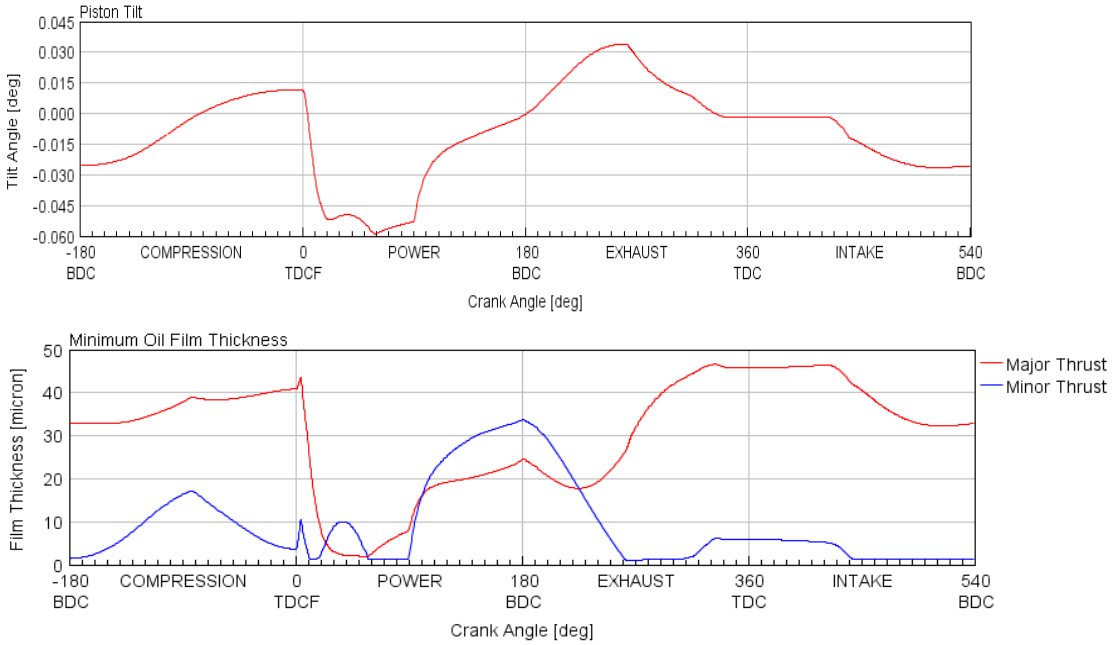

Figure 7.16 : Piston Skirt – Full Load – Piston Tilt, Oil Film Thickness – 1200 RPM

The modelling of the oil transient thermal behaviour and the oil viscosity variation due to shear thinning is observed. But this behaviour of the oil is highly dependent on the Input data of the oil. i.e low Shear and high Shear viscosities of the oil and density variation with temperature must be provided with a high accuracy.

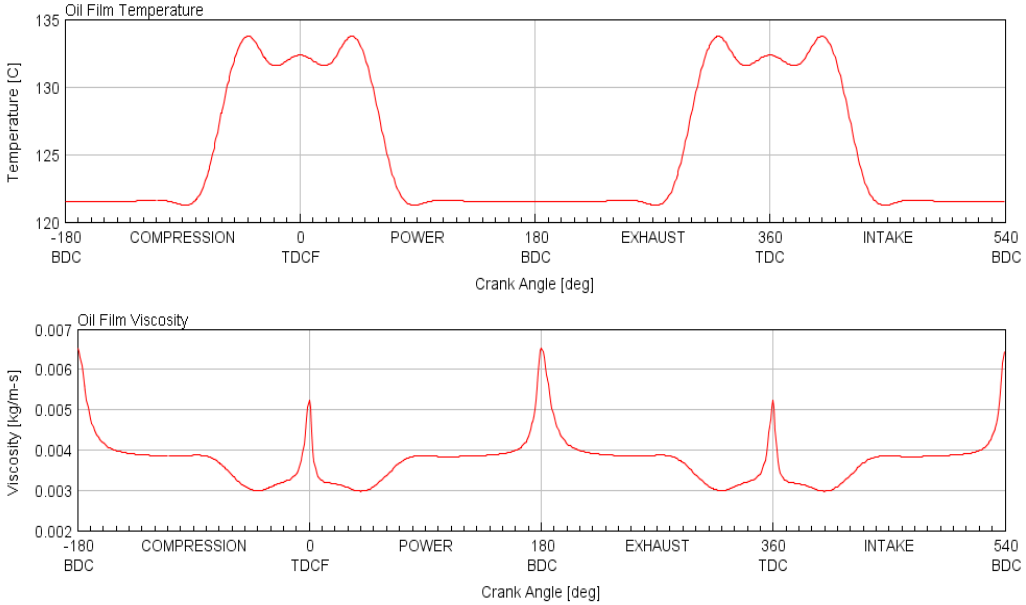

Figure 7.17: Oil film temperature and Viscosity variation – Motored – 1200 RPM

7.2.3 Bearings

Several parametric plots are available in order to analyse the performance of the Bearings – The journal orbit plots of the Big End, Small End and the Main bearings are presented below.

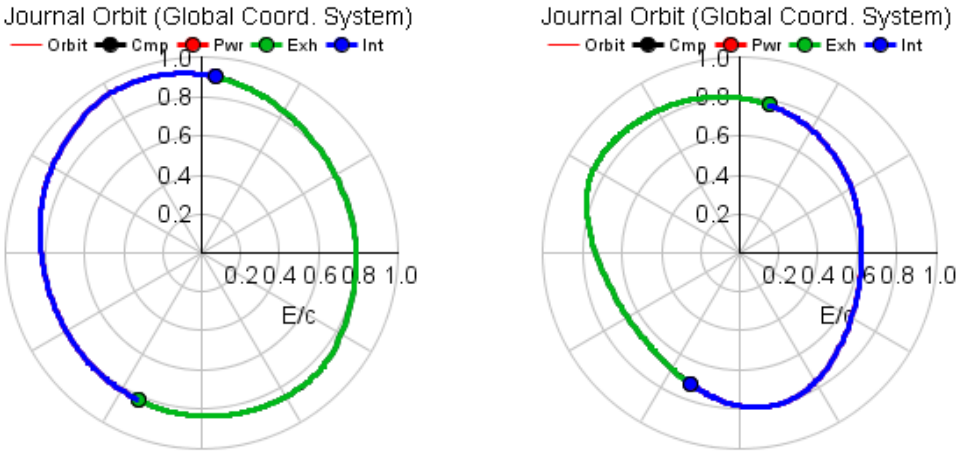

Figure 7.18: Main, Big End Bearing Journal Orbit – Motored – 1200 RPM

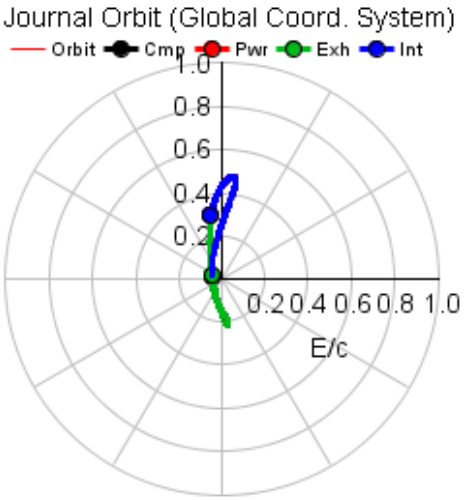

Figure 7.19: Small End Bearing Journal Orbit – Motored – 1200 RPM

We can observe the characteristic motion of the journal through the bearing housing from these orbit plots. The eccentricity/clearance ratio is minimal on the all the bearings due to the motoring condition. And, the Small End bearing motion is almost vertical due to the inertia of the gudgeon pin and the oscillating piston masses.

The motion of the Main bearing is fairly concentric due to motion of the crank and the high inertia of the crankshaft journals. The Big End bearing, however, is subjected to rocking motions from the angular motion of the bearing housing which is embedded into the connecting rod.

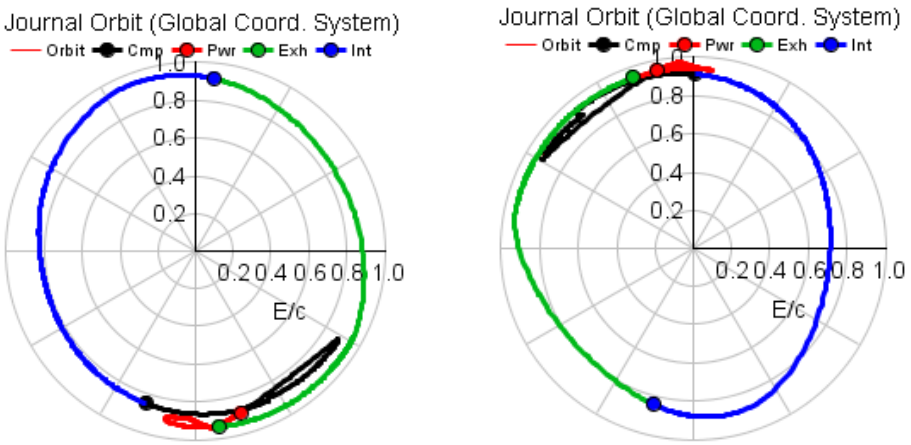

Figure 7.20: Main, Big End Bearing Journal Orbit – Full Load – 1200 RPM

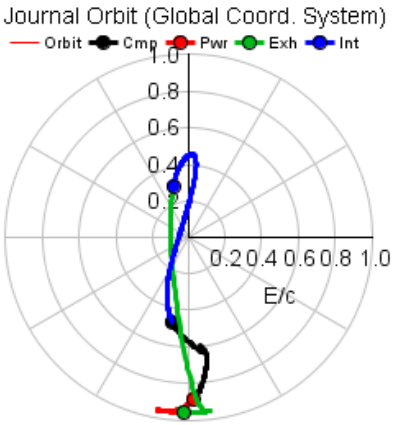

Figure 7.21: Main, Big End Bearing Journal Orbit – Full Load – 1200 RPM

In the Firing conditions at 1200 RPM, the Bearing eccentricity/clearance ratios are very high for all the bearings. This is due to the extremely high Gas pressure forces. The forces exerted on the small end bearing causes the journal to move towards the bottom shell and thereby create a high degree of 'oil shear'. The Big End bearing begins to have a part of the load 'carried' by the surface, as it enters the mixed lubrication regime due to the eccentricity exceeding 99% of the bearing radial clearance, and the Main bearing also has a higher eccentricity. In the Mobility model, since the oil film between the Bearing and the Journal is always modelled as a squeeze film therefore the effect of cavitation at higher rpms is not observed. This could be a potential reason for the Big End bearing friction estimation to be lower at higher RPMs as seen in section 7.1.

The instantaneous power losses of the Bearings in motored and fired conditions are shown below.

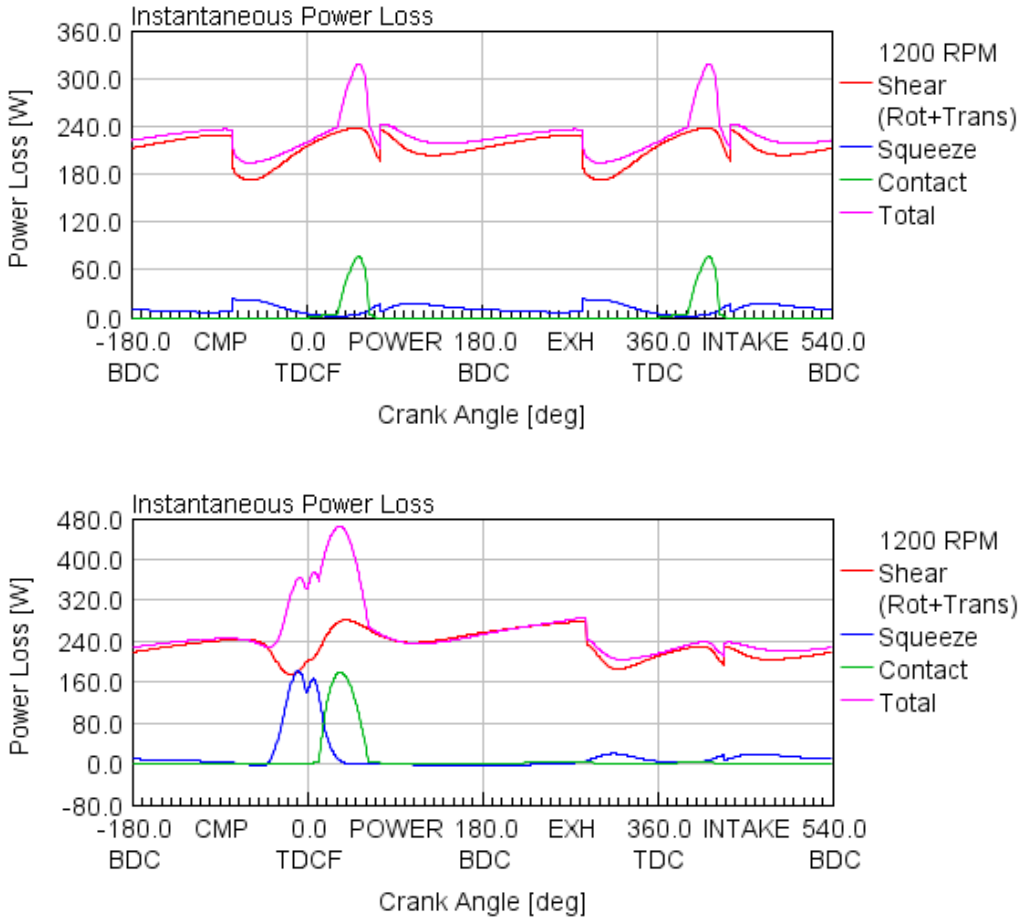

Figure 7.22: Instantaneous Power Loss – Main Bearing 1 – Motored and Full Load – 1200 RPM

As it can be seen, the biggest contribution to the power loss in the bearings is the shear forces due the bearing rotation and translatory motion. The fired condition causes the highest power loss to be concentrated around the region of the cycle where the Cylinder firing occurs for each bearing.

As explained in section 5.1, the bearings are simulated using the Mobility/Impedance method. Both these methods are map based solutions and therefore result in the calculation of the oil film begins modelled as a ‘squeeze film’ in all conditions. As a result of this, the cavitation effects in the Journal Bearings cannot be observed. This feature is available on the Journal Bearing HD simulation object. It involves the simulation of the Journal Bearings using a full 3 dimensional Reynold’s Equation solution and the complete model of the EHL solution. This method was not used for the 1-d modelling scheme, due to the required computing resources and long runtimes. [10].

The Y-forces (vertical) of all Main bearings on the MD13 Crankshaft under fired and motored conditions are shown below.

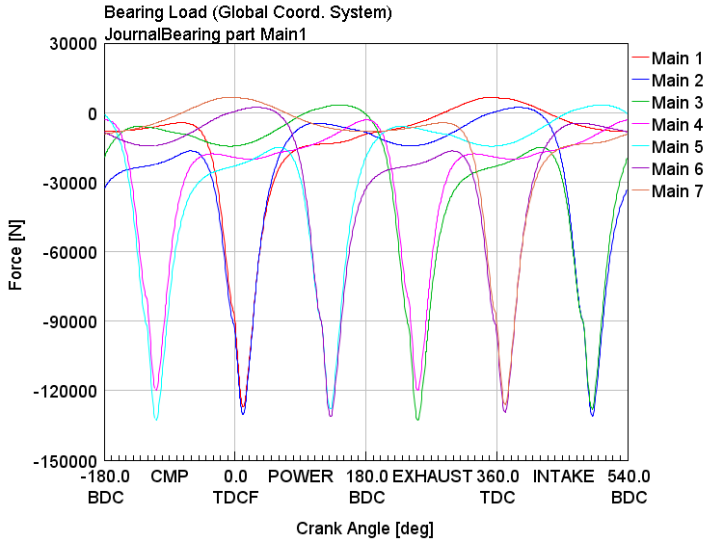

Figure 7.23: Main bearing loads – Full Load – 1200 RPM

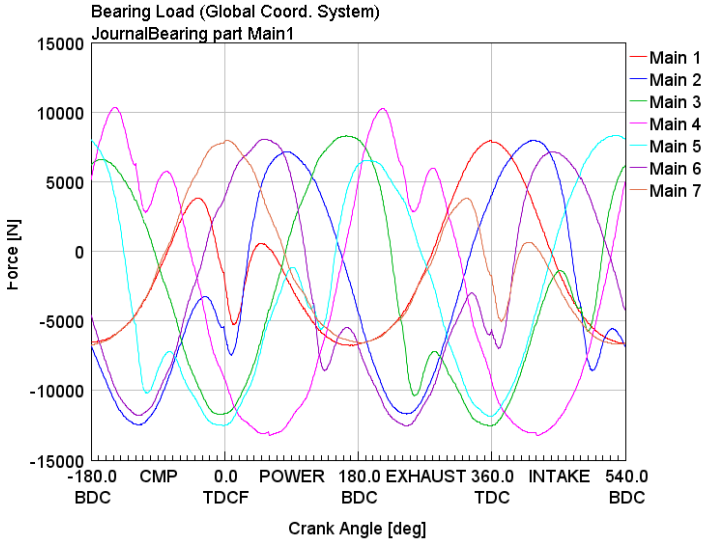

Figure 7.24: Main bearing loads – Motored – 1200 RPM

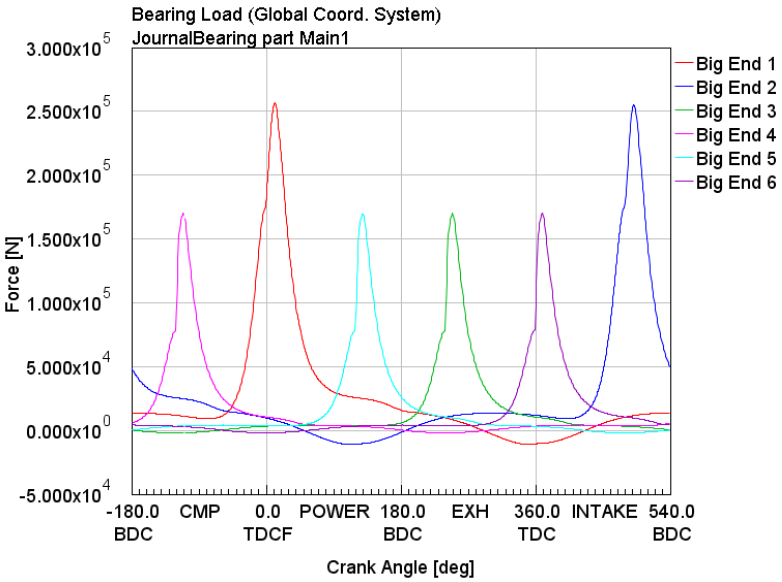

Figure 7.25: Big End Bearing loads – Full Load – 1200 RPM

Both the cases shown above have been simulated by modelling a flexible crankshaft. The stiffness of the crankshaft is provided as sub model inputs to the crank webs, the Journals and the crankpins. This allows the crankshaft to be modelled as a quasi-static 3D-beam, and also engages the bearings appropriately.

The flexible Crankshaft model shows significant bearing performance over fired and motored conditions, and these effects are not captured by the rigid Crankshaft model, hence, all the simulation trials are performed using the flexible Crankshaft model.

8 Friction Reduction Strategies

The simulation models developed using Gamma technologies' GT-Suite and the MIT lc2dm piston simulation program have been tested for various cases of motored and fired running conditions. The fidelity of the models have been fairly established, for the Volvo MD13 engine. In order to study an effect of parameter variation and to perform a sensitivity analysis of the models to change in parameters, the following test strategies are proposed. Apart from being tests for the models, these strategies are potential friction reduction methods.

Possible Friction Reduction Strategies – For motored engine friction

- Possibility of a 12 Counterweight Crankshaft design as a replacement of the existing 4 counterweight design on the MD13.
- Reduction in Main bearing diameter
- Reduction in Oil Control Ring Tangential Force (Ring Tension)
- Change in Piston Skirt length

Each of these strategies targets a specific sub model of the simulation model, and will establish the fidelity of the models in situ.

8.1 12 Counterweight Crankshaft

The current design of the MD13 engine consists of 4 counterweights which are positioned on the webs 1, 6, 7 and 12. The counterweights are efficiently positioned in a unique combination, in order to balance the crankshaft completely in the first order. The 4 counterweight design also provides a lighter Crankshaft in comparison to the 8 counterweight design, which was used previously on the MD13 engine.

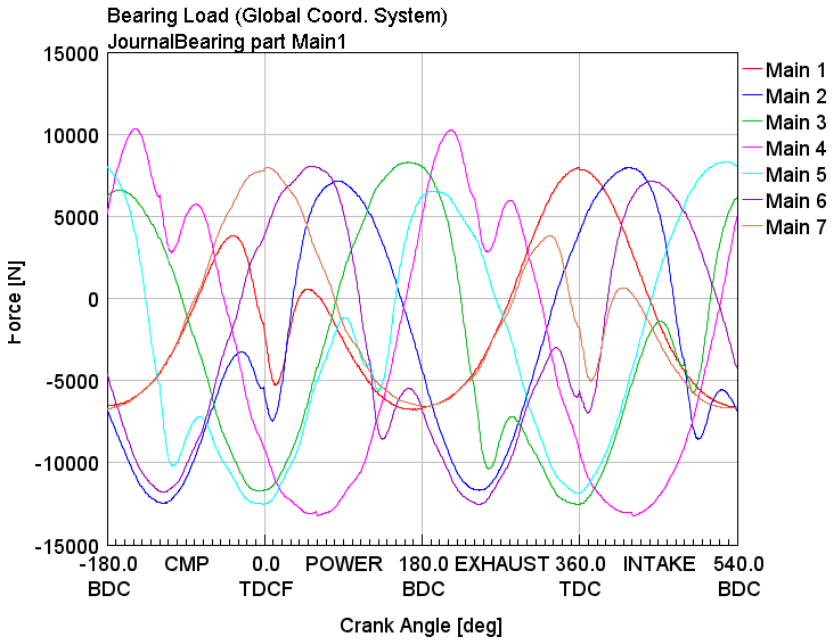

Figure 8.1: Main bearing Y Loads – Motored – 1200 RPM – 12 counterweights

The Main bearing Y-forces for all the bearings on the 4 counterweight design crankshaft are as shown in Figure 8.1.

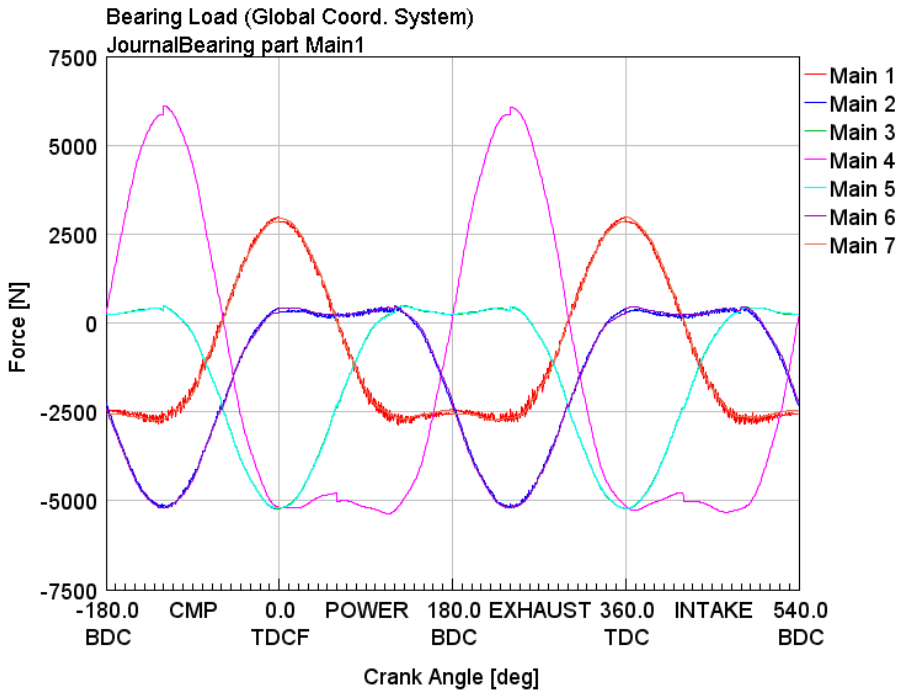

Figure 8.2: Main bearing Y Loads – Motored – 1200 RPM – 4 counterweights

The Main Bearing forces for the 12 Counterweight version of the crankshaft are shown in Figure 8.2.

The change in the FMEP of the Main Bearings due to this modification is presented in the graph below.

Despite increasing the total weight of the crankshaft, the 12 Counterweight design provides a reduced friction performance due to the proper balance of the crankshaft through the 12 counterweight design. The effective distribution of the crankshaft weight provides an advantage to the bearings in terms of the friction reduction.

These results are not conclusive because the effect of the counterweight assembly on the Stresses on the crankshaft are not analysed, and the primary requirement is to maintain the stiffness of the crankshaft at its optimum point, thereby ensuring the life of the engine.

8.2 Reduction in Bearing Diameter

Downsizing the crankshaft bearings provides a direct reduction in friction power loss, by reducing the mass of the crankshaft and also by reducing the overall area of the oil film within each journal bearing. This effect is demonstrated by a reduction in the diameter of the main bearing of the crankshaft by a few millimetres. The resulting change in the stiffness of the Crankshaft will have to be simulated using an FEM tool such as Ansys or AVL Excite in order to determine the change in the flexural rigidity of the crankshaft due to this change.

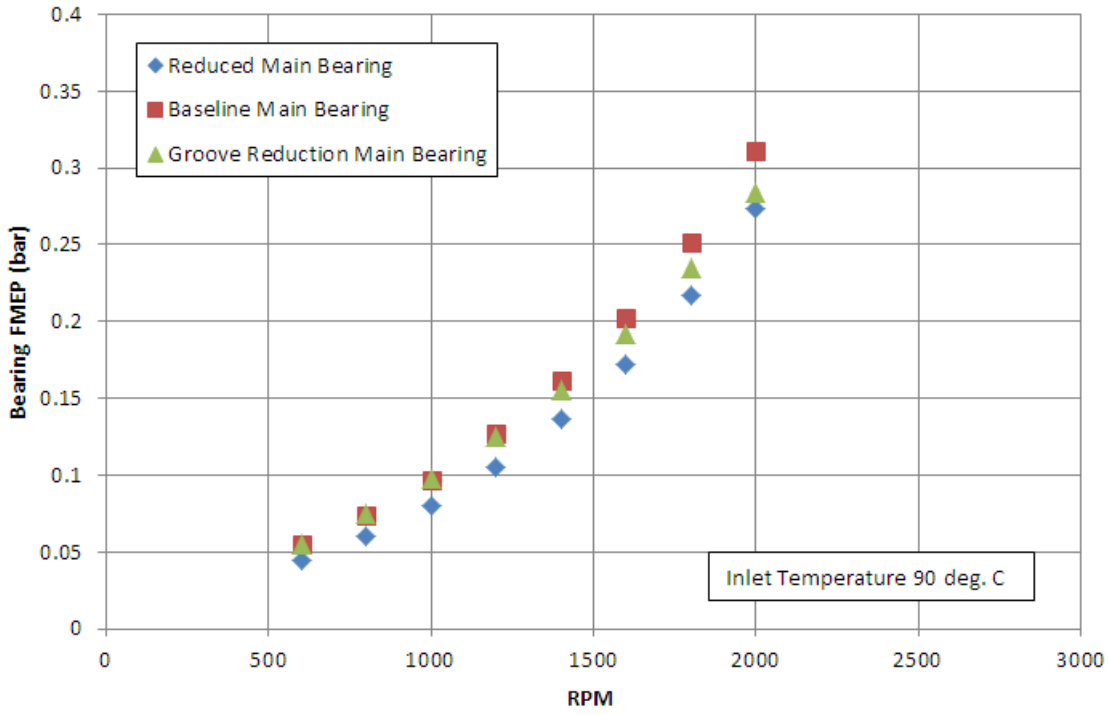

Figure 8.3:Main Bearing Friction Reduction – Motored – 1200 RPM

An interesting possiblity seen in the graph above is the reduction of the width of the oil feed groove in the upper shell of the main bearing by 1 mm on the MD13 Crankshaft, with the dimensions of the bearing same as the beasleine bearing. This provides a small reduction in the friction performance of the bearing. Coupled with a 3 mm reduction in Bearing diameter, this could lead to a considerable drop in the friction power loss from the bearings.

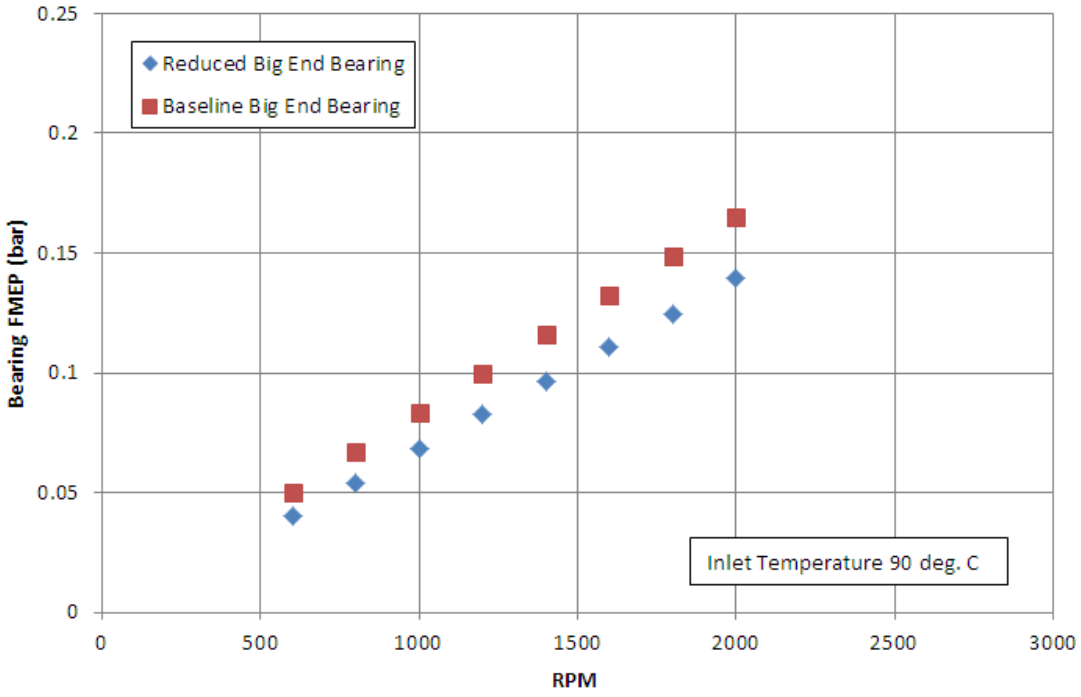

Figure 8.4: Big End Bearing Friction Reduction – Motored – 1200 RPM

The results from the Big End bearings also show the same trend as the main bearings with respect to the diameter reduction.

8.3 Reduction in Oil Control ring Tangential Force

The oil Control Ring contributes to half of the ringpack friction in motored condition. By lowering the Ring tensions (i.e tangential force) on the oil control ring, a minor reduction in the friction of the ring is expected. The performance of the oil control ring is fairly similar in both motored and fired operating conditions. But, a major concern in the lowering of the OCR tangential force is the predicted increase in the blow by gas leakage into the crankcase. Plots of the comparative change in ring tangential force and resulting change in blow by are shown below. The blow by gas predictions are made using the MIT lc2dm program, where the same ring parameters are simulated.

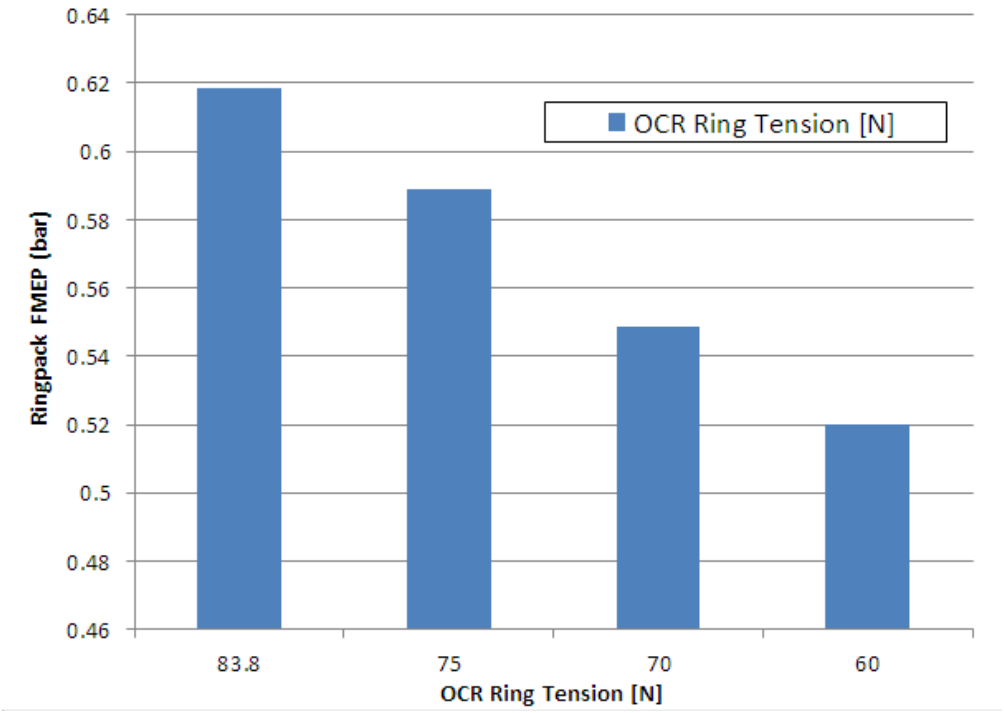

Figure 8.5: Oil Control Ring Tangential Force reduction comparison – Full Load – 1200 RPM

As expected, the reduction in the Oil Control Ring tension provides a reduction in the Ringpack FMEP, for the fired load cases. The plots of the instantaneous power loss on the Oil control ring, provide an ilicit response of the simulation tool to the change in this input parameter.

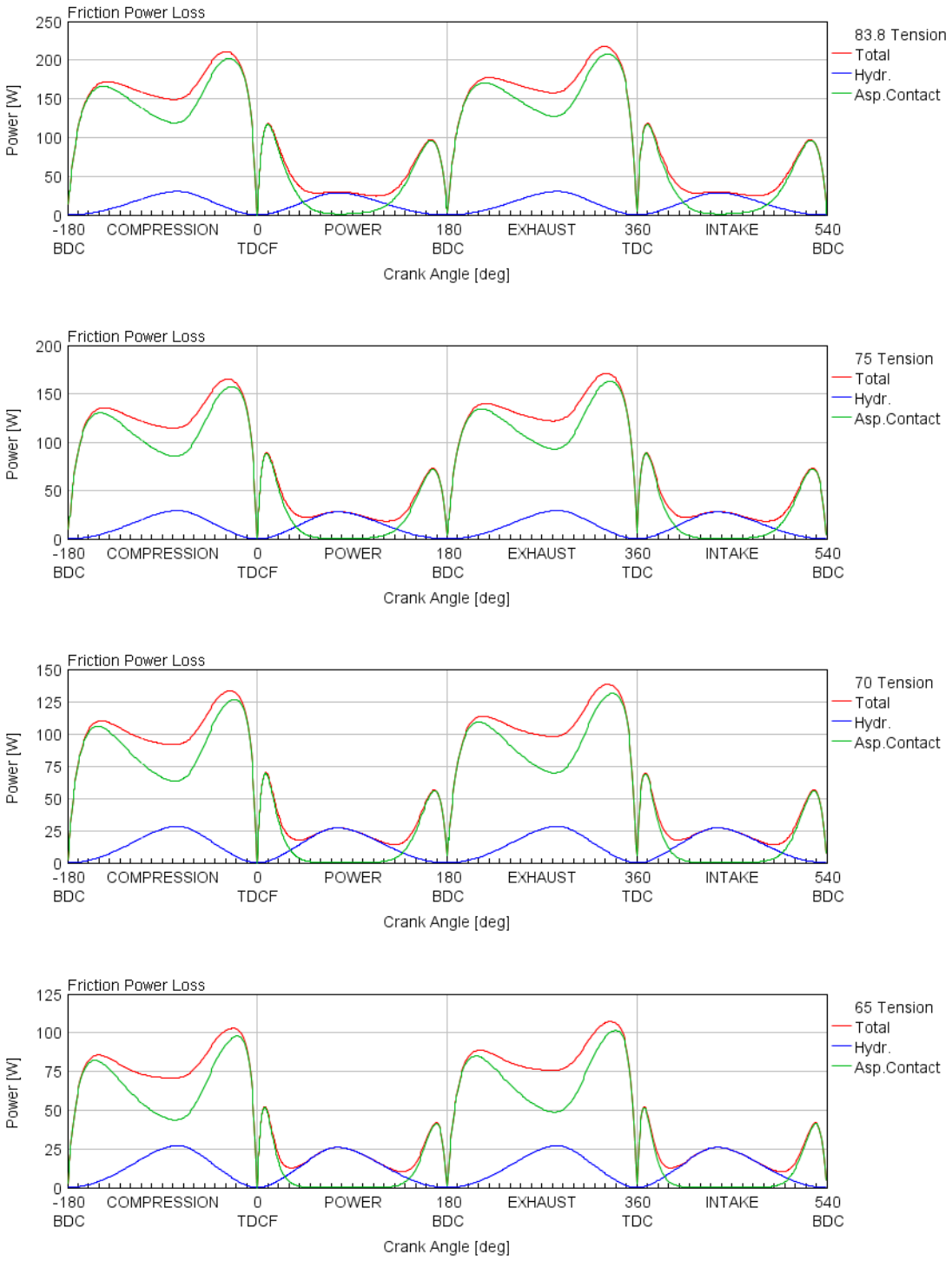

Figure 8.6: Oil Control Ring Tangential Force reduction – Full Load – 1200 RPM – Instantaneous Power Loss comparison

A massive change in the Oil Control Ring tension, can cause a severe blow to the blow by gas leakage, the plots of the blow by gas through the Oil control ring for various tangential forces are presented below.

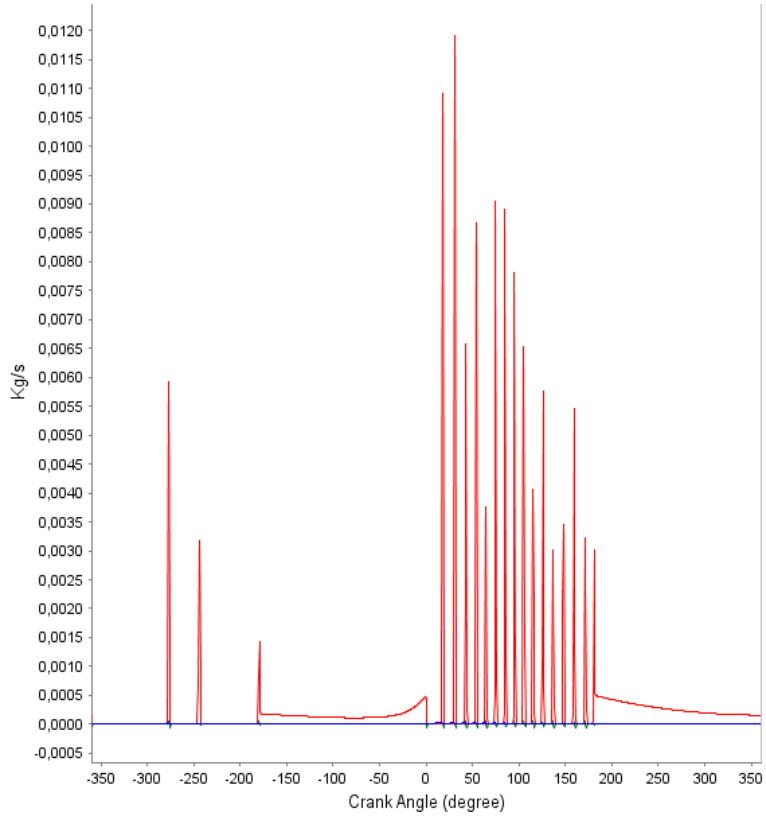

Figure 8.7: Oil Control Ring (83.8 N Tangential Force) blow by gas leakage – Full Load – 1200 RPM

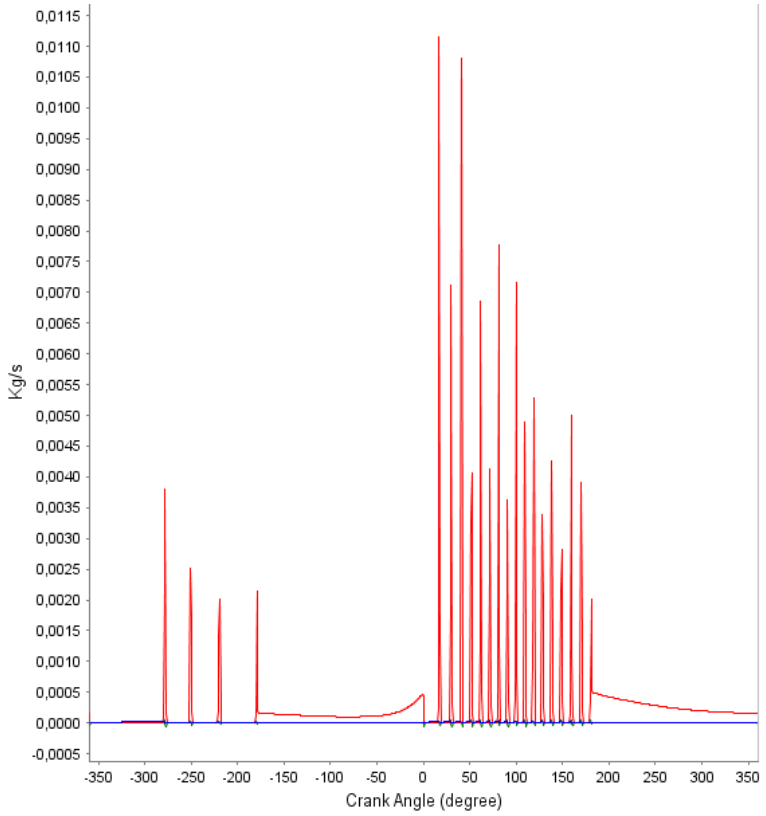

Figure 8.8: Oil Control Ring (75N Tangential Force) blow by gas leakage – Full Load – 1200 RPM

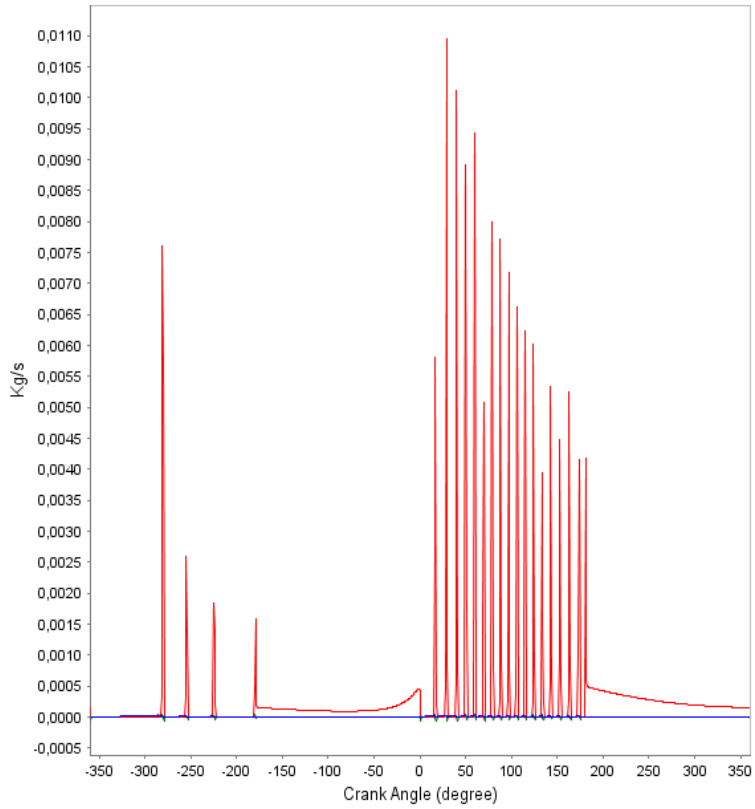

Figure 8.9: Oil Control Ring (70 N Tangential Force) blow by gas leakage – Full Load – 1200 RPM

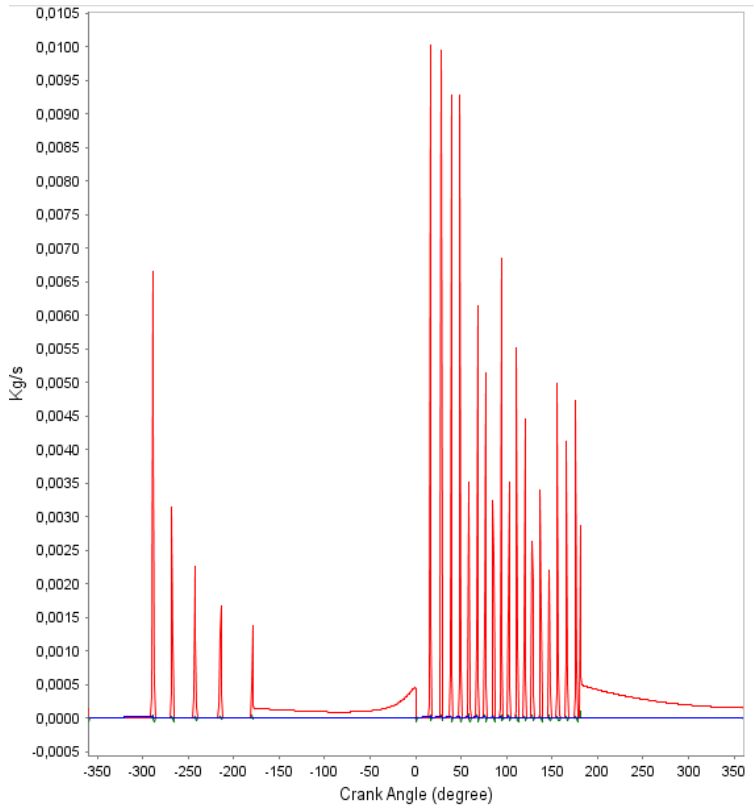

Figure 8.10: Oil Control Ring (65N Tangential Force) blow by gas leakage – Full Load – 1200 RPM

Form the above plots generated using the MIT program, it can be noted that the Oil Control Ring effective change in tangential force does lead to a minor change in the blow by gas leakage through the ring, and this phenomenon has to be weighted against the reduced friction power loss by means of a floating liner rig tests or actual engine operational tests for confirmation of the simulation prediction.

Also, further simulation study is useful with this design change, in order to draw a conclusion on the Ring parameterization. But, this also demonstrates the response of the model to the constitutional parameters for the ringpack.

8.4 Reduction in Skirt length

A reduction in skirt length can also influence the hydrodynamic friction power loss to a considerable extent due to the large area of the skirt. For these simulations to be completely effective, a skirt profile input is required for the skirts. Since the actual profile of the Volvo MD!3 engine piston skirt could not be measured, a profile was assumed based on the CAD information of the piston that was available. From this information, a basic shape representing the ovality and the radial skirt profile was estimated. This profile is the same in a cold state but changes due to the thermal deformation of the skirt as the engine operates at significantly high temperatures.

An extract of the assumed face skirt profile is shown below.

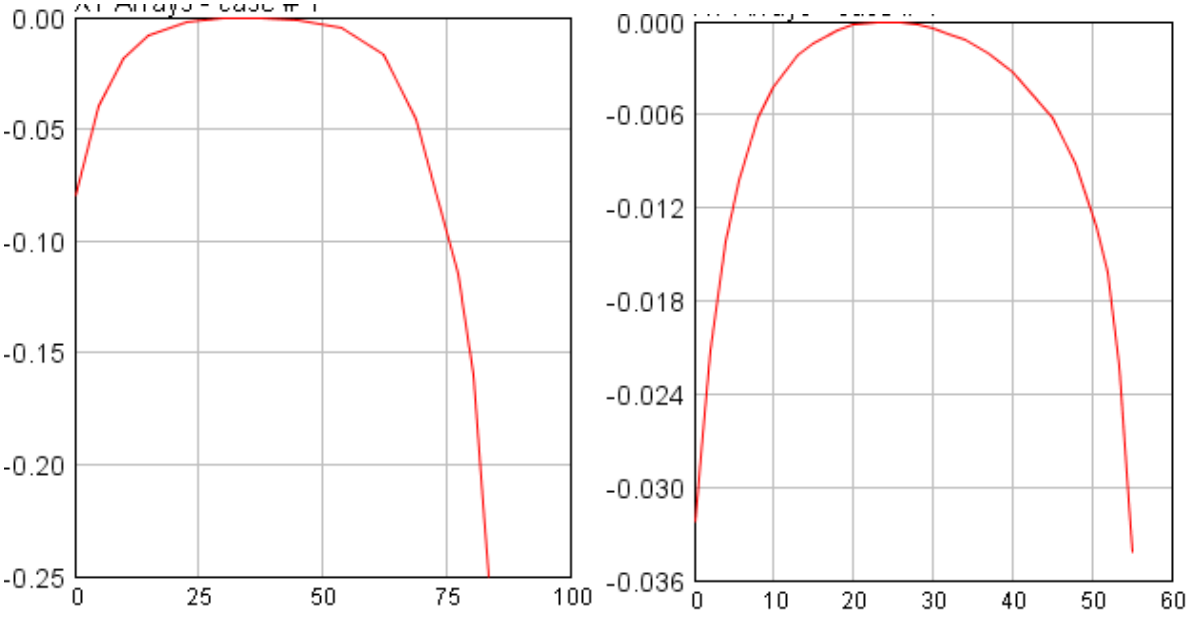

Figure 8.11: Piston skirt ovality and axial profile – Volvo MD 13 approximation

By using these profiles, the position of the skirt on the MD13 piston is altered to four different positions, which are,

Table 4: Skirt dimensions

Position No.	Reduction Edge	Skirt Length
1	Baseline	55
2	Top	52
3		50
4	Bottom	52
5		50

Note: Top and Bottom indicate the edges of the skirt Major and Minor thrust pads, from which the height of the skirt is reduced. The resulting changes in the skirt profile due to the variation in skirt length are accounted in the measurements.

The resulting change in FMEP is shown below.

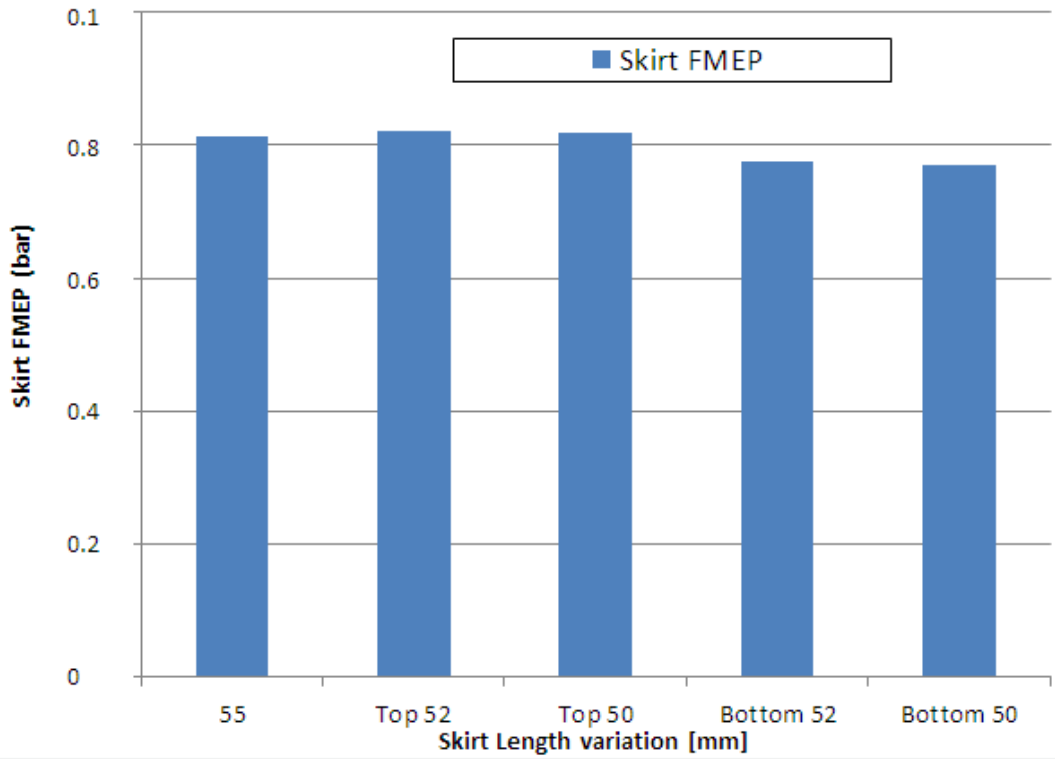

Figure 8.12: Skirt dimension friction comparison – Full Load – 1200 RPM

The variation in the FMEP of the skirt is not high with the small changes in the length of the skirt, due to the minor influence of the end zones of the skirt in the hydrodynamic friction power loss contribution. Also, the most important function of the skirt is to prevent the piston from slapping against the face of the liner when the combustion gas pressure is applied on the piston crown as the piston is at firing TDC. Therefore the parameter variation for the skirt is managed in a way so as to maintain the skirt from major asperity contact and being capable of reproducing the same or better piston slap resistance.

9 Conclusions and Recommendations

From the complete report presented from Chapters 1 through 8, it is significant, that the models that have been developed using gamma Technologies' GT-Suite and the MIT lc2dm have been analysed for various conditions, both motored and fired. A few hundred simulation cases have been run using the combination of the Friction model on GT-Suite and the blow-by model from the MIT program.

From the observations from the models, the following conclusions can be drawn, and the recommendations for Future work are presented in this chapter.

9.1 Conclusions

Through sound physical models based on strong physics backgrounds and the present of minimal tuning factors provides a solution to the early development stage for new engine designs and friction reduction technology. The fidelity of the models have been established through the comparison of the results with the Engine Strip tests conducted by FEV and by presenting parameter variation towards reducing friction power loss.

The models contain very few tuning parameters, most of which have been set to thje default values. The model calibration to the test conditions is fairly simple, and can be used to perform simple and fast verifications for friction performance.

The GT-Suite friction model presents a clear picture of the physics behind the solutions, although some improvements could make the tool, a complete solution for Friction, Blow-by and Oil Consumption simulations. The blow-by model used as part of the MIT lc2dm psim solution, is a complete model, including axial groove ring dynamics, groove ring interactions, and a the effective modelling of the gas pressures and blow-by conditions.

Owing to the split sub-routines for the various components, the models use different solution techniques to solve the individual sub models, thereby the solution speed is very fast. Also, the Master-Slave option to deactivate the solutions for multiple Piston Cylinder Units, by phasing the solution for the ringpack and the skirt increases the solution time by almost 3-4X. Additionally, options to split the CPU intensive Bearing solutions to multiple threads, while maintain the main routine on a Master thread, provides excellent parallel computing capabilities, while using a standard simulation computer, without the need for extensive computing resources.

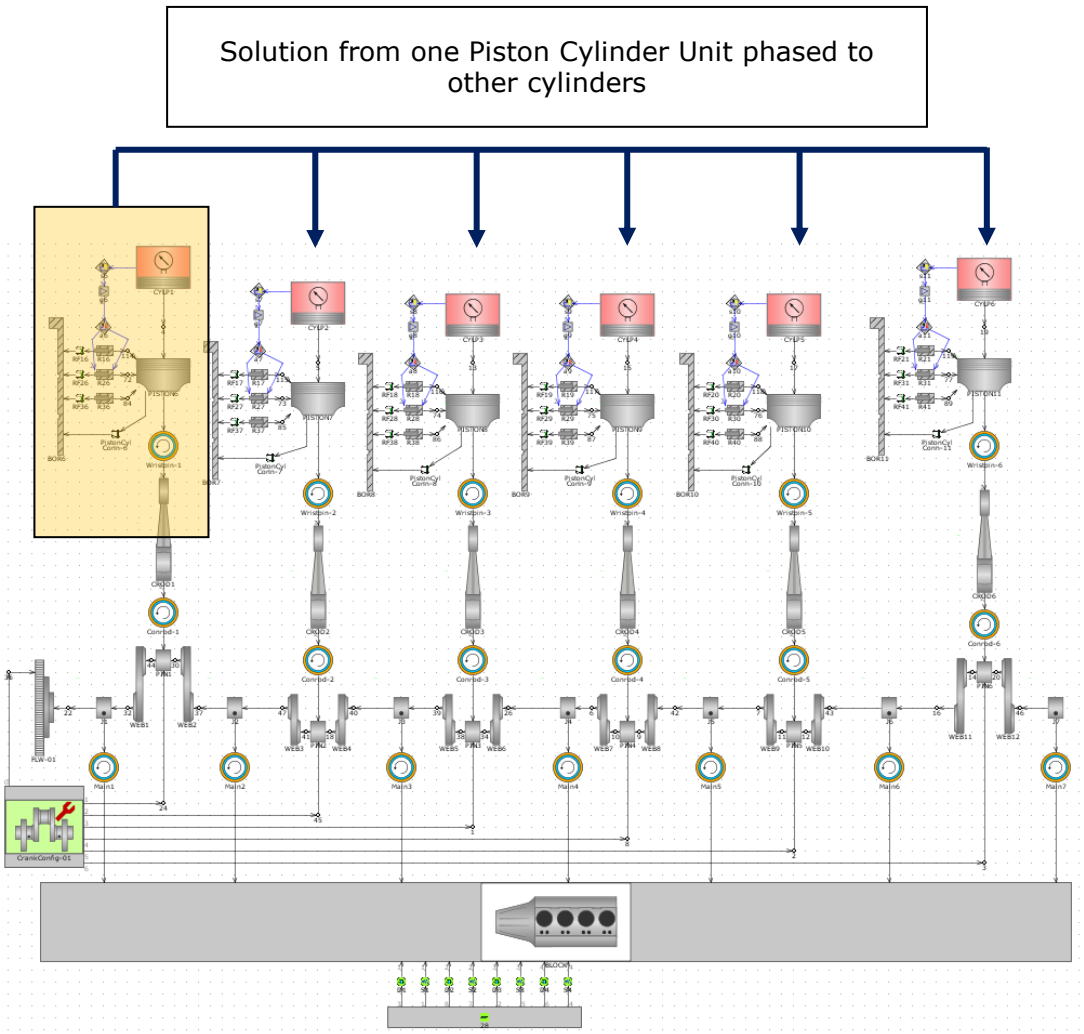

Figure 9.1: GT-Suite PCU solution translation

The major drawbacks of the models observed from the Model Validation chapter observed are two-fold.

a) The Bearing models based on the Mobility and the Impedance approaches always model the oil film as a 'squeeze film' and calculate the effects of the oil shear and squeeze as two separate phenomena based on positions or states of the journal within the bearing housing. This does not provide a possibility to model the mass conserving solution for the oil film, and thereby the model does not simulate the elasto-hydrodynamic nature of the oil film in the bearings. Also this model does not contain a calculation for the cavitation effects due to the absence of the mass conserving solver.

b) The absence of an integrated ring-groove axial dynamics solver and a ringpack blow-by model inhibit the complete estimation of the friction performance of the rings and the concomitant effects of the ring dynamics.

The parameter variations between the models show the robust responses of the models and the simulation physics. The models also confirm the physical intuition towards the friction performance.

Comprehensively, it can be concluded that, the parameters of an engine cranktrain are complex and highly interdependent, but these mathematical models have enabled significant progress towards understanding the influence of these parameters on the performance of the engine cranktrain.

9.2 Recommendations for Future Work

By establishing a better relationship with the development team at Gamma Technologies and at the Massachusetts Institute of Technology, several improvements can be brought about to the models.

The introduction of a finite element based universal hydrodynamic film solver, and the introduction of an elasto-hydrodynamic bearing model. Also, the detailed models for the axial ring groove dynamics and integration of the blow-by models is essential.

With the development of the models becoming more and more complex, tuning of these models will become necessary, and this is best analysed by performing engine tests by using a floating liner rig test bench. Model calibration can be carried out easily by using results from the bench.

Combination of the fast-running cranktrain friction models with a full system lubrication model can prove effective to calculate oil consumption from the cranktrain components.

The modelling and simulation of other engine friction components and their validation against similar tests would be a good compliment towards the building of a 'virtual engine lab' which represents a collection of engine simulation models. Primarily, this involves the Oil Pumps, Coolant pumps and the valvetrain.

10 References

[1] Moughon L., (2006),: Effects of Piston Design and Lubricant selection on Reciprocating Engine Friction, *Massachusetts Institute of Technology,* Thesis Publications, June 2006.

[2] Kamada Y., Ahlberg J., Aixala L., (2009) Comparative Study of friction between Nissan Diesel GE13 and Volvo HDEP engines. Volvo Group Trucks Technology, Internal Report.

[3] Wong V., Tian T., Lang H., Ryan J. et al. (1994): A Numerical Model of Piston Secondary Motion and Piston Slap in Partially Flooded Elasto-hydrodynamic Skirt Lubrication, *SAE Technical Paper* 940696, 1994, doi:10.4271/940696

[4] Pinkus, Oscar and Sternlicht, Beno, "Theory of Hydrodynamic Lubrication", *McGraw Hill*, 1961.

[5] Frene J., Nicolas, D., Degueeurce, B., Berthe D., Godet, M., *Hydrodynamic Lubrication: Tribology Series* (vol 33), Elsevier, 1997.

[6] Greenwood, I. and Tripp, J.H., "The Contact of Nominally Flat Surfaces", *Proc. I. MechE*, Vol 185, pp 625-633, 1971.

[7] Patir N. and Cheng H.S., "Application of Average Flow Model to Lubrication between Rough Sliding Surfaces", *Trans. of ASME*, Vol.101, 1979, pp.220-230.

[8] Keribar, R. and Dursunkaya, Z. "A Comprehensive Model of Piston Skirt Lubrication" *SAE Paper* 920483, 1992

[9] Booker, J. F., "Dynamically Loaded Journal Bearings: Numerical Application of the Mobility Method", *ASME Journal of Lubrication Technology*, Vol. 93, Jan. 1971, pp. 168-176.

[10] GT Suite Mechanical Theory Manual (2014); *Gamma Technologies,* February 2014, As part of GT-Suite 7.4 Build 1.

[11] R. Keribar, Z. Dursunkaya and M.F. Fleming, "An Integrated Model of Ring-Pack Performance", *Trans. A.S.M.E.* Vol.113, 1991, pp 382-389.

[12] Dursunkaya, Z., Keribar, R. and Ganapathy, V., "A Model of Piston Secondary Motion and Elastohydrodynamic Skirt Lubrication," *ASME Trans, J Trib*, 116, pp 777-785, 1994.

[13] Junker, Heinz K., Pistons and Engine Testing, *Mahle Gmbh (Ed.)*, 2012.

[14] Junker, Hienz K., Cylinder components, *Mahle GmbH (Ed.)*, 2012.

[15] Smedley G., (2002),: Piston Ring Design for Reduced Friction in Modern Internal Combustion Engines, *Massachusetts Institute of Technology,* Thesis Publications, June 2002.

[16] Tian T., “Modelling the Performance of the Piston Ringpack in internal Combustion Engines”, *Massachusetts Institute of Technology,* Thesis Publications, June 1997.

[17] Tian T., “Dynamic behaviours of piston rings and their practical impact. Part 2: Oil transport, friction and wear of ring/liner interface and the effects of piston and ring dynamics”, *Proc Instn Mech Engrs,* Vol 216, Part J: J engineering Tribology, 2002.

[18] Tian T., “Dynamic behaviours of piston rings and their practical impact. Part 1: ring flutter and ring collapse and their effects on gas flow and oil transport”, *Proc Instn Mech Engrs,* Vol 216, Part J: J engineering Tribology, 2002.

[19] Tomanik, E. "Piston Ring Conformability in a Distorted Bore", *SAE Technical Publications,* SAE Paper 960356, 1996

[20] McCool J. I., “Extending the Capability of the Greenwood Williamson Micro contact Model”, *ASME Trans. J Trib,* Vol. 122, July 2000.

[21] McCool J. I., “Relating Profile Instrument Measurements to the Functional Performance of Rough Surfaces”, *ASME Trans. J Trib,* Vol. 109, April 1987.

Appendix A

Input parameters for GT-Suite model – Cranktrain Dimensions

Sensitive details about the engine have been omitted from this list in accordance with the Volvo Confidentiality policy.

Parameter	**Value**			Unit
SAE Oil Name	SAE-15W40	SAE-10w30		
Piston/Connecting Rod				
Cylinder Bore	131.01			mm
Half Stroke (Crank Throw)	79			mm
Piston Mass	3557			g
Connecting Rod Length	267.5			mm
Connecting Rod Mass	5730			g
Connecting Rod Rotating Mass	4060			g
Piston Rings	**Top Ring**	**Scraper Ring**	**Oil Control Ring**	
Ring Mass	35.00	43.00	16.00	g
Ring Thickness	3.38	2.55	2.98	mm
Ring Width	4.70	4.75	3.75	mm
Ring Face Roughness	measured	measured	measured	
Land Dia below Ring	130.6880	130.4860	130.8760	mm
Position above Piston Pin	62.78	53.10	46.85	mm
Base Free Dia for Ring Tension	139.00	136.00	138.50	mm
Reference Temp for Ring Tension	25.00	25.00	25.00	deg C
Skirt Length	55			mm
Position of Top of Skirt	21			mm
Pad Angle Major Side	90			deg
Pad Angle Minor Side	90			deg
Bearings	**Main**	**Big End**	**Small End**	
Bearing Diameter	108	99	58	mm
Bearing Length	37	47	47.5	mm
Oil Inlet Temperature	90	92	96	deg C
Ambient pressure	1	1	1	bar
Journal Surface Roughness	1.02E+01	1.50E-01	1.50E-01	micron
Bearing Surface Roughness	1.50E-01	1.50E-01	1.50E-01	micron
Flywheel				
Mass	35.14			kg
Flywheel Length	55			mm
Mass Offset	0			mm

Appendix B

McCool surface decomposition, example surface of Top ring surface presented. Actual surface measurements withheld – Volvo Confidentiality policy.

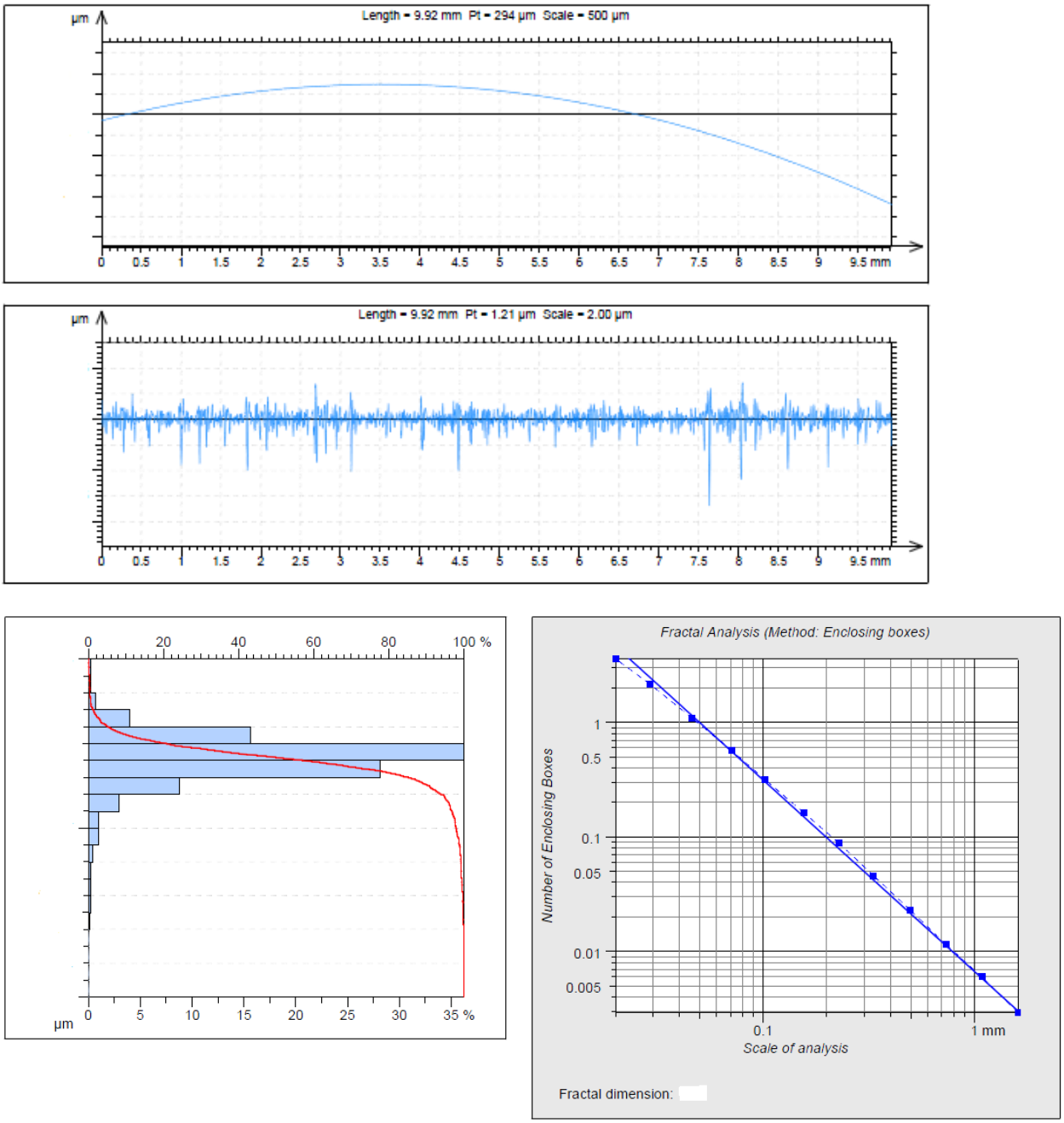

Figure A.1: Measurement information – From Profilometer – Top Ring

SurfaceRoughness_TopRing_Roughness

Profilometer Data Analysis and Extraction of SIGMA, ETA, BETA:

Number of data points 1985
Total stylus travel ..... 9.92 mm
Stylus resolution ..... 4.99748 micron
Mean surface height (datum) ..... -4.53629E-06 micron
Max. surface height (rel. to datum) ..... 0.155 micron
Min. surface height (rel. to datum) ..... -0.179 micron
Standard deviation ..... 4.049809E-02 micron
Standard deviation for points above datum ..... 3.920216E-02 micron
Standard deviation for points below datum ..... 4.178791E-02 micron

McCool Method

Spectral Moment M0 ..... 1.536809E-15 m^2
Spectral Moment M2 ..... 3.798872E-05
Spectral Moment M4 ..... 6.811014E+06 1/m^2
* ETA (Asperity density) ..... 5491.56 1/m^2 x1e6
* SIGMA (Std. dev. of asperity peaks) ..... 3.920216E-02 micron
* BETA (Mean radius of asperity peaks) ..... 254.683 micron
SIGMA*ETA*BETA 5.482841E-02
(SIGMA/BETA)^0.5 ..... 1.240666E-02
(SIGMA*ETA*BETA)^2*(SIGMA/BETA)^0.5 ..... 3.729633E-05

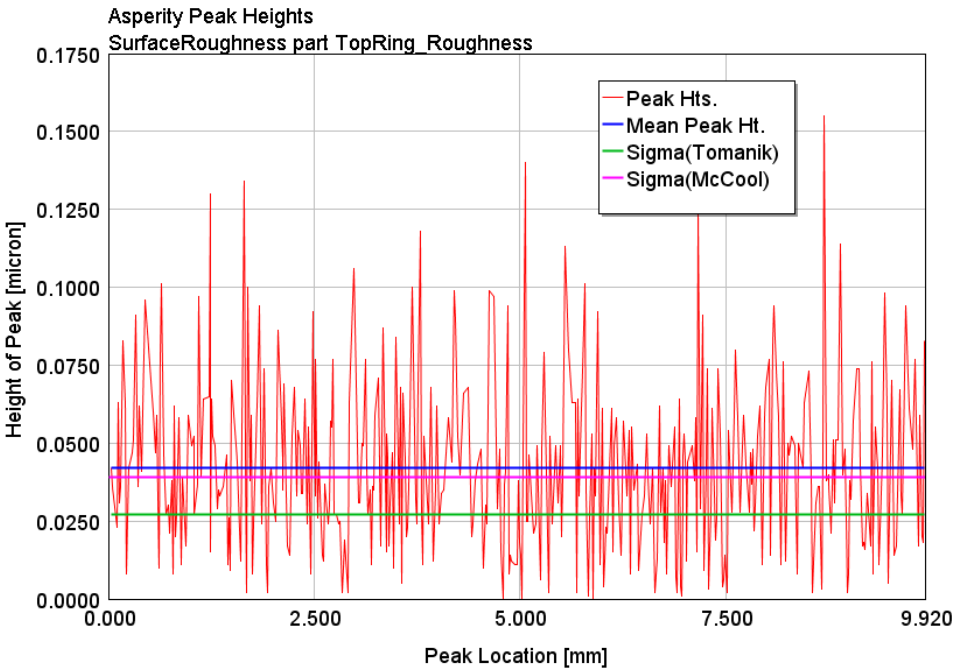

Figure A.2: Asperity Peak Height decomposition – McCool – Top Ring

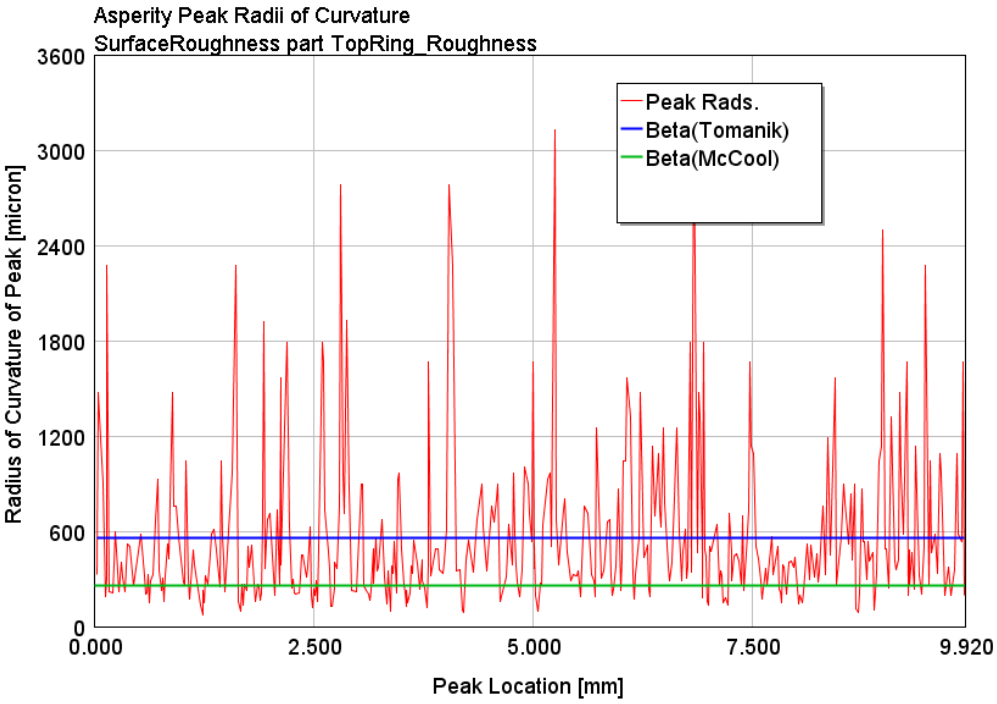

Figure A.3: Asperity Peak Radii of Curvature decomposition – McCool – Top Ring